

Scuola di Ingegneria Industriale e dell'Informazione Dipartimento
di Chimica, Materiali e Ingegneria Chimica "Giulio Natta"

Tesi di Laurea Magistrale in Ingegneria Chimica



POLITECNICO
MILANO 1863

**STRATEGIES FOR SELECTIVE FLUORESCENT
FUNCTIONALIZATION OF CELLULOSE-BASED
NANOMATERIALS USED FOR WATER
REMEDICATION**

Relatore: Prof. Carlo PUNTA

Correlatore: Dott.ssa Laura RIVA

Dott. Andrea FIORATI

Camilla FLEMATTI

Matricola n. 899296

Anno accademico 2018-2019

“Tomorrow belongs to those who hear it coming”

(David Robert Haywood-Jones)

ESTRATTO

L'inquinamento ambientale è diventato uno dei principali problemi nel corso degli ultimi decenni. In particolare, la bonifica delle acque rappresenta una delle maggiori sfide per la comunità scientifica, incoraggiata anche da una sempre più consapevole presa di coscienza da parte della popolazione riguardo la salute dell'ambiente. Tra le varie soluzioni proposte, i nanomateriali ingegnerizzati (ENMs) si sono dimostrati tra le tecnologie migliori per la rimozione di inquinanti come gli ioni dei metalli pesanti.

Alla luce di questa recente tendenza, proponiamo un nuovo nanomateriale a base di cellulosa, già oggetto di studi di eco-design. Il nostro materiale è composto da due polimeri diversi: nanofibre di cellulosa TEMPO-ossidate (TOCNFs) e polietilenammina ramificata (bPEI), reticolati nella forma di aerogel. Questo nanomateriale si è dimostrato essere efficiente, sia nella rimozione degli inquinanti sia per quanto concerne l'aspetto di eco-sostenibilità. Tuttavia, servono ulteriori studi per verificare eventuale bioaccumulo dei nanomateriali in organismi acquatici.

Obiettivo della mia ricerca è stato il grafting della poliammina con vari fluorofori al fine di controllare il comportamento del polimero nell'ambiente marino. La presenza di gruppi carbossilici su TOCNF e amminici su bPEI ha permesso il grafting selettivo su entrambi i gruppi funzionali, usando fluorofori rilevabili all'UV-Vis a lunghezze d'onda diverse (**Figure 1**). In questo modo è stato possibile monitorare il degrado del nostro materiale co-polimerico nell'acqua di mare.



Figure 0.1. Fluorofori usati per la funzionalizzazione dei polimeri.

L'obiettivo delle sintesi è stato quello di graftare almeno il 20 % delle ammine primarie presenti sulla superficie della poliammina. Applicando gli stessi criteri per il grado di funzionalizzazione dei gruppi carbossilici di TOCNFs e, non superando questa percentuale, sono quindi rimasti sufficienti gruppi reattivi liberi per promuovere il cross-linking necessario alla formazione dell'aerogel.

ABSTRACT

Environmental pollution has become one of the main issues in the last decades. In particular, the water remediation has risen as major challenge for the scientific community, which is also pushed by an increasing awareness of population about the matter. Among the solutions to this issue, Engineered NanoMaterials (ENMs) have shown to be one of the best ways for the removal of heavy metal ions from sea water.

Considering this recent trend, we propose a new cellulose-based nanomaterial, on which an eco-design study has already been carried out. This material is composed by two different polymers: TEMPO-Oxidized Cellulose Nanofibers (TOCNFs) and branched polyethyleneimine (bPEI), combined in the form of aerogels. This nanomaterial has proved to be effective in both the removal of pollutants and eco-safety. However further investigation was necessary to explore possible bioaccumulation of these materials in aquatic organisms. Hence, the focus of my work was the grafting of both the polyamine and nanocellulose with different fluorophores, in order to check the behaviour of the ENMs in the marine environment.

The presence of carboxylic groups on TOCNF and amino moieties on bPEI allows the selective grafting on both these chemical groups, considering various UV-Vis detectable fluorophores with different emission wavelength (see **Figure 1**). In this way it is possible to monitor the degradation of our co-polymeric material in sea water.

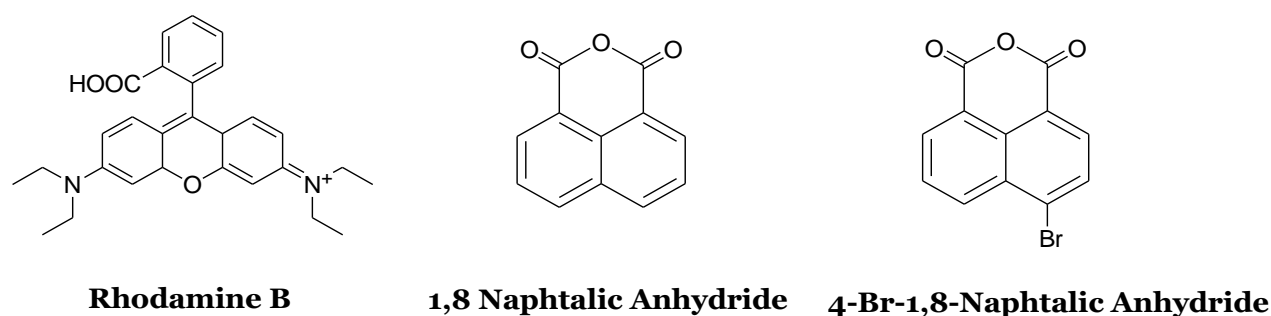


Figure 0.2. Fluorophores used for the functionalization of the polymers.

The aim of the synthesis was to graft at least the 20 % of the primary amine groups on the surface of the polyamine; the same criteria was used for the functionalisation degree of carboxylic groups on TOCNF. This is because it is necessary to keep some reactive groups free in order to favour the cross-linking that leads to the formation of the aerogel.

Table of Contents

ESTRATTO	IV
ABSTRACT	V
Table of Contents	VIII
List of Figures and Tables	XI
1. Introduction	1
1.1 General overview	1
1.2 Cellulose	3
1.2.1 General features	3
1.2.2 Cellulose sources	4
1.2.3 Hierarchical structure	4
1.2.4 Applications	6
1.3 Nanocellulose	7
1.3.1 General features	7
1.3.2 Types of Nanocellulose	9
1.3.3 Properties	12
1.3.4 Production Methods	3
1.4 Synthesis of Co-Polymeric Nanosponges Systems with TEMPO-Oxidized Cellulose Nanofibers and branched Polyethyleneimine	6
1.4.1 TEMPO-Oxidized Cellulose NanoFibers (TOCNFs) Error! Bookmark not defined.	
1.5 Nanosponges	11
1.5.1 State of the art of the material	11
1.5.2 Adsorption	16
2. Results and Discussion	19
2.1 Preparation of the materials	19
2.1.1 F-bPEI1a and F-bPEI1b	20
2.1.2 F-bPEI2 and F-bPEI3	21
2.1.3 Model compounds 1,2,3	23
2.1.4 Compounds 4 and 5	25
2.1.5 Compound 6	27
2.1.7 Preparation of sponges	27
2.2 UV-vis discussion	30
2.2.1 UV-vis analysis with Rhodamine B	30

2.2.2 UV-vis analysis with 1,8 Naphthalic Anhydride and 4-Br-1,8-Naphtalic Anhydride	32
2.3 Ecotoxicological tests	33
3. Materials and Methods	36
3.1 General	36
3.2 Cellulose oxidation with the TEMPO, NaClO and KBr system	36
3.3 Tempo Oxidised Cellulose NanoFibers (TOCNFs) titration	37
3.4 Sponges general procedure	39
3.5 Reference table	41
3.6 Synthetic procedures	44
3.6.1 Synthesis of F-bPEI1a	44
3.6.2 Synthesis of F-bPEI1b	45
3.6.3 Synthesis of compound 1	46
3.6.4 Synthesis of F-bPEI2	49
3.6.5 Synthesis of compound 2	50
3.6.6 Synthesis of F-bPEI3	51
3.6.7 Synthesis of compound 3	52
3.6.8 Synthesis of compound 4	54
3.6.9 Synthesis of compound 5	54
3.6.10 Synthesis of compound 6	56
3.6.11 Preparation of the sponges	57
3.7 UV absorption spectroscopy	58
3.7.1 UV-vis analysis of compound 1 and F-bPEI1b	59
3.7.2 UV-vis analysis of compound 2 and F-bPEI2	62
3.7.3 UV-vis analysis of compound 3 and F-bPEI3	66
4. Conclusion and future perspective	71
5. Bibliography	73

List of Figures and Tables

Figure 1. Fluorofori usati per la funzionalizzazione dei polimeri.....	IV
Figure 2. Fluorophores used for the functionalization of the polymers.....	V
Figure 3: Hierarchical structure of wood biomass and the characteristics of cellulose microfibrils ¹⁵	5
Figure 4: SEM image of cellulose nanocrystals.....	10
Figure 5: SEM of bacteria producing a bacterial cellulose pellicle, ²⁸	11
Figure 6: SEM image of cellulose nanofibers taken from ³⁵	12
Figure 7: Redox reaction of nitroxide radical.....	8
Figure 8: Mechanism of cellulose TEMPO-oxidation and highlight of the separation of the fibrils under alkaline medium. (⁷⁵ - modified).....	9
Figure 9 : schematic procedure for the preparation of the nanosponges: A) TOCNFs dispersion in water at 2.5% w/v concentration and sonication to obtain a homogeneous dispersion; B) bPEI addition to the solution; C) Fast freezing of the solution in molds; D) Freeze-drying for bulk water; thermal treatment for enhancing amidation; E) Thermal treatment for enhancing amidation; F) Washing of the material to remove the non-reticulated components; Material ready for the metal adsorption essay;	13
Figure 10: Preparation of bPEI-TOCNF sponges with citric acid ⁷⁷	13
Figure 11: SEM images of cross section of bPEI-TONCF 2:1 (left side) and bPEI-TONCF-CA 2:1-18 (right side) nanosponges with increased magnification. The presence of citric acid seems to improve the development of sheet-like internal porous structure.	15
Figure 12: comparison between α -CNS (blue bars) and A-CNS (orange bars) adsorption capacity at the equilibrium (q).....	16
Figure 14: SEM-EDX image of a-CNS cross section. A) Cd(II) adsorption from 50 ppm MilliQ water solution. B) Zn (II) adsorption from 50 ppm MilliQ water solution.	17
Figure 2.1: ¹ H-NMR spectrum of F-bPEI1b in D ₂ O with enlightening on the aromatic portion.....	21
Figure 2.2: ¹ H-NMR spectrum of F-bPEI2 in D ₂ O with enlightening on the aromatic portion	22
Figure 2.3: ¹ H-NMR spectrum of F-bPEI3 in D ₂ O with enlightening on the aromatic portion	23
Figure 2.4: UV spectra at different concentration of RB in HCl 0.1N.....	30
Figure 3.1: ¹ H-NMR spectrum of F-bPEI1 concentrated in D ₂ O.....	46
Figure 3.2: ¹ H-NMR spectrum of compound 1 in CDCl ₃	48
Figure 3.3: IR spectra of blanc bPEI, and derivative functionalized with Rhodamine B. In the spectra of compound 1 and F-bPEI1b it is possible to observe a peak at 1175 and between 1500-1750 cm ⁻¹ , relative to the imidic bond.....	48
Figure 3.4: ¹ H-NMR spectrum of F-bPEI2 in D ₂ O.....	49
Figure 3.5: ¹ H-NMR spectrum of compound 2 in CDCl ₃	50
Figure 3.6: IR spectra of blanc bPEI, and derivative functionalized with 1,8-Naphtalene Anhydride. In the spectra of compound 2 and FbPEI2 it is possible to observe a peak at 1700 and 1656 cm ⁻¹ ; these peaks are relative to the stretching of the imidic bonds.	51
Figure 3. 7: ¹ H-NMR spectrum of F-bPEI3 in D ₂ O.....	52
Figure 3 8: ¹ H-NMR spectrum of compound 3 in CDCl ₃	53
Figure 3.9: IR spectra of blanc bPEI, and derivative functionalized with 4-Br,1,8-Naphtalene Anhydride. In the spectra of compound 3 and F-bPEI3 it is possible to observe a peak at 1700 and 1656 cm ⁻¹ ; relative to the stretching of the imidic bonds and a peak at 700 cm ⁻¹ , peculiar of the alkyl halide.	53
Figure 3.10: IR spectra of oxidised cellulose, and derivative functionalized with APTES and then with Rhodamine B. In the spectra of compound 4 and compound 5 it is possible to	

observe a peak at 3000 cm^{-1} ; relative to the stretching of the primary and secondary amines and a peak at 1175 and between 1500-1750 cm^{-1} , relative to the imidic bond55

Figure 3.11: IR spectra of oxidised cellulose, and derivative functionalized with Rhodamine B. In the spectra of compound 6 it is possible to observe a peak at 1400 cm^{-1} ; relative to the double bond C-C of the aromatics57

Figure 3.12: UV spectra at different concentrations of compound **1** in HCl 0.1N59

Figure 3.13: calibration lines of compound **1**, expressed in mg/mL and $\mu\text{mol/mL}$61

Figure 3.14: UV-vis spectra of F-bPEI1b in HCl 0.1N at different concentrations.....61

Figure 3.13: UV spectra at different concentrations of compound **2** in HCl 0.1N63

Figure 3.14: calibration lines of compound **2**, expressed in mg/mL and $\mu\text{mol/mL}$ 65

Figure 3.15: UV spectra of F-PEI2 in HCl 0.1N at different concentrations.....65

Figure 3.16: UV spectra at different concentrations of compound **3** in HCl 0.1N67

Figure 3.17: calibration lines of compound 3, expressed in mg/mL and $\mu\text{mol/mL}$68

Figure 3.18: UV spectra of F-PEI3 in HCl 0.1N at different concentrations69

Table 1: properties and applications of Nanocellulose ⁴²1

Table 2.1: Different ratio of non-functionalized-bPEI and F-bPEI1b in each sponge28

Table 2.2 : Different ratio of non-functionalized-bPEI and F-bPEI2 in each sponge28

Table 2.3 : Different ratio of non-functionalized-bPEI and F-bPEI3 in each sponge29

Table 2.2: concentrations and measured absorption of RB31

Table 3.1: abbreviation and corresponding compound41

Table 3.2: concentrations and measured absorptions of compound **1**60

Table 3.3: concentrations and measured absorptions of F-bPEI1b.....62

Table 3.4: fluorophore present in each sample of F-bPEI1b and corresponding degree of grafting62

Table 3.5: concentrations and measured absorptions of compound **2**.....64

Table 3.6: concentrations and measured absorptions of F-bPEI2.....66

Table 3.7: fluorophore present in each sample of F-bPEI2 and corresponding degree of grafting66

Table 3.8: concentrations and measured absorptions of compound **3**67

Table 3.8: concentrations and measured absorptions of compound **3** **Error! Bookmark not defined.**

Table 3.9: concentrations and measured absorptions of F-bPEI3.....69

Table 3.10: fluorophore present in each sample and corresponding degree of grafting70

1. Introduction

1.1 General overview

Over the last decades, several efforts have been made to find suitable materials able to provide environmental remediation. Water treatments are studied with particular attention, since hydric quality is more and more and rapidly decreasing. This is due to many factors, such as population growth, climate change and increasing pollution. Some of the main issues to consider are the costs and the challenge in the treatment of either ground- and waste- water, that combined with an always growing awareness of the environmental risk lead to a continuous improvement and innovation. ¹

Some technologies already used are biological treatments with suitable enzymes or microorganism, phytoremediation, permeable reactive barriers using biological organism or chemical processes, chemical precipitation, absorption (activated carbon), oxidation, natural and synthetic zeolites with synthetic resins (ion exchange) and some physical methods.

Among all various materials and technologies proposed, engineered nanomaterials (ENMs) have shown a great potential and lots of researches are in progress to exploit their properties. In fact, nanoremediation has risen as a new clean-up method which is cheaper, more effective from an environmental, social and economic point of view, able to perform decontamination processes in situ, minimizing the addition of further chemicals.

Anyway, the lack of a unique legislative assessment is slowing the spread of these emerging technologies. ²

Since their nanometric size, ENMs display a high and reactive surface area and, moreover, they can be tailored according to the specific needs, making them an excellent material with almost infinite applications in several industrial areas.

The increasing consciousness about environment and human health is however cornering the use of these new materials because there aren't enough data available to ensure their safety, provoking debates regarding the balance between the commonly known goodness of nanoremediation and the unknown risks. ³ The main problem regards their mobility, which could lead to eco-toxicological issues (probable *Trojan horse* behavior in the carriage of pollutant matters). ⁴

Nanostructured cellulose-based materials with a micro-dimensional scaffold may overcome the potential hazard connected with the use of ENMs.

These materials are particularly attractive thanks to their wide availability and low cost, since they are cellulose-based derived from cotton, starch, paper and other renewable sources.

The last decade investigations proved that nanocellulose has a broad application spectrum: it can be used for food science, packaging, catalysis, energy storage devices and, more important for our purposes, for water remediation. ⁵

Moreover, the hydroxyl groups on the backbone of glucose units can be exploited with other substances, modifying the molecular properties according to the material.

1.2 Cellulose

1.2.1 General features

Cellulose is a linear macromolecule formed by β -1,4-linked D-glucopyranose rings and it is the most abundant polymer on Earth. It is also one of the most important structural elements in plants and bacteria: its purpose is the maintenance of their structure. These mentioned living species have a continuous daily production of cellulose (*e.g.*, a tree generates about 10 g of cellulose per day, with a global annual production of cellulose of about 1.5×10^{12} tons).⁶

The mass ratio of plants and animals is 1000:1, and cellulose plays a major role as one of the biggest plant constituents. This sustainable polysaccharide has remarkable physical and chemical properties, making it interesting in a broad range of applications, including fine chemicals.

Cellulose is a colourless, odourless, tasteless nontoxic solid polymer and exhibits promising properties such as excellent mechanical strength, biocompatibility, hydrophilicity, relative thermal-stabilization, high sorption capacity, and alterable optical appearance.⁷ Moreover, it is insoluble in water and in most organic solvents, chiral and biodegradable.

The single polymer chains assemble into fibers through intermolecular hydrogen bonds and hydrophobic interactions. The terminal groups of every cellulose chain give directional asymmetry. The reducing end of the chain has a hemiacetal group, while the non-reducing end bears a pendant hydroxyl group.⁸

Most of the polymer's properties are related to its chain length (degree of polymerization), that is the number of glucose units composing the molecule. Cellulose from wood pulp has chain length between 300-1700 units, cotton (and other plant fibers) and bacterial cellulose have length-range of 800-10'000 units.⁹ The shorter is the chain, the more the polymer is soluble in water. Generally speaking, it is soluble in many kinds of ionic liquids.¹⁰

Cellulose is a straight chain polymer; this property allows the adoption of a quite stiff rod-like conformation, helped by the equatorial conformation of the glucose residues. The bond between the units is made through condensation of the hydroxyl group present on the monomer, forming microfibrils with high tensile strength, the fibers are then meshed into a polysaccharide matrix.

Cellulose derivatives are obtained through the reaction (full or partial) of the hydroxyl groups (-OH) with several reagents, obtaining materials characterized by

different functional. In current industrial practice, cellulose-based polymers are renewable resources.

Cellulose is mostly employed to produce paper, paperboard and card stock, with small quantities converted into a huge variety of derivative products. Moreover, its wastes can be used to produce biofuels.

1.2.2 Cellulose sources

The most important source of cellulose is lignocellulosic biomass, which is composed of cellulose, hemicellulose, and lignin of vegetal origin. It contains 30–50 wt % cellulose,¹¹ 19–45 wt % hemicellulose,¹² and 15–35 wt % lignin.¹³ Together these polysaccharides form a heteromatrix that varies in its composition and structure as a function of the biomass source.

Other sources include:

- agricultural residues;
- tree trunks and dead forest matter;
- energy crops;
- food waste;
- municipal and industrial biowaste such as used paper, carton, and wood from demolition sites.

1.2.3 Hierarchical structure

Wood and plants are cellular hierarchical bio-composites projected by nature and they essentially consist of semi-crystalline cellulose microfibril-reinforced amorphous matrix of hemicellulose, lignin, waxes, and extractive and trace elements.

The architecture of the hierarchical structure of cellulose may be described as follow: the smaller components are linear glucan chains, that combine in crystalline cellulose microfibrils 3-4 nm wide (30-40 cellulose chains each), then bundles of microfibrils are formed, leading to cell walls, fibers, plant tissues and finally trees or other plants.

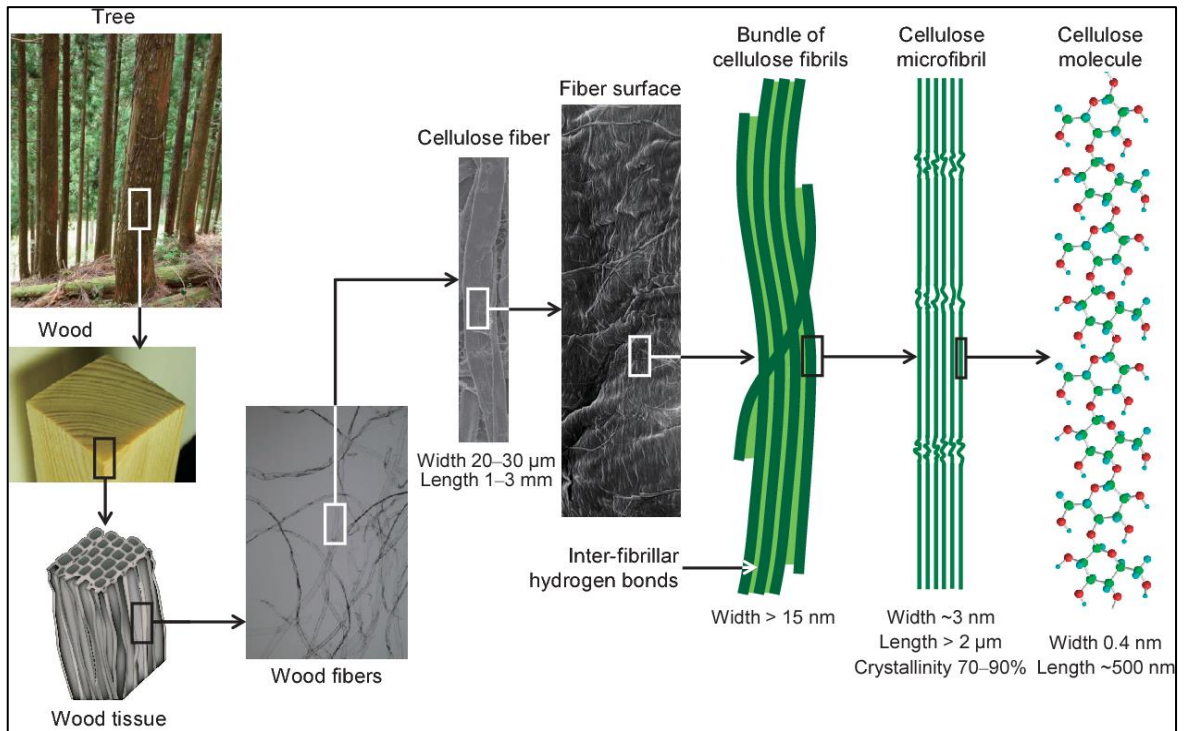


Figure 1.1: Hierarchical structure of wood biomass and the characteristics of cellulose microfibrils ¹⁵

1.2.4 Applications

From an industrial point of view, cellulose has been used as building block in the production of many products, including paper, cellophane films, explosives, textiles, and dietary fibers. ⁸ It has been traditionally burnt and used as load-bearing materials for constructions. In addition, there are much more sophisticated applications for cellulose and its derivatives, for instance in pharmaceutical industry, such as bioadhesive, mucoadhesive, osmotic (both semi-permeable membrane formulations and central core) drug delivery systems. Cellulose can be also used for pharmaceutical coating processes, for extended release (ER) solid dosage (coated ER formulations and ER polymeric matrices) and for enteric coated solid dosage. Pharmaceutical industries also use cellulose as compressibility enhancer, gelling, thickening and stabilizing agent, filler in solid dosage, binder in granulation processes and disintegrating and taste masking agent. ¹⁶

1.3 Nanocellulose

Cellulose fibrils are formed through cellulose biogenesis and hydrogen bonds and van der Waals forces stabilize them ¹⁷. The fibrils contain crystalline and amorphous regions, and the latter are more favorable in releasing nanoscale components through mechanical, chemical and enzymatic processes. The amorphous region can be treated with strong acids producing nanocrystalline cellulose, which is used as filler phase in bio-based polymeric matrix obtaining nanocomposites with superior thermal and mechanical properties. ¹⁸

1.3.1 General features

Nanotechnologies with cellulosic substrates have generated enormous attention during the past few decades. Various methods, such as chemical, biochemical and mechanical ones provide manners to modify nanocellulose, underlining properties like flame retardancy, transparency, and high flexibility, expanding traditional applications of wood deriving materials.

Sustainable development requires products crafted from renewable, environmentally friendly sources, presenting low health and safety risks, and economically affordable. Its high Young's modulus and surface area of several hundreds of square meters per gram encourage the investigation of many new alluring properties and applications. Nanocellulose employments foresee the production of a variety of high-value goods with low environmental impact. Nowadays, the industrial production of nanocellulose is in the range of tons per day. ¹⁹The term "nanocellulose" includes a lot of cellulose-based materials and their chemical and physical properties change typically according to their source and extraction method: cellulose nanocrystals (CNCs), cellulose nanofibers (NFC), and bacterial nanocellulose (BNC). The surface chemistry is crucial for the processability and the functionality of the incoming products.

When threaded together, nanocellulosic materials may form highly porous and mechanically strong matters. Moreover, due to the formation of strong networks possessing high tensile strength, they are the suitable material for the reinforcement of bio/nanocomposites, answering to the public request of non-petroleum based polymers. ^{20, 21} From an engineering perspective, the addition of rigid particles to polymer matrices produces lots of desirable effects, *i.e.* improved stiffness, a reduction in the thermal expansion coefficient, and increase in creep resistance and fracture toughness. Polymers NC-reinforced were found to be more efficient,

moreover have better mechanical properties than those crafted using conventional micro- or macrocomposite materials. A limitation to some application could be nanocellulose hydrophilic nature, but this restraint can be overcome by surface modification techniques. Carboxymethylation, amidation, esterification, etherylation, silylation, sulfonation, and phosphorylation are surface modifications aiming to the alteration of the properties and the extension of the applications. Nanocellulose may be functionalized with polymers, performing the grafting-to, grafting-from, or grafting through methods.

Nanocellulose has been employed in a wide range of composites, combined with nanocarbons, polymers, and inorganic materials composites due to compatibility issues.

1.3.2 Types of Nanocellulose

As previously reported, there are three main classes of nanocellulose: CNCs, CNFs and BNC, classified according to their morphology and source.

Cellulose is biosynthesized in plants forming partially crystalline fibers. The crystalline regions are at first weakened and then destroyed by means of mechanical shearing or acid hydrolysis, yielding to the expected nanocellulose. The amorphous parts have different physical properties with respect to crystalline cellulose, nanoparticles are formed disrupting the fibrils at amorphous points. Mechanical shearing or controlled acid hydrolysis can be both used to deconstruct cellulose nanofibers, yielding different structures depending on the chosen approach.²² Nanometer-long and highly crystalline rod-like fragments, CNCs, results from acid hydrolysis. CNFs are produced by means of mechanical shearing techniques, that destroy cellulose fibers into their substructural nanoscale units, which are usually longer, being micrometric in length.²³ BNC is produced through a bottom-up approach employing cultures of bacteria.

1.3.2.1 Cellulose Nanocrystals

CNCs, also known as nanowhiskers, show elongated crystalline rod-like shapes, and higher rigidity compared to NFC since wider amorphous proportions are removed.

One of the most used techniques employs strong acid hydrolysis, especially with sulfuric acid. A typical procedure for the separation of CNC starts with alkali and bleaching pretreatments, with subsequent acid hydrolysis, washing, centrifugation, dialysis, and ultrasonication to obtain a suspension which may be further lyophilized (freeze-drying or spray-drying) if required.²⁴ The reaction conditions and the cellulose source both influence many of the achieved properties of CNCs, such as the degree of crystallinity, the aspect ratio, dimensional dispersity, and the morphology.

²⁴ CNCs combine high axial stiffness (105–168 GPa), high Young's modulus (20–50 GPa), high tensile strength (~9 GPa), low coefficient of thermal expansion (~0.1 ppm/K), high thermal stability (~260°C), high aspect ratio (~10–70), low density (1.5–1.6 g/cm³), lyotropic liquid crystalline behavior, and shear thinning rheology.²⁵ Natural and synthetic polymers can be coupled with CNCs, obtaining new composites. Moreover, the surface can be modified with many different techniques that alter the self-assembly behavior of CNCs in suspensions and checking the interfacial properties present in the composites. CNCs offer composite materials with improved mechanical properties, low density and high surface area.²⁵

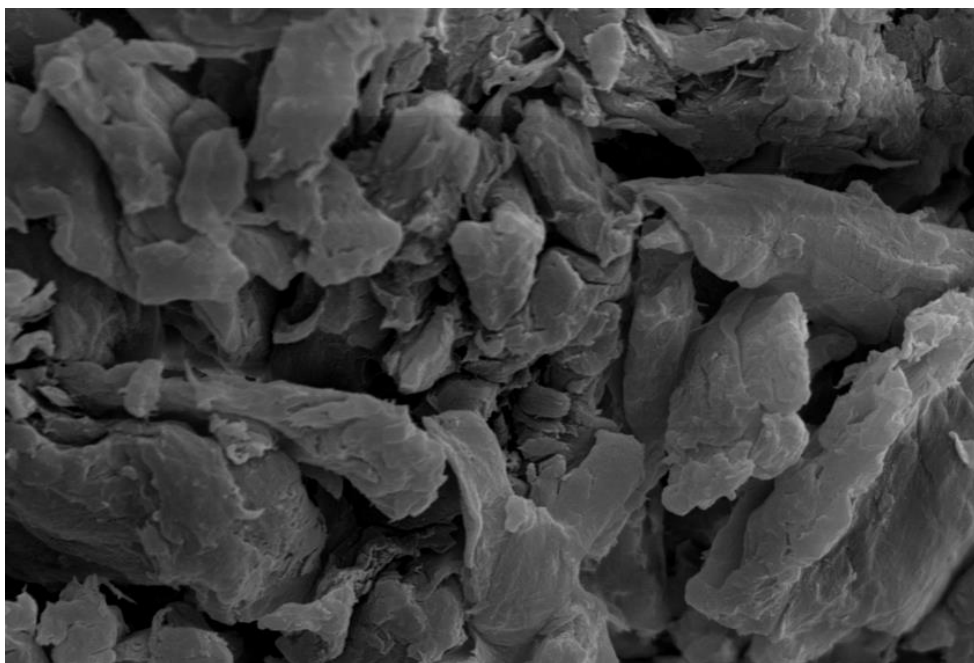


Figure 1.2: SEM image of cellulose nanocrystals

1.3.2.2 Bacterial Nanocellulose

Bacterial nanocellulose is produced by cultivating bacteria like the *Gluconoacetobacter xylinus* family²³, *Agrobacterium*, *Pseudomonas*, *Rhizobium*, and *Sarcina*,²⁶ for some days in an aqueous culture media with glucose, phosphate, carbon, and nitrogen sources. Cultivation conditions, nutrient source, oxygen ratio, bacterial strain type, incubation time, and cultivation in a bioreactor, for instance, regulate the properties and structures of BNC tubes.²⁷

Gluconacetobacter xylinus CGMCC No. 1186 has been incubated with either fructose or glucose in silicone tube bioreactors. The employment of fructose improved the nanocellulose yield.

The change of the reactor alters the amount of dissolved oxygen and therefore the structure of the obtained tubes.

The cell membrane of the bacteria applied to produce BNC is made of a cellulosic network arrangement of ribbon-shaped fibrils that are not even 100 nm wide, assembled from bunch of much finer nanofibrils,²⁸ 2–4 nm in diameter. The fibrils are rather straight and continuous and have little polydispersity in terms of their dimensions. The high crystallinity (84–89%) of the bundles provides outstanding intrinsic properties.²⁹

Next to an elastic modulus of 78 GPa, BNC is demonstrated to have high water retention capacity and a molecular weight up to 8000 Da,³⁰ allowing the possibility

to use BNCs as scaffold with attractive magnetic, optical, and mechanical properties thanks to their low apparent density and elevate surface area. ³¹

BNC joins high physical strength, a greatly hydrophilic surface, and an interpenetrating structure, endorsing this material for biomedical applications. ³²

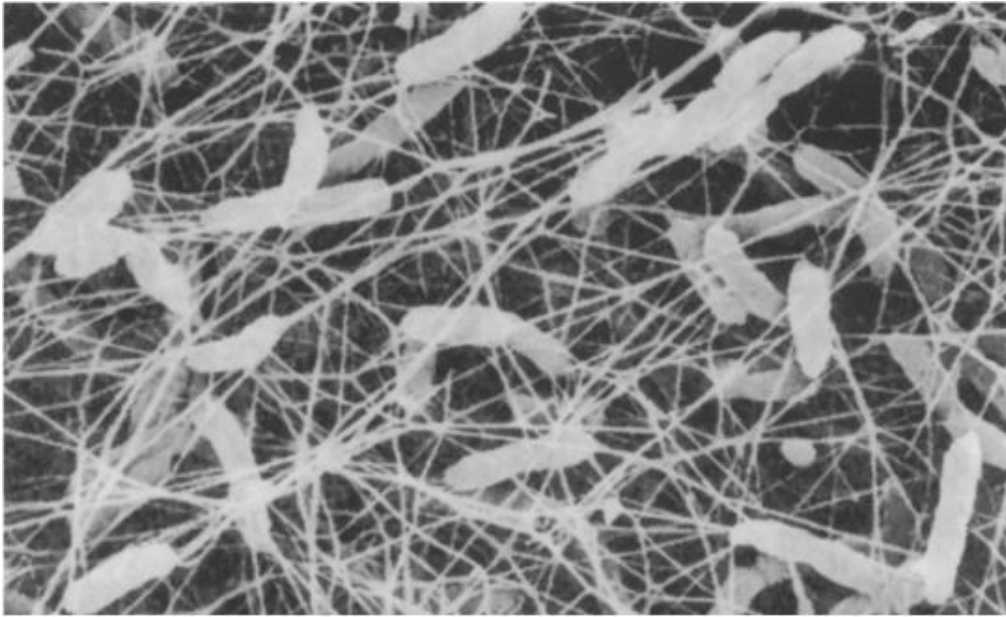


Figure 1.3: SEM of bacteria producing a bacterial cellulose pellicle, ²⁸.

1.3.2.3 Cellulose Nanofibers

CNF is a bundle of extended cellulose nanofibers. The cellulose chains are entangled and elastic with a large surface area. CNFs are made of many amorphous regions, with soft, long chains of widths varying from ten to a few hundred nanometers and lengths on the micrometer scale. ³³

Among various approaches for NCs isolation, *i.e.* chemical, biological and mechanical, the latter is the most employed. High pressure homogenization, cryocrushing, and grinding are some of the mechanical treatments used to extract cellulose nanofibers. ³⁴ Similar to CNCs, the fundamental properties of CNFs also vary according to the raw material and the *ad hoc* extraction process employed. Due to the different possibility of treatments, the final nanofiber can have a wide variability in its shape, degree of fibrillation, morphology and properties. This allows to tailor the process in agreement with the required characteristics of the desired product.

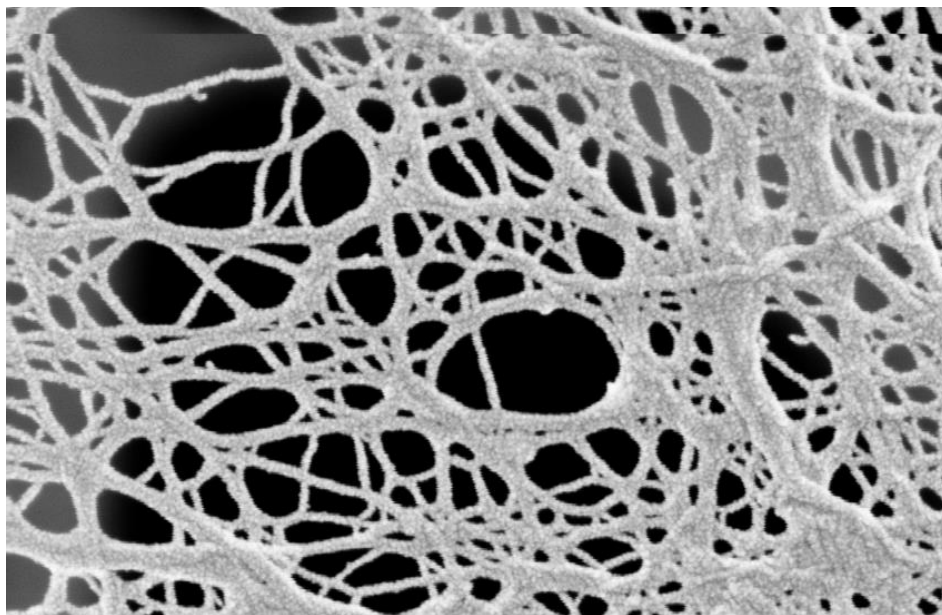


Figure 1.4: SEM image of cellulose nanofibers taken from ³⁵

1.3.3 Properties

Nanocellulose can be defined as cellulose particles with at least one dimension smaller than 100 nm. They originate from crystalline cellulose microfibrillar structures and possess high strengths, high elastic moduli and large surface areas, they are largely available, nontoxic, biodegradable and biocompatible. [10] Nanocellulose, produced by environmentally friendly means, can therefore combine outstanding properties with small or negligible carbon footprints compared with inorganic and petroleum-based nanomaterials. The efficient production of wood cellulose fibers using modern pulping and bleaching technologies on an industrial scale can yield an inexpensive raw material for nanocellulose production costing 60 cents per dry kg. ³⁷

Thanks to its versatility, NC can be applied in many fields, *i.e.* biomedics, reinforcement of polymeric matrix, packaging, films, paper, microelectronics, optics, catalysis, as flame retardant, energetical and environmental.

The reinforcement effect of NC can be characterized by its properties in both ordered (crystalline) and disordered (amorphous) regions of the nanoparticles. NC composites then provide better dispersion, high surface area, promising wettability, improved interfacial bonding, and homogenous composites materials. The hydrophilicity is due to the abundance of hydroxyl group, which gives NC composites biodegradability and green characteristics.

This means that nanomaterials of such nature could play a significant role in the nanotechnology research domain. The typical extraction methods from biomass sources are mechanical, chemical and enzymatic. ^{38,39}

NCs possess many desirable properties with respect to conventional materials, which are:

1. Their production does not require high-temperature processes resulting in low emission of carbon dioxide.
2. They are more sustainable and environmentally friendly compared to their petroleum-based polymer counterparts.
3. Moreover, the increased surface area-to-volume ratio and quantum size effects of CNs produced from cellulosic sources increase the amount of adsorption sites and offer the possibility of tuning the surface properties of CNs through molecular modification, allowing them to be tailored according to the specific
4. They have good mechanical strength and dispersibility in water, making them ideal for use in filtration membranes and as flocculants, respectively.

In cellulose fibrils, there are some regions where the cellulose chains are arranged into highly ordered structure (crystallites), and disordered regions (amorphous), from which nanometric matters can be extracted with suitable approaches. ^{40,41} The released nanoparticles show diameters of 5 to 30 nm and lengths of 100 to 500 nm in the case of nanocrystals, or lengths of 100 nm to several micrometers if nanofibers.

Table 1.1: properties and applications of Nanocellulose ⁴²

Features of Nanocellulose	Properties	List of Applications
Cellulose Nanocrystal (CNC)	<ul style="list-style-type: none"> - High strength - High aspect ratio - Low toxicity - Biodegradability - Chiral nematic structure 	<ul style="list-style-type: none"> - Reinforcing material in polymeric matrix - Paper reinforcement - Bio applications - Controlled drug delivery - Tissue engineering scaffold - Cosmetic application - Food packaging - Rheology modifier - Bioimaging application - Electronic applications
Cellulose Nanofiber (CNF)	<ul style="list-style-type: none"> - High tensile strength - Flexural properties - Good dispersion - Mimic to real cellulose material 	<ul style="list-style-type: none"> - Interior automotive part - Antireactive films - Substrates to determine cellulase activity
Bacterial Nanocellulose (BCN)	<ul style="list-style-type: none"> - Non-toxic to cells - Highly pure - High modulus high crystalline structure - High hydrophilicity - Ultrafine network 	<ul style="list-style-type: none"> - Biomedical applications - Tissue engineering scaffold - Artificial skins - Optical transparent film - Diaphragms in speakers and headsets - Filtration membrane in water treatment - Binder in paper production - Fire-retarding properties in synthetic paper

Morphology, physical properties and dimension of nanocellulose change significantly with the different natural source and extraction process. Mechanical properties of nanocellulose are better than their starting biomass due to a more uniform morphological structure. The average modulus of nanocellulose is 100 GPa, much higher than the base cellulosic materials. ⁴³ Nanocellulose has both cellulose I (native cellulose) and cellulose II (regenerated cellulose fibers). ⁴⁴ Thermal degradation property of nanocellulose depends on extraction method and resources. The enhanced thermal stability of nanocellulosic materials compared to their source cellulose is due to their higher crystallinity, flexible structure and removal of low

thermal stable lignin materials. ⁴⁵ CNs-based adsorbents are ideal to remove dyes, heavy metal ions, pharmaceuticals and several other contaminants in wastewater. ⁴⁶

1.3.3.1 Adsorption/decontamination

Several properties of NC make them excellent candidates for use in water/wastewater treatment processes, ⁴⁶ some of them are:

- a) Surface area: the high surface area will provide more active sites for the adsorption of contaminants, hence the removal capacity of many different types of contaminant is improved.
- b) Aspect ratio: the high aspect ratio of NCs makes the formation of percolated (for CNCs) and entangled (for CNFs) networks easier at low concentrations making them effective flocculating agents.
- c) Surface functionality: the high density of surface hydroxyl groups facilitates the functionalization of NCs with a wide variety of functional groups (sulfate ester, carboxyl, amine, and aldehyde groups), small molecules and nanoparticles or grafting with polymers. This alluring property of NCs is advantageous with respect to their applications across various water/wastewater treatment processes, such as adsorption, absorption, membrane filtration, flocculation, catalytic degradation and disinfection.
- d) Mechanical strength: the high mechanical strength and crystallinity of NCs increase the stiffness and chemical resistance of NC-incorporated adsorbents and membranes for use in a wide range of operating conditions. The high surface tension and stability of NCs in water improve the wetting characteristics and reduce the bio-fouling of the NC incorporated adsorbents and membranes.
- e) Availability: the supply of NCs for commercial applications is endless compared to other nanomaterials as many organizations and companies, have the capability of producing NCs in large quantities.
- f) Colloidal stability: the colloidal stability and aggregation of NCs will greatly affect the efficacy and applicability of NCs in water/wastewater treatment processes.

Adsorption is a widely utilized technique for the removal of contaminants in water. It is a surface phenomenon, where contaminants (adsorbates) are concentrated at the solid surface (adsorbent) from its surrounding liquid medium. The preferential accumulation of adsorbates on the adsorbent surface is due to forces of attraction. If these forces are weak, such as Van der Waals ones, it is called physisorption, when the adsorbate and adsorbent form chemical bonds, is chemisorption. The latter may

also occur due to other types of interactions, such as electrostatic attractions, π - π interactions etc. [16],[17] Among many other methods employed, adsorption is a water treatment process that provides unfailing results in delivering high quality treated water when implemented using a properly designed system.

Heavy metals constitute a group of contaminants that are considered a serious threat to humans and the environment because of their toxic nature and other adverse effects. Many of these heavy metals are found in industrial effluents originating from anthropological activities. They are not biodegradable, so tend to accumulate in the food chain. Thus, it is essential to develop adsorbents to remove these toxic contaminants from wastewater. Recent studies have shown that CN-based adsorbents may provide the removal of these heavy metal ions, thanks to the high surface area of CNs and the numerous functionalities introduced onto their surface empower CN-based adsorbents to remove various heavy metal ions present in water. ⁴⁶

1.3.4 Production Methods

Before the mechanical, chemical or enzymatic treatment, alkali and bleaching pretreatments are required. The primary purpose of pretreatment is to remove certain quantity of lignin, hemicellulose, wax and oils covering the outer surface of the fiber cell wall. Alkali treatments depolymerise the native cellulose structure, defibrillates the outer cellulose microfibrils and exposes short length crystallites. Then, bleaching treatment is necessary in order to remove the cementing material completely from the fiber. ⁴⁹ Apart from cellulose nanocrystal and cellulose nanofibers, some strains of bacteria can produce nano size BNC if in favorable conditions.

1.3.4.1 Mechanical methods

Depolymerization of lignin and hydrolyzation of hemicellulose can be obtained through pretreatment at high temperature steam explosion with alkali. Then, lignin is quickly oxidized by chlorine, that accelerate the degradation of lignin. Formation of various groups such as hydroxyl, carbonyl and carboxylic groups makes the lignin solubilization in the alkaline medium easier. Acid coupled steam treatment aids to disintegrate fibrils leading to the formation of the nanocellulose.⁵⁰ Before the mechanical treatment, pretreatments such as grinding, acid hydrolysis, decrystallization and derivatization are used. Extracted cellulose has spherical shape

with diameter of less than 200 nm.⁵¹ Nanocellulose can be derived from the cellulose-derived biomass by high pressure homogenization. The biomass could be suspended using high speed stirring coupled with ultrasonication treatment prior to the high-pressure homogenization.⁵² Ionic liquid can be used to treat the lignocellulosic biomass prior to the mechanical treatment. The ionic liquid permeates through the microstructure of cellulose and subsequently, attacks the hydrogen bonds between cellulose molecules. The high-pressure homogenization breaks the bonds, both inter and intra molecular, therefore, nanocellulose is disintegrated. Extracted nanocellulose has a width of 10–20 nm.

1.3.4.2 Bacterial method

Nanocellulose obtained by using bacterial method has similar chemical structure as with nanocellulose extracted from the lignocellulosic biomass by following chemical and mechanical methods. In addition to this, ultrafine nanofiber network formed by an appropriate culture medium exhibits unique properties e.g. high purity, uniform morphology, good water absorption capacity, excellent mechanical properties and flexibility.⁵³ Biomaterial grade BNC could be synthesized by aerobic cultivation of the bacterium *Gluconacetobacter xylinus* (synonym *Komagataeibacter xylinus*) in a glucose enriched medium.^{54,55}

1.3.4.3 Chemomechanical Treatment (Kraft Pulping)

Chemical pretreatments aim to remove non-cellulosic materials (waxes, ashes, lignin, pectin, and hemicellulose).

Hemicellulose is a random, amorphous material dissolved from the lignin structure by breaking the bonds between the carbohydrates and lignin with acid–alkaline pretreatment.⁵⁶ A pretreatment can reduce the energy consumed by mechanical processing of an order of magnitude (from between 20 000 and 30 000 kWh/ton to 1000 kWh/ton).⁵⁷ Alkaline treatment targets the removal of the lignin content and the degradation of hemicelluloses, though hemicellulose is later completely removed via hydrolysis. Reaction conditions should be controlled, to prevent cellulose degradation.

Once cellulose is recovered, acid hydrolysis is without any doubt the most common chemical treatment used to obtain nanocellulose crystals. The hydronium ions penetrate the amorphous regions of cellulose chains and hydrolytically cut glycosidic bonds, releasing individual crystalline cellulose nanoparticles. Acid hydrolysis is

usually evaded for the isolation of NFCs since it may destroy the amorphous regions leading to CNCs upon homogenization/ultrasonication.

Acid hydrolysis is the method used industrially⁵⁸, but the major drawback is the huge amount of chemical wastes, even when efficient recycling strategies are used.

Otherwise, nanocellulose can be recovered using oxidative processes. Cellulose may be oxidized with TEMPO radicals before the mechanical treatment.¹⁴

1.3.4.4 Chemical method

Between the removal of hemicellulose and the acid hydrolysis, the cellulosic source can be chemically treated with for example dimethyl sulfoxide to swell the polymeric matrix, allowing an easier diffusion of the acid within the domain structure of lignocellulosic biomass and the disruption of the nanowhisker.⁵⁹ In this kind of treatment, the yield of NC is strictly correlated to the content of lignocellulosic biomass and to the operation conditions, *i.e.* acid concentration, time and temperature. To get maximum yield and to preserve the morphology of the starting material the optimization of experimental parameters is paramount.⁶⁰ Yield and nano dimension are inversely proportional to acid treatment time of cellulosic biomass.⁶¹ A green approach to prepare nanocellulose from the lignocellulosic biomass could be the use of liquid catalyts. In fact, the ionic liquid floods through the microstructure of cellulose with a following attack of the hydrogen bonds between cellulose molecules. Ionic liquid-based catalyts demonstrate several advantages such as wide range of electrochemical stability, good electrical conductivity, high ionic mobility, selective dissolution properties to many organic and inorganic substances as well as excellent chemical and thermal stabilities.⁶² Nanocellulose crafted from bleached hardwood craft pulp oxidized by 2,2,6,6-tetramethylpiperidine-1-oxyl (TEMPO) is strongly affected by ultrasound, since the nanofibrils prepared with ultrasound assisted process is thinner, includes more carboxylic functionality, higher degree of fibrillation and yield.⁶³⁻⁶⁶

1.4 Synthesis of Co-Polymeric Nanosponges Systems with TEMPO-Oxidized Cellulose Nanofibers and branched Polyethyleneimine

12

Over the last two decades, scientists are investigating the properties of this class of oxidating catalysts. The ability to perform a selective oxidation of sugars hydroxyl groups to carboxylic and/or aldehyde moieties, the shorter times, gentler and well controlled reaction conditions makes the oxidation of polysaccharides with TEMPO very appealing. ⁶⁷

There are further advantages compared with classic oxidation catalysts, which are:

- high reaction rate;
- high conversion ratio;
- high selectivity;
- partial decrease of molecular weight of polysaccharides during the process (if controlled);
- low cost as co-oxidant.

Moreover, KBr or NaBr can be added to improve the rate of oxidation reaction. ⁶⁸

Cellulose and its nanofiber form are perhaps the most investigated polysaccharides for TEMPO oxidation.

Preparing TOCNFs for the creation of new bio-based applications is one possible solution to address the challenge of dealing with the valorization of byproducts/wastes from paper and wood industry. Wood cellulose material can be easily converted to individual micro- and nanofibers of different lengths, sizes and diameters. These characteristics are involved in TEMPO chemistry and can lead to various TOCNFs. ¹⁴

Thanks to their specific chemical, mechanical and physical properties, TONCFs have recently found several interesting applications, spacing from biomedicine, energy, sensing to environmental remediation. ¹⁴ They can be used as additives in already existing formulations, nanostructured in aero- and hydrogels and films for sophisticated applications. This versatility is due to the oxidative process, that implies the selective introduction of carboxylic moieties in the backbone of the polysaccharide.

Carboxylic groups bring at least three different contributions:

1. they promote the defibrillation of cellulose at basic pH, since the negatively charged cellulose chains undergo electrostatic repulsion;
2. they can take part in the cross-linking process of the fibrils, causing intermolecular hydrogen bonding with other chains of the polymer, or promoting ionic electrostatic interaction that lead to the formation of composites or favoring the formation of covalent bonds;
3. they can behave as hook for the modification of the carbohydrate via grafting with active molecules, broadening the chemo-physical properties of the materials. ⁶⁹

TOCNFs, when employed as green additives, are mainly used for the modulation of the mechanical properties of the finished material.

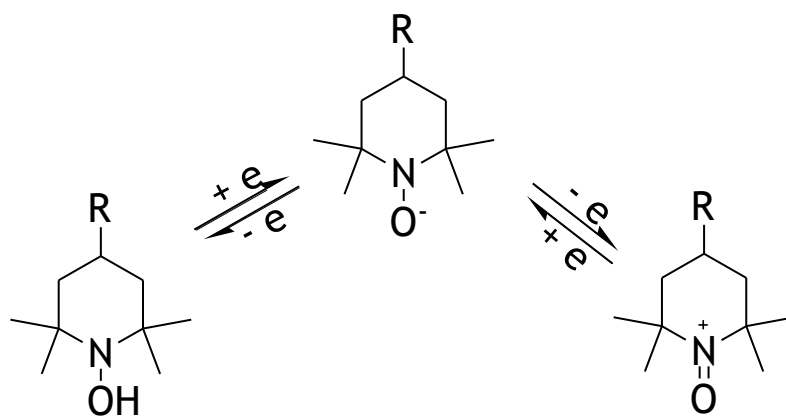
The inclusion of TOCNFs in composites is maybe the most common use for these polymers, with many researches operating to find advanced high-performing materials. The negatively charged carboxylates formed on the skeleton of the fibrils advise the chance to prepare micro- and nano-gels by ionic/ionic interactions with cations. ⁷⁰

Hybrid organic composites offer more versatility for the design of novel materials with increased properties. When negatively charged TONCFs are combined with single-walled carbon nano-tubes or carbon dots, transparent and printable films are gained, obtaining flexible materials highly conductive in the first case and strongly luminescent (under UV excitation) in the second one. ^{71,72}

The abundancy of carboxylic groups on the skeleton of the structure suggested the opportunity to use poly-amine polymers like branched-polyethyleneimine (bPEI) for an effective ionic/ionic interaction and/or cross-linking, allowing to enlarge the functionalization possibilities even on the amino groups.

1.4.1.1 Properties and applications

2,2,6,6-Tetramethylpiperidine-1-oxyl radical (TEMPO) is a secondary amine nitrogen oxide (*i.e.*, a nitroxyl radical) with an unpaired electron delocalized between the N and O atoms.



Scheme 1.1: Redox reaction of nitroxide radical

This cyclic nitroxyl radical is among a redox series of compounds (hydroxylamine, nitrosonium ion, TEMPO) coming from electron transfer. During the oxidation of sugars, the nitrosonium ion deriving from TEMPO is reduced into hydroxylamine when weakly alkaline conditions are applied. For the regeneration of TEMPO, the nitrosonium ion reacts with the hydroxylamine and the catalyst is continuously regenerated in the reaction mixture by a primary oxidant, usually sodium hypochlorite. Following this mechanism, primary alcohol oxidation occurs with a high degree of selectivity.⁶⁷

The use of non-metal oxidation catalysts, such as TEMPO and its derivatives, have more and more increasing interest for many reasons:

- several of their derivatives are cheap and commercially available,
- these catalysts are user-friendly under aqueous system reaction conditions,
- these catalysts can react with all common oxidizing agents to produce oxoammonium salt,
- these catalysts are very resistant to auto-oxidation.⁷³

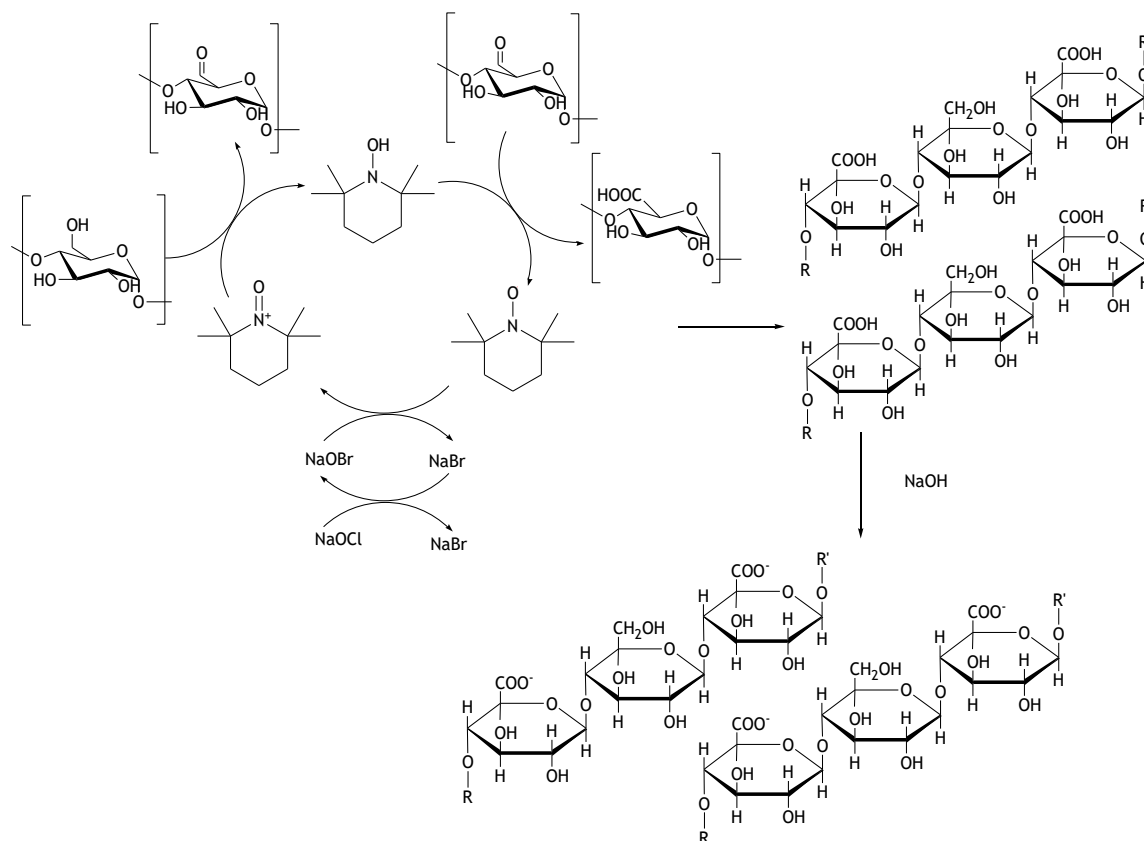
For these reasons, TEMPO radical and its derivatives are usually employed as highly regio-selective oxidation reactants to industrially produce specific synthesis of chemical, cosmetics, pharmaceuticals, flavors, and fragrances.²⁵

1.4.1.2 Structure and mechanism

Cellulose in its nanofibrillated form is more effective for the introduction of functional groups onto its structure, since it is difficult to access to the hydroxyl

moieties of the bulk because of the strong hydrogen bonds in the native form. Nanofibrils, on the other hand, have higher chemical accessibility, so they are easily functionalized.⁷⁴ Nevertheless, the nanofibrillation of cellulose is not a minor task, because of the above mentioned hydrogen bonds, which make the process very energy intensive, provoking structural damage to the fibrils.¹⁴ The use of chemicals, such as TEMPO, for nanofibrillation prevents it. The introduction of carboxylic moieties during the oxidation of cellulose eases the defibrillation of cellulose in water because of the electrostatic repulsion of the single fibrils at basic pH.⁶⁹

One of the most employed methods to obtain CNFs through oxidation is the already mentioned TEMPO/KBr/NaClO system. In fact, TEMPO favors the selective conversion of primary alcohols on the C6 position of the glucose units to the matching carboxylic groups.¹⁴ These are deprotonated under basic conditions, favoring the separation of the fibrils by charge repulsion, as can be seen in Figure 5.



Scheme 1.2: Mechanism of cellulose TEMPO-oxidation and highlight of the separation of the fibrils under alkaline medium. (⁷⁵– modified).

TOCNFs show intrinsic adsorbent properties due to the electrostatic attraction effects of carboxylate moieties.⁷⁴ Anyway, the adsorption performances are not excellent, and the fibrils are easily spread in water. That is why a reticulation process is suggested with the aim to achieve a stable material with better adsorption properties.

Performing a reticulation of TONCFs with branched polyethyleneimine (bPEI) brings to amide bonds formation between the primary amine of bPEI and the carboxylic groups of TOCNFs. Hence, the nanofibers are cross-linked with the polyamine, obtaining a highly porous, sponge-like material.

1.5 Nanosponges

Water-stable and effective sorbent material can be prepared through a thermal procedure. Furthermore, the amine moieties now brought accelerate the adsorption of cations and polar organic substances, endorsing this material for water remediation from heavy metals and organic pollutants. ^{74,76}

To guarantee the cross-linking of the fibrils and accomplish a porous structure, two steps are crucial: freeze-drying for the removal of bulk water employed during the preparation (to avoid the alteration of the three-dimensional structure); thermal treatment, to enhance the reticulation process between $-NH_2$ of bPEI and $-COOH$ of the oxidized cellulose. ^{76,77}

Many application of likewise obtain matters are found in literature, such as drug delivery, ⁷⁷ sensing in solution,⁷⁸ water remediation through adsorption of organic or inorganic pollutants. ^{74,76}

1.5.1 State of the art of the material

Over the last years, the research group where I did my research activity has developed this innovative material, improving its formulation to make it this nano-sorbent material the more eco-safety as possible.

The upstream reasonings to reach the goals were:

- The use of proper building blocks, better if they are renewable and sustainable derivatives
- The possibility to work with nano-structured microdimensional scaffold, in order to keep the goodness of the nano-scale but erasing the issues of nano-size.
- A constant check of the eco-design from the beginning of the study, to be able to apply *ad hoc* modifications.

The first formulation involved a TOCNFs (3 % w/v) in a water solution of bPEI (25 kDa), with a TOCNFs-bPEI ratio 1 : 2. This ratio proved to ensure a good compromise among the mechanical stability, shape recovery capability in both wet and dry conditions and porous structure.

The solution then underwent the freezing and thermal protocols to form xerogels. The material was grinded to obtain a fine powder, preventing the risk of diffusional limitations and so enhancing the adsorption capabilities.

Unfortunately, ecosafety tests proved that the artificial sea water used for the assay provoked a great inhibition effect on the biota employed, making the material unsuitable for environmental remediation. It was hypothesized that this effect was due to the release of toxic compounds present in the nanosponge. Hence, a major focus on bPEI was necessary. bPEI is fundamental for the reticulation and the heavy metal ions adsorption, but it is also known to have a cytotoxic effect. It was thought to add a new -COOH carrier, such as citric acid (CA) to enhance the extent of imidic bonds in the material in order to decrease the bPEI release. A new formulation was then proposed, which is essentially the same as the original one, but with the addition of 18 % in mmol of CA for each mmol of NH_2 on bPEI. The introduction of the acid allowed also to avoid the use of more severe reaction conditions. In fact, only a small portion of cellulose can be successfully oxidized, and with large excess of oxidant. This new component will bond with the primary amines of bPEI, increasing the stability and the mechanical-chemical properties of the material.⁷⁷ Moreover, the employment of CA permitted to reduce the ratio between TOCNFs and bPEI to 1 : 1 w/w, since the branched polymer was better fixed. Another improvement was the purification phase. The washing was no longer performed with methanol but with water in order to prevent the possible hydrolysis of amide bonds. In the following Figures, a schematic representation of the preparation of the material and when the addition of citric acid takes place.

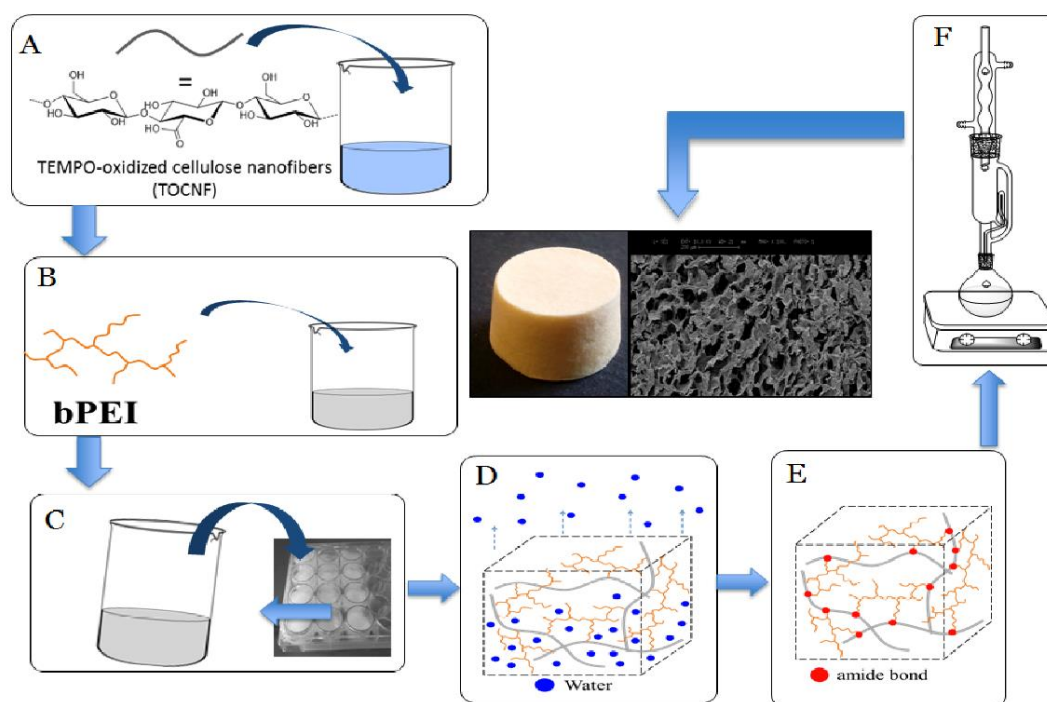


Figure 1.5 : schematic procedure for the preparation of the nanosponges: A) TOCNFs dispersion in water at 2.5% w/v concentration and sonication to obtain a homogeneous dispersion; B) bPEI addition to the solution; C) Fast freezing of the solution in molds; D) Freeze-drying for bulk water; thermal treatment for enhancing amidation; E) Thermal treatment for enhancing amidation; F) Washing of the material to remove the non-reticulated components; Material ready for the metal adsorption essay;

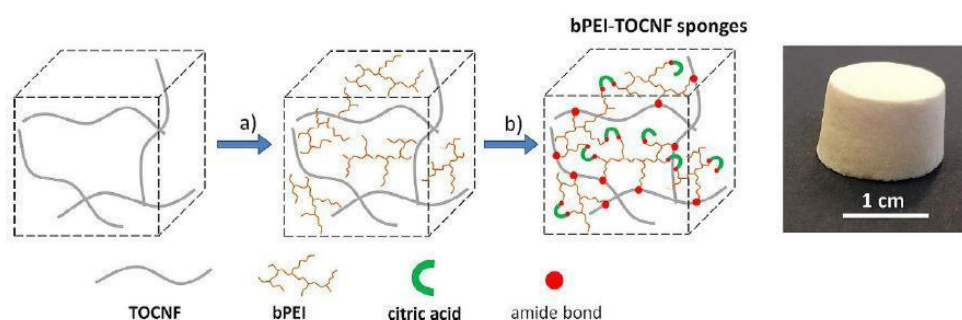


Figure 1.6: Preparation of bPEI-TOCNF sponges with citric acid ⁷⁷

The materials described in ^{76,77} were totally characterized with Fourier-transform infrared (FTIR) and ¹³C CP-MAS NMR spectroscopy, scanning electron microscopy (SEM), micro-computed tomography (μ -CT) and elemental analysis.

In the next Figure, SEM images at different magnification of NS with citric acid, showing the improvement of reticulation.

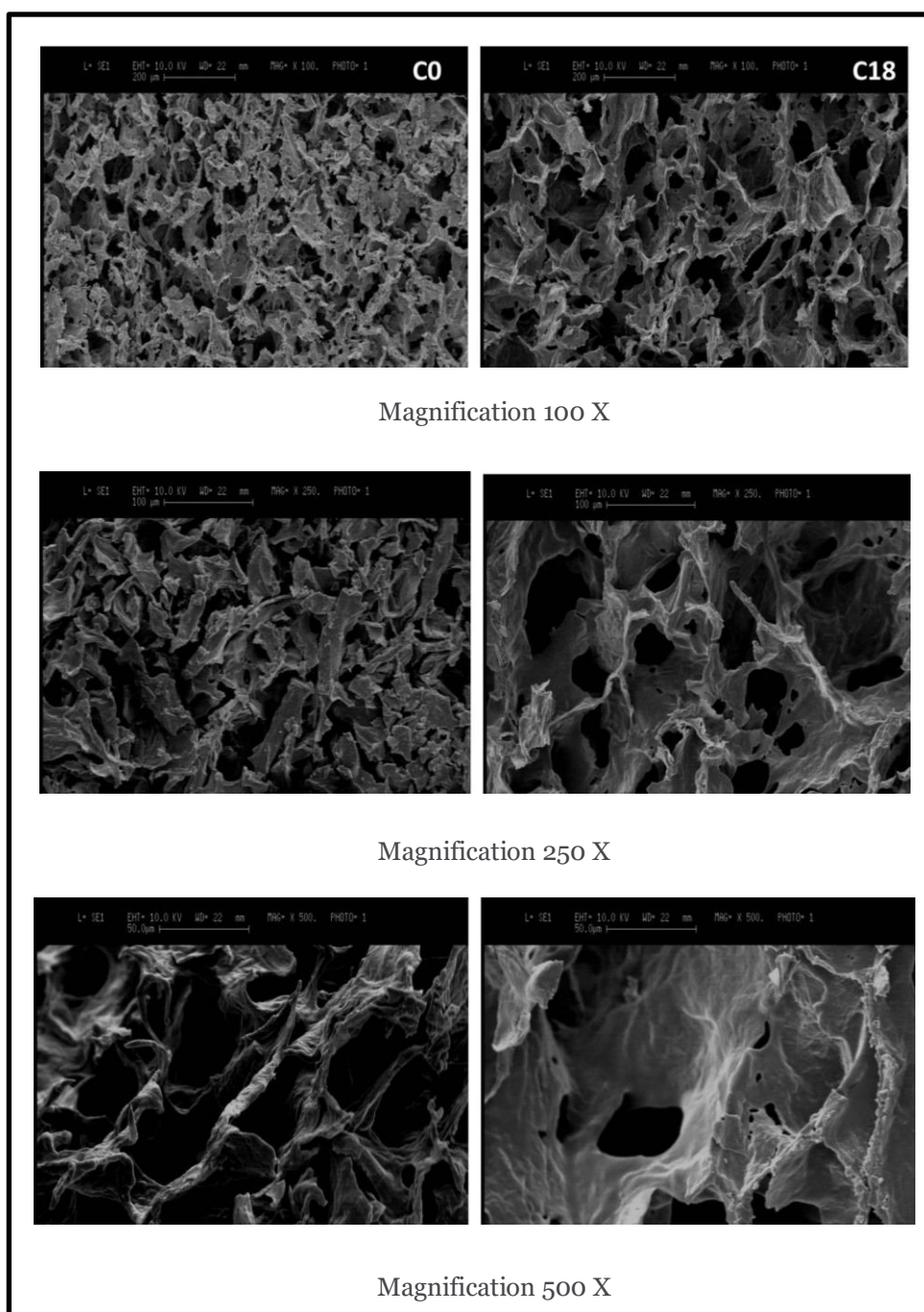


Figure 1.7: SEM images of cross section of bPEI-TONCF 2:1 (left side) and bPEI-TONCF-CA 2:1-18 (right side) nanosponges with increased magnification. The presence of citric acid seems to improve the development of sheet-like internal porous structure.

1.5.2 Adsorption

To test the adsorption properties of the nanosponges, the group in which I did my activity used MilliQ water and artificial sea water (ASW), as reported in ⁷⁹.

The tests were performed for each formulation, outputting improved results along with the improvement of the formulation.

1.5.3.1 Adsorption tests for the first formulation

At first, adsorption experiments with mono contaminated MilliQ water solutions were made. Weight for weight, the powder proved to have better decontamination efficiency with respect to the sponge, as shown in Figure 12, taken from ⁷⁹.

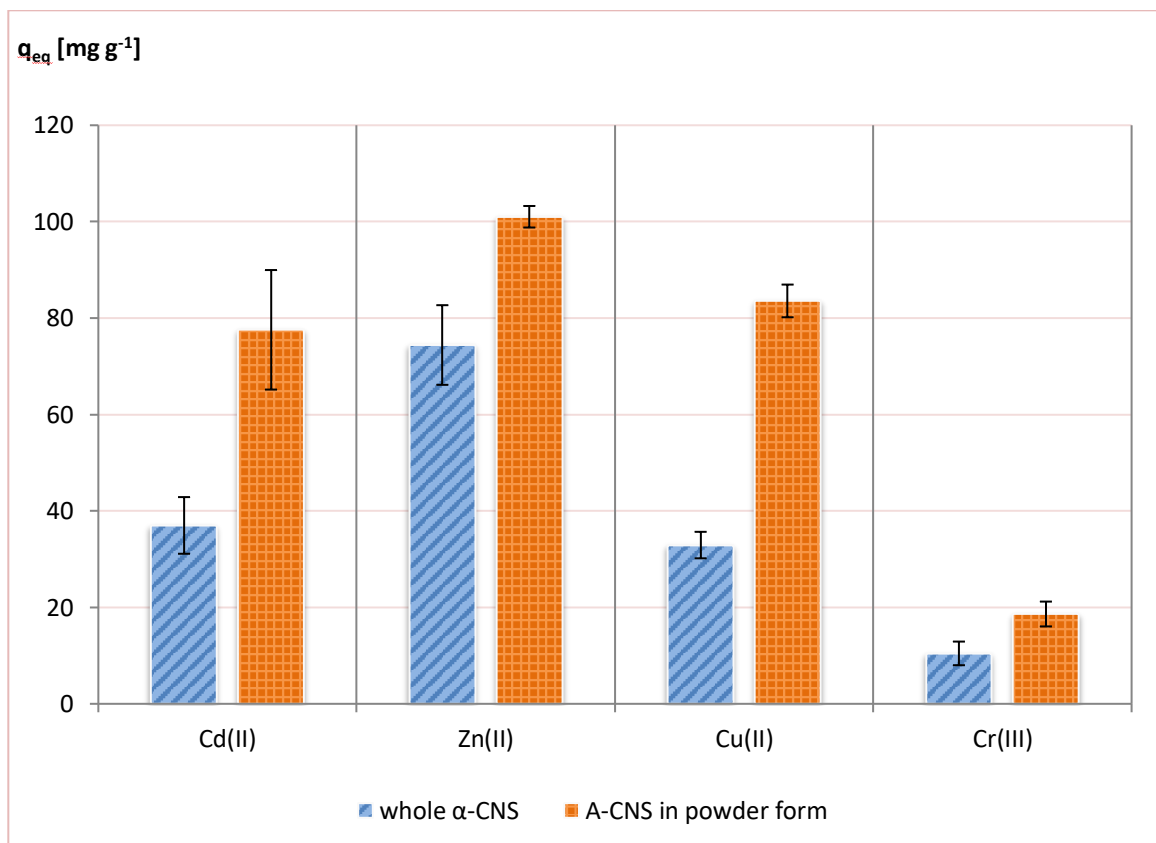


Figure 1.8: comparison between α -CNS (blue bars) and A-CNS (orange bars) adsorption capacity at the equilibrium (q).

Figure 13 shows how the metal ions diffusion in the material is not uniform, meaning that diffusional kinetic limitation of the solution in the sample were still present, in which the Sem-EDX image prove a non-uniform distribution of the metal ions in the

material. ⁷⁹ In both cases, the green dots are the metal ions present in the mono contaminated MilliQ water solution.

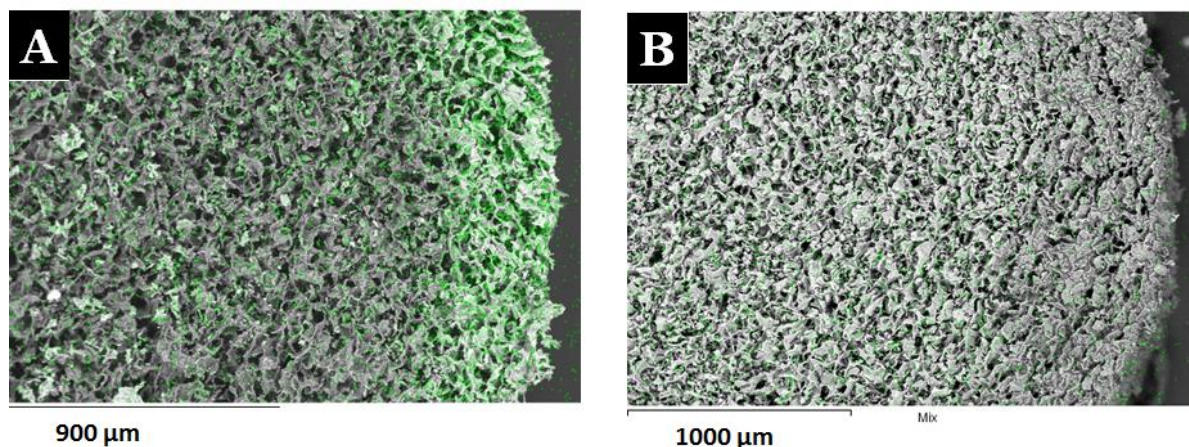


Figure 1.9: SEM-EDX image of a-CNS cross section. A) Cd(II) adsorption from 50 ppm MilliQ water solution. B) Zn(II) adsorption from 50 ppm MilliQ water solution.

The adsorption tests with ASW proved to be better than the ones in MilliQ water, probably due to a change in the pH of the solution. The weakly basic pH blocks the protonation of NH_2 groups, so they can fulfil their chelation purpose regarding the transition metal ions they must capture.

1.5.3.2 Adsorption tests for the second formulation

The adsorption tests performed on the second type of nanosponges (B-CNS, with CA) were essentially the same as the former case. The removal efficiency of the new set of material did not show significant changes, meaning that the addition of CA in the formulation did not affect the goodness of the original adsorbing performance, but it only provided enhanced stability of the sorbent material and the possibility to decrease the amount of toxic polymer in the synthesis of the sponges.

To prove that the new formulation would not damage its remediation environment, A-CNS and B-CNS were used to decontaminate samples of ASW at different dilution, which was employed to conduct a growth inhibition assay of a probe marine biota (*D. tertiolecta*). The results were very promising, even if a small quantity of

bPEI would still detach from the material while conditioning ASW, causing little growth inhibition of the organic matter. Anyway, since the actual chemistry of sea water is more complex than the standard one, it is reasonable to think that the little amount of bPEI released could be complexed by organic organisms, organic and inorganic colloids and particulate matter existing in the marine environment, decreasing the toxic risk.

Unfortunately, *in vivo* exposure tests performed on mussels showed how B-CNS cannot be considered an eco-safe material. ASW treated with this batch of nanosponge affected negatively the lysosomal membrane stability (LMS) of the mussels used for the assay. This is probably due to a still too high bPEI release.

It was then attempted the same kind of tests with NCs with half the content of bPEI with respect to the previous one (C-CNS). Not only most probe organisms were no longer affected by the newly conditioned water, but also the adsorption efficiency increased. In fact, using a Langmuir model approach (non-linear regression) for the interpolation of the data, it was possible to see how the initial slope of the isotherm regarding C-CNS is higher than the one of A-CNS.

So, the adsorption is faster, since more of the 90% of the pollutant equilibrium value were entrapped within two hours of contact time.⁷⁹ The new material was also tested with typical concentrations of bilge water solution, and the removal of the heavy metal ions was more of the 90%.

Apart from the above shown outstanding adsorption properties of this nanomaterial, the presence of both carboxylic and amino moieties allows the possibility to functionalize individually each component, broadening the already vast application fields of this innovative and versatile material. My activity consisted in the selective grafting of both functional groups with fluorophores, to be able to follow the environmental destiny equally of cellulose and bPEI.

2. Results and Discussion

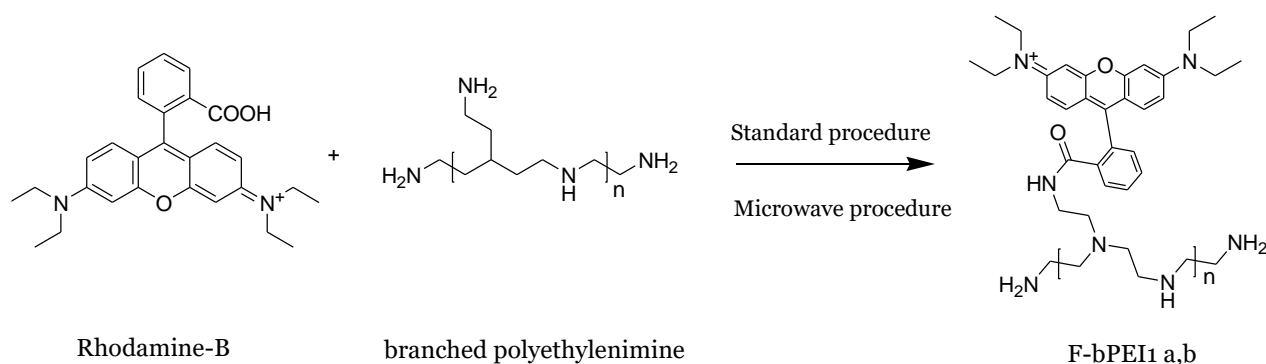
The NS described in the introduction have already proved their sorbent capability in the removal of pollutants ions, even when tested in solutions with a concentration of heavy metal ions comparable to the ones in the real conditions of application. The ecotoxicological tests done on the material demonstrated that one of the polymers forming the composite material (bPEI) is toxic, arising problems for the potential bioaccumulation in the marine environment, with the associated risks for its inhabitants. Hence, it was thought to functionalize selectively the material with fluorescent probes in order to follow the destiny of both polymeric components (nanocellulose and bPEI), taking advantage of the different functional moieties on their backbones (-COOH for TOCNFs and -NH₂ for bPEI). It is still not completely clear if the two polymers have distinct or shared fates. The fluorophores were chosen for their different excitation and emission wavelengths, so that it could be possible to monitor the behavior of the two polymers individually. The grafting of the fluorophores was performed according to both standard procedures and innovative ones by using a microwave reactor, choosing the best pathway for each synthetic step. The final NS were prepared with different ratios of functionalized and non-functionalized bPEI. In this way it was possible to understand and define the right concentration of sensor to be put into the material in order to be harmless for the marine biota. To accomplish this task two different and complementary analysis were required: the UV spectroscopy and ecotoxicological tests. The former was indispensable to determine the effective grafting degree on the polymer, in order to be able to quantify the amount of fluorophore present in each NS, the latter to define which one among the different dilutions was suitable for our purpose.

2.1 Preparation of the materials

For some of the compounds here reported, different synthetic pathways were used: the traditional strategy found in the literature and the microwave reactor. The latter proved to be more efficient, either in the yield of the products, in saving of the now needless co-reactants and, finally, in the reaction conditions. The possibility to push both temperature and pressure at the most suitable values for the specifically reaction allowed a significant increase in the purity of the product, and this brought to faster and easier operations downstream, such as the purification of the crude product. Moreover, the microwave reactor had two other advantages: the multistep reactions

took place in just one-pot and, more important, the reaction time decreased considerably, permitting to change the reaction conditions (both physical and chemical). In this way, it was almost immediate to evaluate the most appropriate improvements to be done.

2.1.1 F-bPEI1a and F-bPEI1b

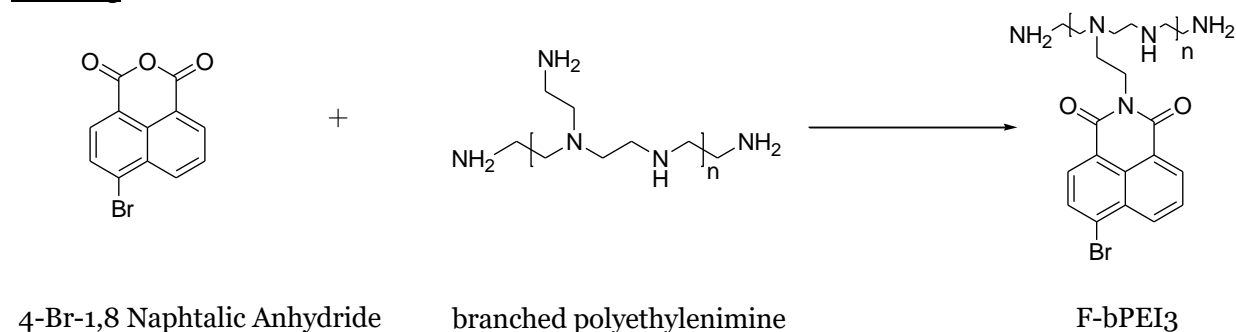


Scheme 2.2.1: the two pathways to synthesize F-bPEI 1

F-bPEI1a was synthesized in two different reaction pathways: the first one using condensing agents, while the second with the microwave reactor. In the first case it was necessary to use condensing agents to promote the formation of the amide bond between the carboxylic groups of the fluorophore and the primary amine of the polymer at room temperature and pressure. In the second case the formation of the desired bond was achieved by the increase of the reaction conditions without the addition of any external agent. A major improvement was the decrease of the reaction time, from 72 hours to 2 hours. In both cases it was mandatory to dialyze the reaction product, since a lot of the fluorophore did not react. Once the procedure was finished, the product was stored. In the case of the standard procedure, the grafted bPEI was frozen for 72 hours and then lyophilized, obtaining a fine hygroscopic powder. Unfortunately, it proved to be a poor choice, since it was very hard to redissolve the polymer in water to prepare the sensing sponges. The successive products were then kept in liquid solution at known concentration for further uses.

Even if it was not possible to establish the extent of the grafting, we know for sure that some fluorophore has reacted. This is proven by both the NMR and IR spectra, with the former showing an aromatic signal, which was not present in the polymer, and the

F-bPEI₃



Scheme 2.2.3: synthetic pathway of F-bPEI 3

The synthesis of these two grafted polymers was done according to what states in the Material and Methods section. Once the dialysis was completed, the product was stored as an aqueous solution at known concentration. On the dialysis membrane some solid residue was present, which was insoluble in most organic solvents, such as water, acetone, ethyl acetate, diethylether, dichloro methane chloroform and dimethyl sulfoxide. In both cases, the NMR and IR analysis proved that the reaction took place. The extent of the grafting was achieved by means of UV spectroscopy.

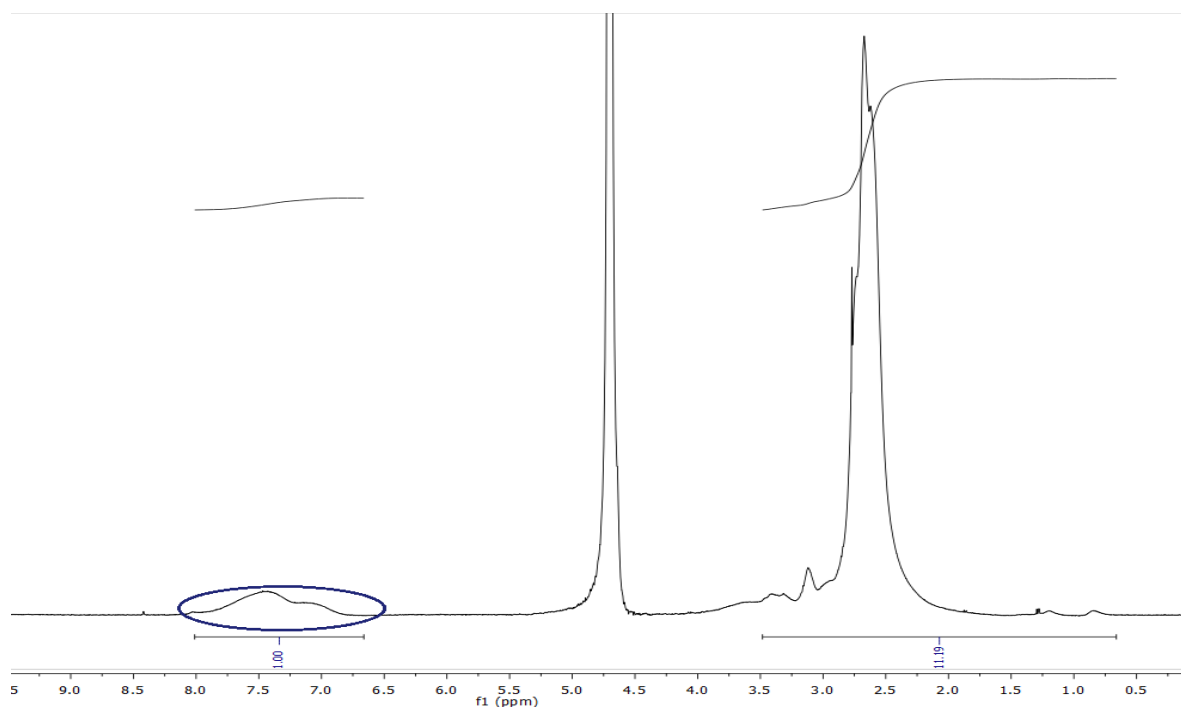


Figure 2.2.2: ¹H-NMR spectrum of F-bPEI₂ in D₂O with enlightening on the aromatic portion

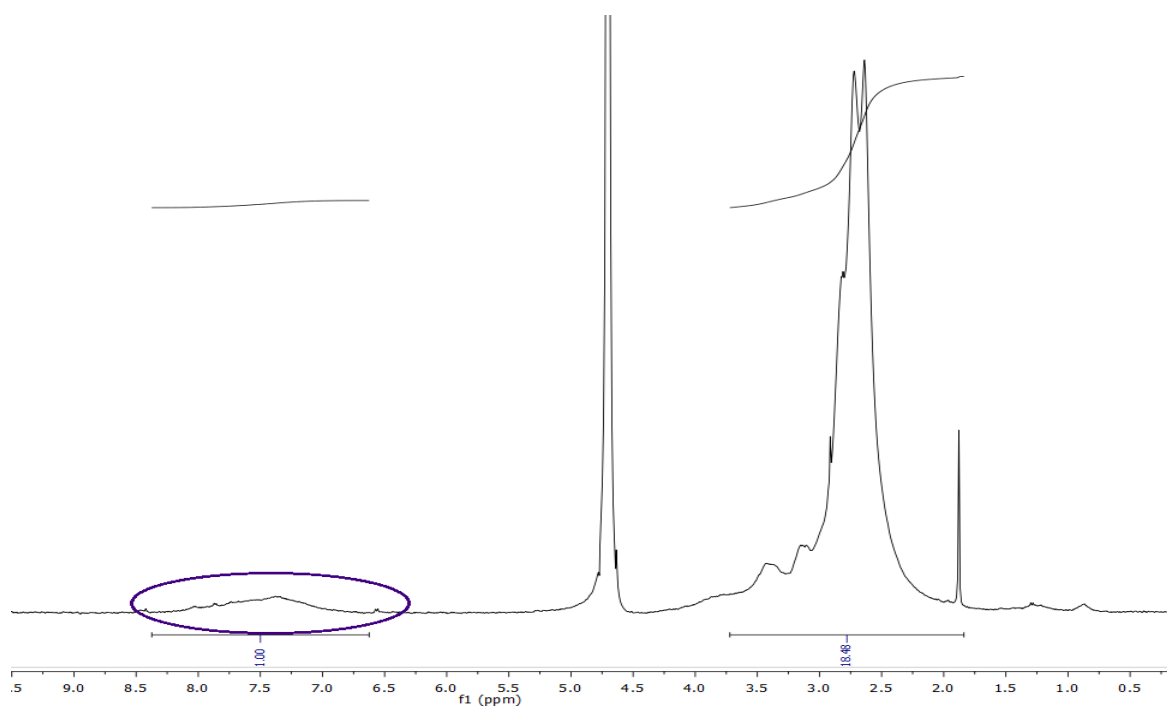
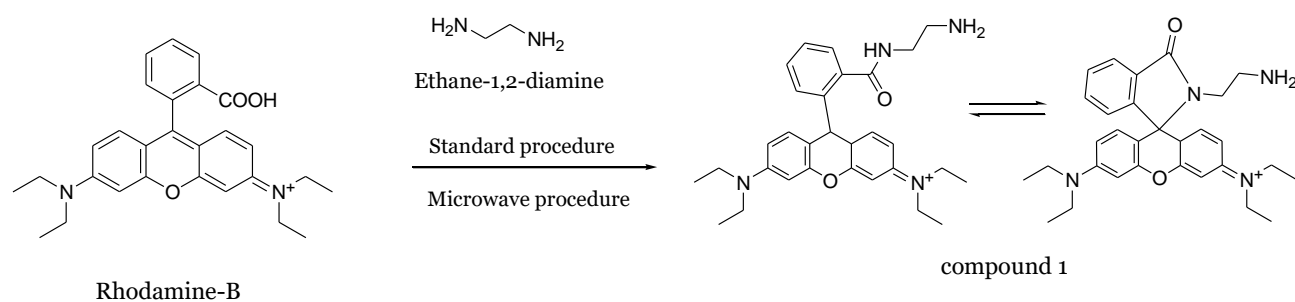


Figure 2.2.3: $^1\text{H-NMR}$ spectrum of F-bPEI₃ in D₂O with enlightening on the aromatic portion

2.1.3 Model compounds 1,2,3

Synthesis of compound 1



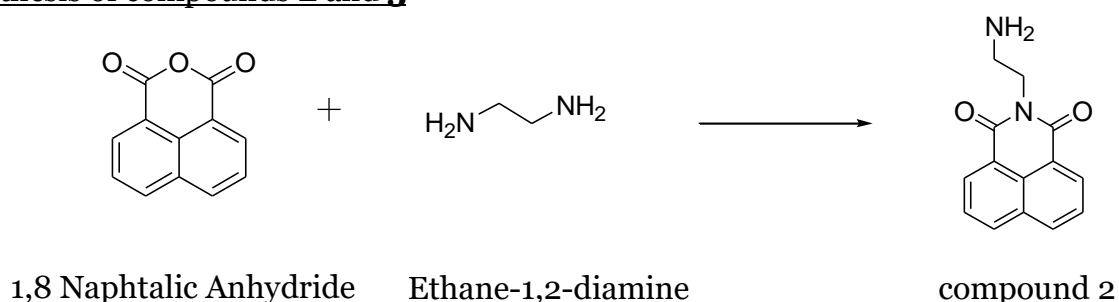
Scheme 2.2.4: synthetic pathway of compound 1

The only purpose of this compound was its use to build an UV calibration line to be able to quantify the amount of Rhodamine-B grafted on bPEI primary amines. In fact, using Ethane-1,2-diamine we obtained a molecule with the same appendage of bPEI, so we can have a reliable behaviour of the UV-vis analysis. The same reasoning was applied for compounds **2** and **3**.

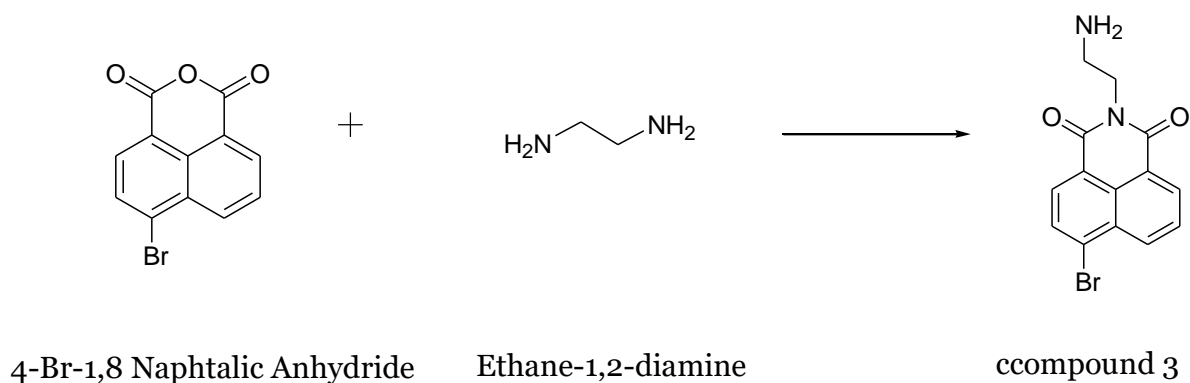
Compound **1** (Rhodamine-B ethylenediamine modified) was synthesized with two different strategies. At first it was used a procedure found in the literature [1], then a second procedure involving the microwave reactor was attempted. The reactor allowed to push the reaction at much higher operating conditions and the reaction time decreased substantially, from five days to 90 minutes. The yield increased to almost reach the unity (yield 95.74%).

Given these very useful advantages (increase of reaction condition and wide reduction of time), when possible, it was chosen to use the microwave reactor over the standard synthetic pathway, to be able to repeat the reactions in a faster and more efficient way, also making them more reproducible.

Synthesis of compounds **2** and **3**



Scheme 2.2.5: Synthetic pathway of compound 2



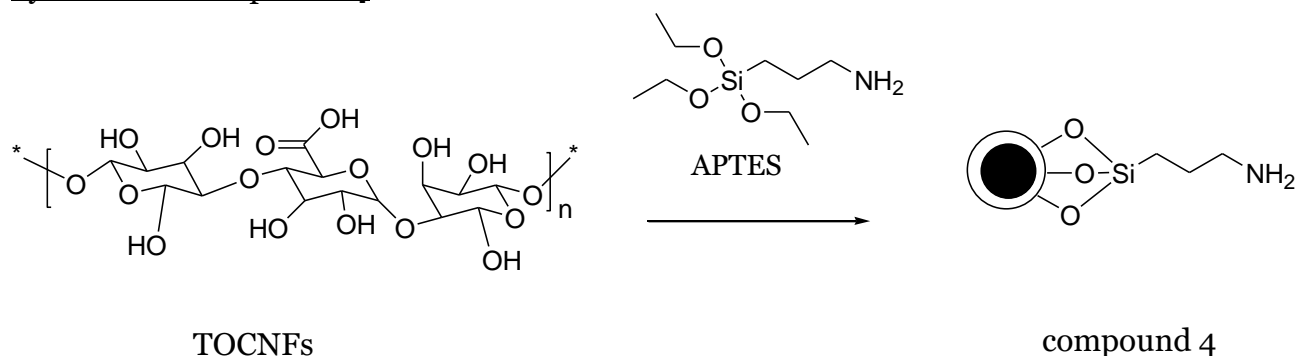
Scheme 2.2.6: Synthetic pathway of compound 3

The synthesis of compounds **2** and **3** was done as reported in the Materials and Methods section without the employment of the microwave reactor, since their

reaction time was reasonable, the reaction conditions led to quite good yields and the products were clean enough for their purpose. The purification was done by means of flash chromatography. The yields were respectively the 68.3% and 78.1%.

2.1.4 Compounds 4 and 5

Synthesis of compound 4



Scheme 2.2.7: synthetic pathway of compound 4

TONCFs were mixed with NaOH to have a basic solution, then sonicated for a better dispersion and lyophilized for an effective water removal. Afterwards, the reaction under inert atmosphere and reflux took place. Then the ICP-OES analysis provided an estimation of the amount of reacted silane, which was 1.31 ± 0.05 w%. At first, the percentage of silicon present in the silane was calculated with Eq 2.1:

Eq 2.1

$$mg_{APTES} : 100 \text{ w\%} = mg_{Si} : X$$

where X is the weight percentage of silicon present in the reacting compound (X = 12,65 w%)

Once the total available Si is known, the grafting obtained was estimated using Eq 2.2:

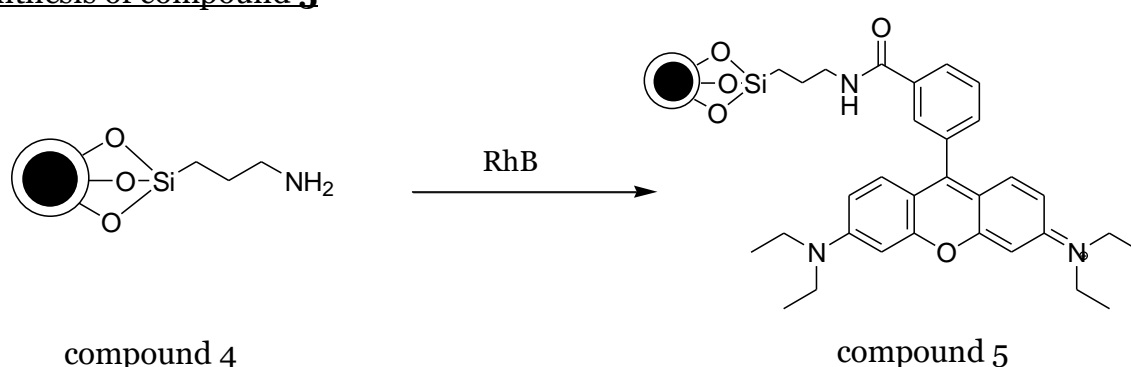
Eq2.2

$$w\%_{Si} : 100\% = w\%_{Si\ ICP} : X$$

where $w\%_{Si\ ICP}$ is the silicon found in a sample ICP-analyzed, thus X is the grafted silane (X = 10%).

The goal of compound **4** was to have primary amines able to bond with the carboxylic moieties present on Rhodamine-B. In this way it was possible to functionalize the modified cellulose through an imide bond, leading to compound **5**.

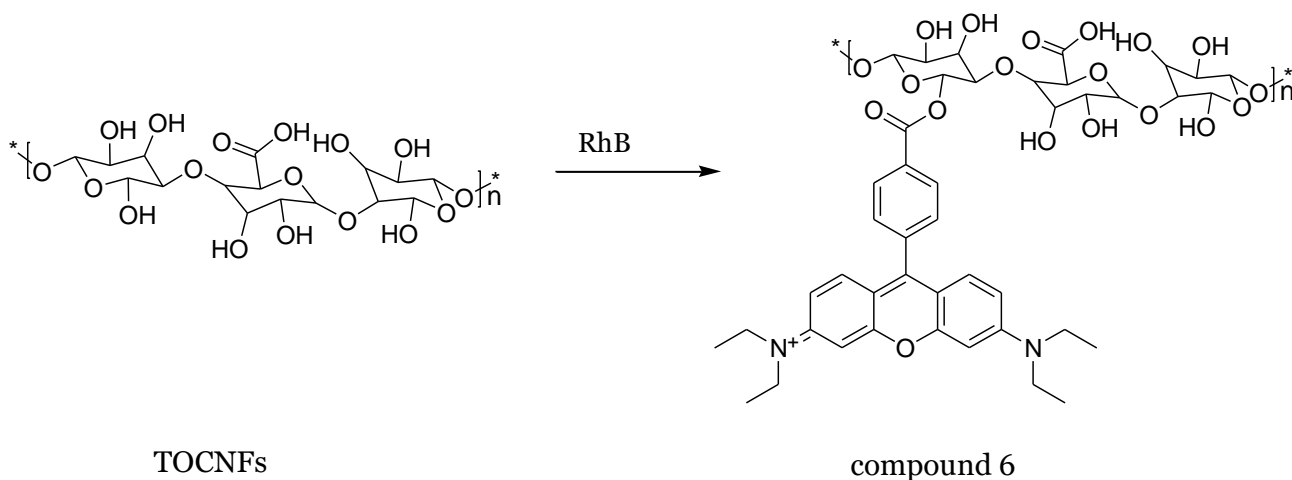
Synthesis of compound 5



Scheme 2.2.8: synthetic pathway of compound 5

Compound **5** was synthesized with the aid of the microwave reactor. Even though the quite severe reaction condition, the yield was low (about 33%). The impurities and unconverted reactant were washed under vacuum using several solvents, as stated in the Material and Methods Section. Even though no NMR analysis was performed (cellulose does not dissolve properly in the solvents), we know for sure that the reactions took place. In the case of compound **4** thanks to the elemental analysis, which proved that silica has reacted with the oxidised cellulose and for both compounds the evidence of the reaction is the IR spectra reported in Figure 3.10, showing the typical signals of imidic bond and of primary amines, both obviously not present on the starting oxidised cellulose.

2.1.5 Compound 6



Scheme 2.2.9: synthetic pathway of compound 6

Compound **6** was synthesized in the exact same condition as compound **5**, except that no amino-giver reactant was employed. In this case no amide bond was formed, instead the obtained product was an ester, derived by the direct condensation of the carboxylic groups present on both TONCFs and Rhodamine-B. Also, in this case, no NMR was done for the same motives of the previous two compounds, but the confrontation between the IR spectrum of compound **6** and oxidised cellulose tells us that Rhodamine-B was successfully grafted on the polymer. In fact, in Figure 3.11 the imidic signal is clearly visible.

The last three compounds were synthesized with a multifunctionalization of the compound material in mind.

2.1.7 Preparation of sponges

In order to prepare the sponges bearing fluorophore probes, the TONCFs obtained as described in the Material and Methods Section were dispersed in water to get a homogeneous suspension 3% w/v. Then water solutions of different ratios of non-functionalized-bPEI and functionalized-bPEI were added as reported in Table 1,2,3

Then the homogeneous mixtures underwent freezing and thermal treatments, according to the standard procedure already reported in the literature.

Table 2.2.1: Different ratio of non-functionalized-bPEI and F-bPEI1b in each sponge

sample	TOCNF [mg]	Functionalized-bPEI [mg]	Non-functionalized-bPEI [mg]	Citric Acid [mg]	Non-functionalized functionalized bPEI ratio
S1a	500	25	475	128	19
S1b	500	50	450	128	9
S1c	500	75	425	128	5.7
S1d	500	100	400	128	4
S1e	500	125	375	128	3
S1f	500	150	350	128	2.3

Table 2.2.2 : Different ratio of non-functionalized-bPEI and F-bPEI2 in each sponge

sample	TOCNF [mg]	Functionalized-bPEI [mg]	Non-functionalized-bPEI [mg]	Citric Acid [mg]	Non-functionalized functionalized bPEI ratio
S2a	500	50	450	128	9
S2b	500	100	400	128	4
S2c	500	150	350	128	2.3
S2d	500	200	300	128	1.5
S2e	500	250	250	128	1

Table 2.2.3 : Different ratio of non-functionalized-bPEI and F-bPEI₃ in each sponge

sample	TOCNF [mg]	Functional ized-bPEI [mg]	Non- functionali zed-bPEI [mg]	Citric Acid [mg]	Non- functionali zed functionali zed bPEI ratio
S3a	500	50	450	128	9
S3b	500	100	400	128	4
S3c	500	150	350	128	2.3
S3d	500	200	300	128	1.5
S3e	500	250	250	128	1

2.2 UV-vis discussion

The UV-vis analysis was used to quantify the degree of grafting of the fluorophore onto the bPEI primary amine.

2.2.1 UV-vis analysis with Rhodamine B

At first, a calibration line of pure Rhodamine-B was built, using acid water (HCl 0.1N) as solvent, in order to have an indication of the concentrations to be used and where to expect the peak of absorption, which results at 557 nm, as shown in Figure 2.4 and Table 2.2

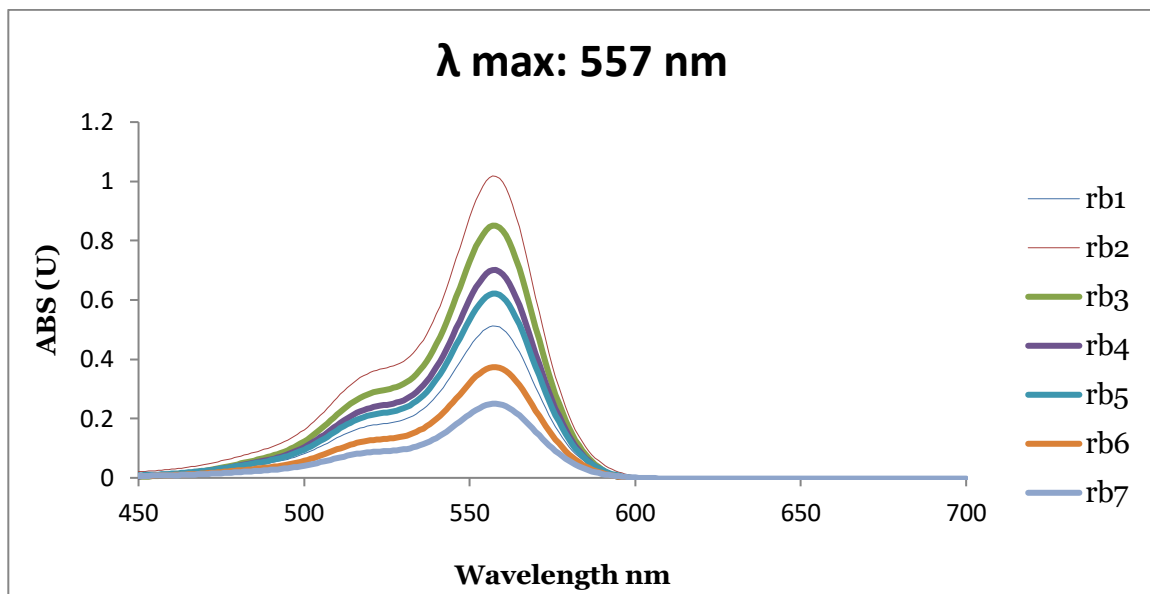


Figure 2.2.4: UV spectra at different concentration of RB in HCl 0.1N

Table 2.2.4: concentrations and measured absorption of RB

Sample	Absorption 557 nm	Concentration (mg/mL)	Concentration (μmol/mL)
RB1	0.512423	0.0036	0.0075
RB2	1.01843	0.0072	0.0150
RB3	0.850843	0.0064	0.0134
RB4	0.700802	0.0055	0.0115
RB5	0.621551	0.0045	0.0094
RB6	0.37323	0.0027	0.0056
RB7	0.250141	0.0018	0.0038

As shown in the previous table, one would expect very little concentration for the UV-vis analysis of compound **1**, since it is the same fluorophore. Unfortunately, this is not true, since we had to use concentration values three order of magnitude higher with respect to the ones reported in Table 2.2. We thought that the reason of this anomaly is because the product is an equilibrium mixture of its open and closed form and maybe this could interfere with the analysis. The last this statement is currently under investigation.

As reported in the Materials and Methods section, the obtained degree of grafting was three order of magnitude higher than the theoretical maximum. So, it was thought to change the solvent. The first attempt was made with DMSO, but the samples did not dissolve even after 72h under vigorous magnetic stirring. Then ethanol was employed, but all the above-mentioned problems remained. It was then decided to try with other fluorophores, such as 1,8-Naphtalic Anhydride and 4-Br-1,8-Naphtalic Anhydride.

2.2.2 UV-vis analysis with 1,8 Naphthalic Anhydride and 4-Br-1,8-Naphtalic Anhydride

1,8 Naphthalic Anhydride

As before, different dilutions of the mother solution of the model compound were made in order to acquire UV-vis spectra at different concentrations, as fully reported in the Material and Methods section.

The linear regression performed on the data reported in Table 3.5 allowed to find the unknown parameters (intercept and angular coefficient) of the calibration line. The resulting lines were:

$$y = 55.968 * x - 0.03373,$$

when concentrations in [mg/mL] were used, and

$$y = 13.447 * x - 0.0368 \text{ in the case of } [\mu\text{mol/mL}].$$

Then the UV-vis analysis of the corresponding grafted polymer was performed, as described in the Material and Methods section.

The calibration line in [$\mu\text{mol/mL}$] was inverted in order to find the amount of fluorophore in each cuvette of F-bPEI₂, obtaining Eq.3.5.

The concentration values in [$\mu\text{mol/mL}$] were divided by the concentration of the F-bPEI₂ [mg/mL], as reported in Table 3.7.

The average grafting value was 0.57 [$\mu\text{mol/mg}$], in agreement with either the theoretical maximum allowable (1.4 [$\mu\text{mol/mg}$]), *i.e.* the feeded stoichiometric amount of fluorophore in μmol divided by the stoichiometric amounts of the polymer and chromophore in mg (nominal value 40.7 %) and the purpose of grafting of the 20% of bPEI primary amine (11.3% of grafted NH_2).

4-Br-1,8-Naphtalic Anhydride

The same approach previously described was used, in this case the model compound was **3**.

Again, through a linear regression of the data of the value reported in Table 3.8, the intercept and angular coefficient of the calibration line were found. The interpolation lines were:

$$y = 43.491 * x - 0.008$$

when expressed in [mg/mL] and

$$y = 13.886 * x - 0.0092$$

if in [$\mu\text{mol/mL}$] the average value of grafted bPEI was 0.30 [$\mu\text{mol/mg}$], also in this case the value was coherent with the theoretical maximum (1.05 [$\mu\text{mol/mg}$]), *i.e.* the reacting stoichiometric fluorophore in μmol divided by the stoichiometric amounts of polymer and chromophore in mg. The nominal value was 0.28 % and the percentage of the bPEI grafted primary amine was 6%.

2.3 Ecotoxicological tests

The ecotoxicological analysis were performed at the University of Siena, Department of Environment, Earth and Physical Science by Prof Ilaria Corsi research group.

Microscopic fragments of NS grafted with Rhodamine-B, 1,8-Naphtalic Anhydride and 4-Br-1,8-Naphtalic Anhydride were observed in dry conditions through optical fluorescence microscope Olympus BX51 at magnification 20x equipped with camera and filter for Rhodamine-B (Ex 522- Em 586; Ex 450-Em 490; Ex 345-Em 460). The images obtained showed fluorescence at the selected wavelength by checking the presence of Rhodamine-B in the NS **S1f** (Figure 2.5). Similar results were obtained also for the NS obtained by grafting bPEI with 1,8-Naphtalic Anhydride (**S2e**) and 4-Br-1,8-Naphtalic Anhydride (**S3e**) (Figure 2.6).



Figure 2.5: Microscopic fragments of NS grafted with Rhodamine-B (S1f)

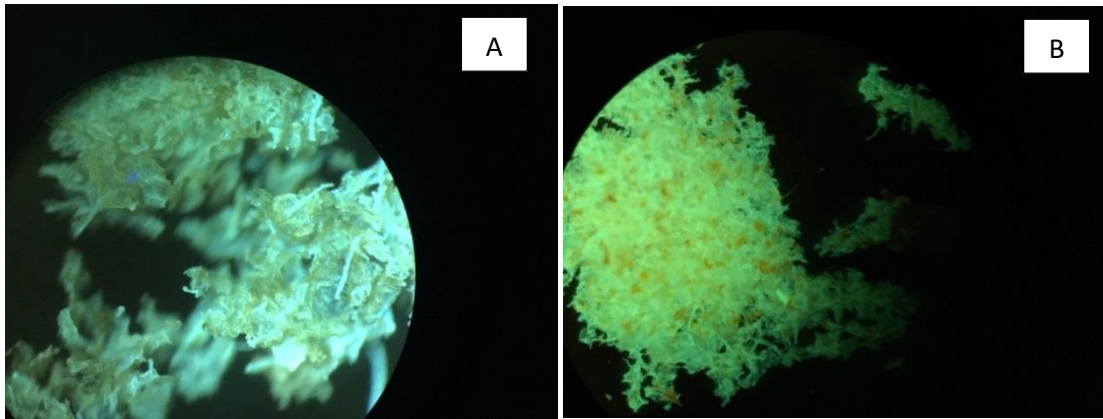


Figure 2.6: Microscopic fragments of NS grafted with 1,8-Naphtalic Anhydride (A, **S2e**) and 4-Br-1,8-Naphtalic Anhydride (B, **S3e**)

Examples of the marine bivalve *M. galloprovincialis* were exposed for 24h to the following amounts of cellulosic NS grafted with RhB (0,120 mg/L; 0,06 mg/L; 0,03 mg/L) in artificial sea water suspension (pH 8, salinity 35 per thousand and T 22°C)

After 24 hours, traces of fluorescence were detected in circulating cells of the specimens exposed to the highest amounts of 0.120mg/L and 0.06mg/L confirming the uptake of NS RhB in the exposed specimens (Figure 2.7). No fluorescence was observed in the specimens exposed to the lowest concentration (0.03 mg/L).



Figure 2.7: In vivo images showing traces of fluorescence in circulating cells in marine bivalves.

At 72 hours in the specimens exposed to the highest concentration (0.120mg/L) aggregates were observed near the byssus (organ that serves the mussel to anchor to the hard substrates) suggesting a clearance in the 72 hours exposure (Figure 2.8). Weak traces of fluorescence have been found in circulating hemocytes.

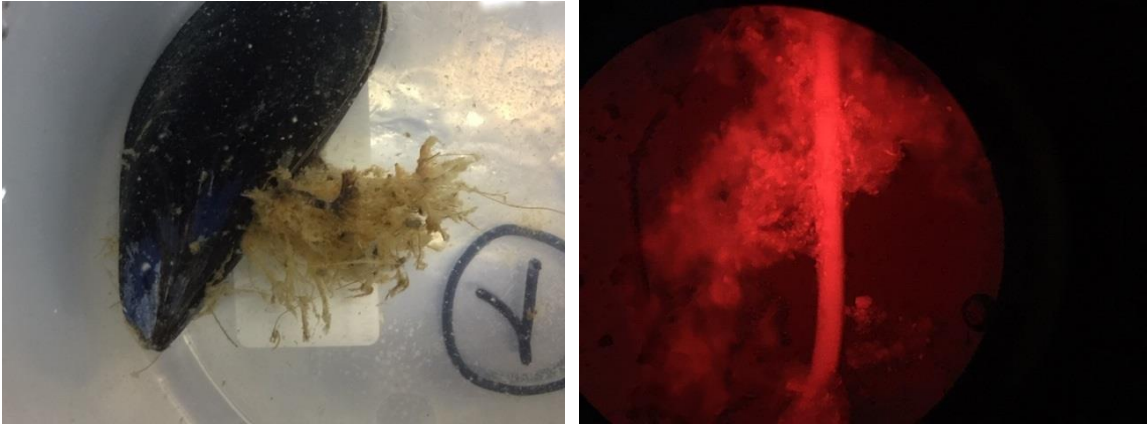


Figure 2.8: In vivo images of byssus showing fibers expulsion after 72 h.

3. Materials and Methods

3.1 General

The reactants used in this work were purchased from Sigma-Aldrich. Cellulose from cotton linters was provided by Bartoli paper mill (Capannori, Lucca).

The deionised water was produced within the laboratories with a Millipore Elix® Deionizer with Progard® S2 ion exchange resins.

The FTIR spectra were produced with a Varian 640-IR FTIR.Spectrometer. All NMR spectra were recorded on a 400MHz Bruker NMR spectrometer. Microwave reactions were conducted in a Biotage® Initiator+. The UV spectra were obtained with a Jasco V-630 BIO Spectrophotometer. A Branson SFX250 Sonicator and a SP Scientific BenchTop Pro Lyophilizer were also used in the following procedures.

3.2 Cellulose oxidation with the TEMPO, NaClO and KBr system

Cotton linters was used as cellulose starting material furnished by Bartoli paper factory (Lucca, Italy). The fibres are short and thick-walled and resemble the most to cotton seed.

30 g of paper were minced with the aid of a domestic mixer with gradual addition of deionised water. In the meantime, 0.645 g of tetramethyl-piperidine-N-oxide (TEMPO) and 4.626 g of KBr were dissolved in 0.5 L of deionised water into a 1L beaker placed on a magnetic stirrer. As soon as the paper was homogeneously blended with water, the suspension was transferred in a 10 L keg with addition of water until a total volume of 1.7 L.

Keeping the solution under stirring, a pH meter and a dropping funnel were installed above the beaker, containing 131 mL aqueous solution of NaClO 10% w/w. NaClO solution was then dropped into the suspension while the pH was monitored and maintained at 10.5-11 by the addition of NaOH 4M.

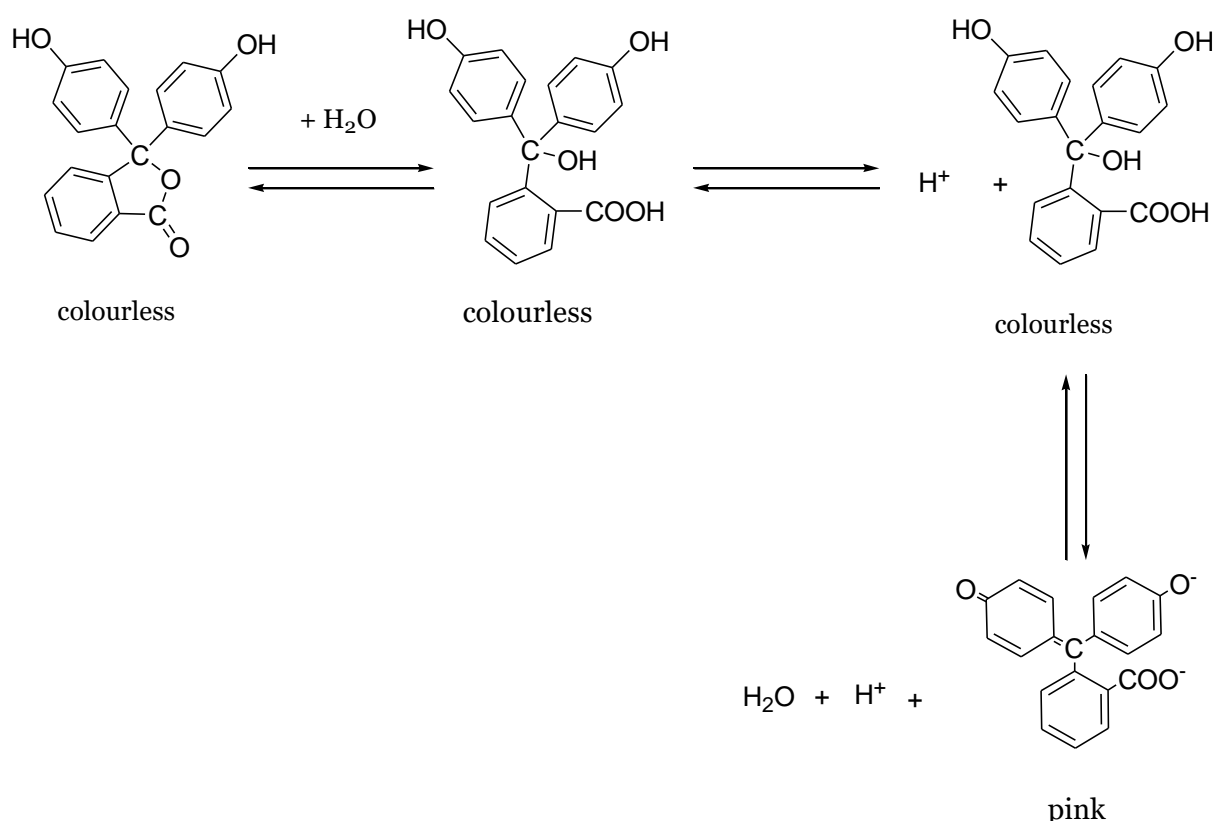
Once NaClO was consumed, some NaOH 4 M was still dripped to keep the pH constant, then the now oxidised cellulose was left stirring overnight. After 16 hours, cellulose was acidified with concentrated HCl to promote the aggregation of the cellulose fibres and an easier separation from water. Then cellulose was filtered on a Büchner funnel and washed with deionised water (2 L, 5-6 times).

For an effective removal of water from the fibres, two washes with acetone (0.5 L each time) were performed (to ensure the complete removal of the solvent, under-vacuum evaporation was used).

The resulting oxidised cellulose was 23.6 g, about the 78.6% of the starting material.

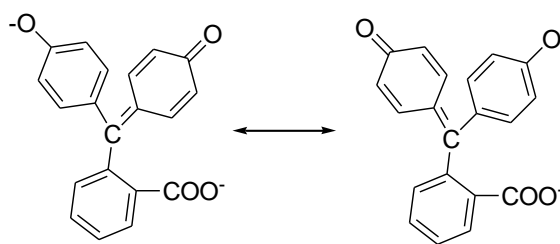
3.3 Tempo Oxidised Cellulose NanoFibers (TOCNFs) titration

To establish the concentration of carboxylic acid on the cellulose structure, a titration with NaOH was performed. The NaOH solution used for the titration of cellulose was initially titrated with hydrogen phthalate potassium, then phenolphthalein was employed as colourimetric indicator. This weak acid is transparent when in acid solution and turns to a bright pink colour when in basic ones. The chromatic change is due to the modification of the structure of the molecule. In the case of phenolphthalein, the detachment of two atoms of hydrogen transforms the lactonic colourless structure in a bright pink quinonic one.



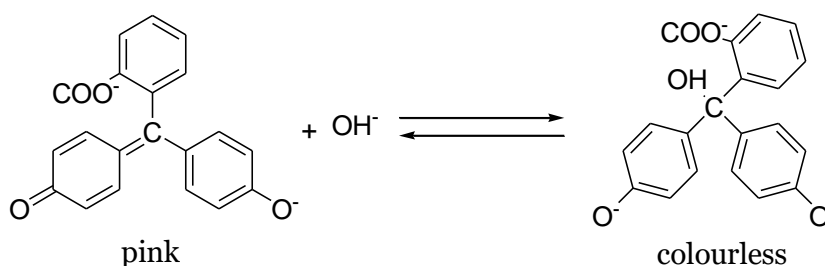
Scheme 3.3.1: phenolphthalein mechanism

The quinone shows also a resonance equilibrium, which is responsible for the colour change.



Scheme 3.3.2: equilibrium forms of phenolphthalein

The colour change happens around pH 9.5, value expected when all the carboxylate groups undergo basic hydrolysis. The reaction stops at a pH value above 13, since the central carbon (the one promoting the conjugation) is blocked.



Scheme 3.3.3: interruption of the reaction

403.3 mg (1.97 mmol) of potassium hydrogen phthalate were dissolved in water with the addition of a few drops of phenolphthalein solution 10 mM in acetonitrile, afterwards the NaOH solution was dripped in the beaker under continuous agitation. To achieve the neutralization of the phthalate, 20.22 mL of soda were required, so the precise titration of NaOH used for the determination of carboxylate groups of the oxidised cellulose was 0.0977 M.

412.8 mg of TOCNF were dispersed in water and sonicated to obtain a homogeneous suspension. A drop of the same phenolphthalein solution was added and the soda solution previously titrated was trickled in the beaker kept stirring: 5.5 mL were necessary to neutralise the carboxylic acids of the cellulose. The concentration of the carboxylic groups was calculated using Eq.3.1:

Eq.3.3

$$[COOH] = \frac{0,0977 \frac{mmol_{NaOH}}{mL_{NaOH}} * 1 \frac{mmol_{COOH}}{mmol_{NaOH}} * 5,5 mL_{NaOH}}{0,4128 g_{TOCNF}} = 1,3 \frac{mmol_{COOH}}{g_{TOCNF}}$$

Equation 3.1: calculation of the carboxylic group present in one gram of TONCF

3.4 Sponges general procedure

In a beaker TONCFs were suspended in a deionised water solution 2.5% w/v. While mixing, granular NaOH was added to the suspension, obtaining a yellowish viscous non homogeneous solution. The beaker was put in an ice bath and the solution sonicated to promote a better separation of the nanofibers. After some minutes the solution was almost transparent and more homogeneous. The solution was acidified with HCl, then it underwent filtration by means of a Büchner funnel, washes with deionised water and finally was resuspended. The procedure was repeated until neutrality. Wet cellulose was removed from the filter paper and weighted. The difference between the initial and latter weight was due to retention of water during the washes. The remaining water needed to get a 2.8-3% w/v TOCNFs solution for the next phase was divided in three portions, one for cellulose, one for the cross-linking polymer (branched polyethyleneimine, bPEI 25 kDa) and the latter for the co-reticulant agent (anhydrous citric acid) in three separated beakers. Concerning bPEI, different ratios of functionalised and non-functionalised polymer were used, and the amount of citric acid employed was calculated according to Eq.3.2 [1]:

Eq.3.4

$$m_{CA} = x g_{bPEI} * 7,4 \frac{mmol_{NH_2}}{g_{bPEI}} * 0,18 \frac{mmol_{CA}}{mmol_{NH_2}} * 192,24 \frac{mg_{CA}}{mmol_{CA}} = y mg_{CA}$$

Equation 3.2: calculation of the amount of CA to be used related to the primary amine of bPEI

Once dissolved in water, they were carefully added to the cellulose solution, kept stirring until a homogeneous hydrogel was obtained, placed in well-plates (about 15.5 mm diameter, each filled for about 2 mL) and rapidly freezed at -35°C. After a few hours, the well-plates were quickly moved to the lyophiliser for 48h, in which was

performed the sublimation of water, thus maintaining the internal structure of the original hydrogels.

After the freeze-drying, the cylindrical-shaped sponges were removed from the well-plates and put in crystallizing dishes for the thermal treatment in the laboratory oven. The initial temperature of 55°C was gradually raised up to 102°C in 4 hours to avoid sudden overheating and prevent the risk of burning the material. Above 100°C the water formed because of the reticulation reactions (formation of amidic bonds) between carboxylic moieties and amines was swiftly evaporated, allowing the formation of the desired reticulation of the material.

After a night in the laboratory oven, the sponges were extracted, showing a yellow and slightly soft texture, that hardened in a quite fast manner while cooling down.

3.5 Reference table

The following table shows the reference codes for all the synthesized chemical compounds and materials.

Table 3.3.1: abbreviation and corresponding compound

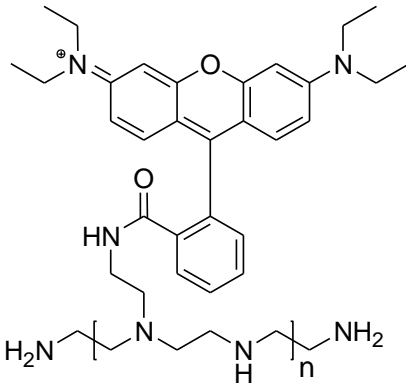
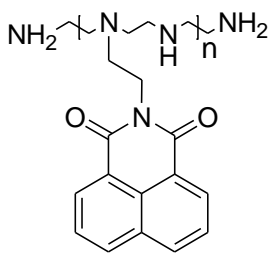
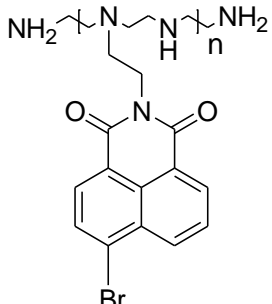
<p>FbPEI1a FbPEIb</p>	 <p>Synthesis with procedure a (condensing agents) Synthesis with procedure b (microwave)</p>
<p>FbPEI2</p>	
<p>FbPEI3</p>	

Table 3.1: (continues)

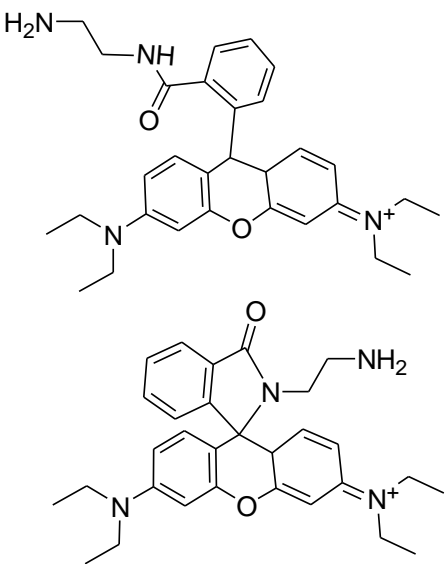
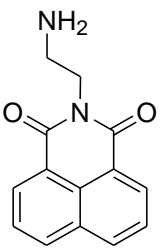
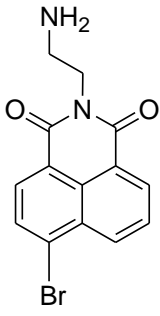
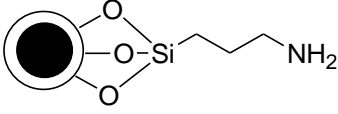
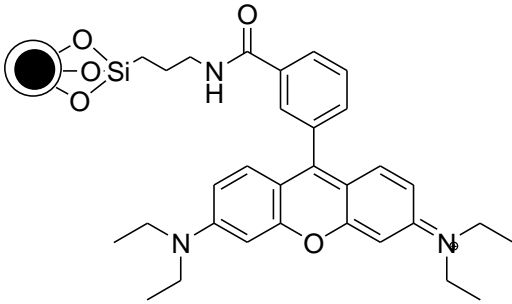
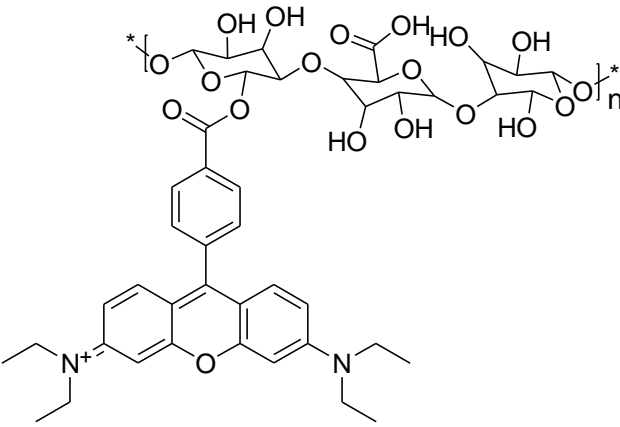
Compound 1	 <p>Chemical structures of Compound 1. The top structure is a complex molecule featuring a central benzofuran core. It has a diethylamino group (-N(CH₂CH₃)₂) at the 2-position, a diethyliminium group (=N⁺(CH₂CH₃)₂) at the 6-position, and a benzamide group (-C(=O)NHCH₂CH₂NH₂) at the 3-position. The bottom structure is a similar benzofuran derivative, but with a benzamide group (-C(=O)NCH₂CH₂NH₂) at the 3-position instead of the benzamide group.</p>
Compound 2	 <p>Chemical structure of Compound 2: A benzimidazole ring system with a primary amine group (-NH₂) attached to the nitrogen atom.</p>
Compound 3	 <p>Chemical structure of Compound 3: A benzimidazole ring system with a primary amine group (-NH₂) attached to the nitrogen atom and a bromine atom (-Br) at the 5-position of the benzimidazole ring.</p>
S1	Sponges with FbPEI1b
S2	Sponges with FbPEI2
S3	Sponges with FbPEI3

Table 3.1: (continues)

Compound 4	
Compound 5	
Compound 6	

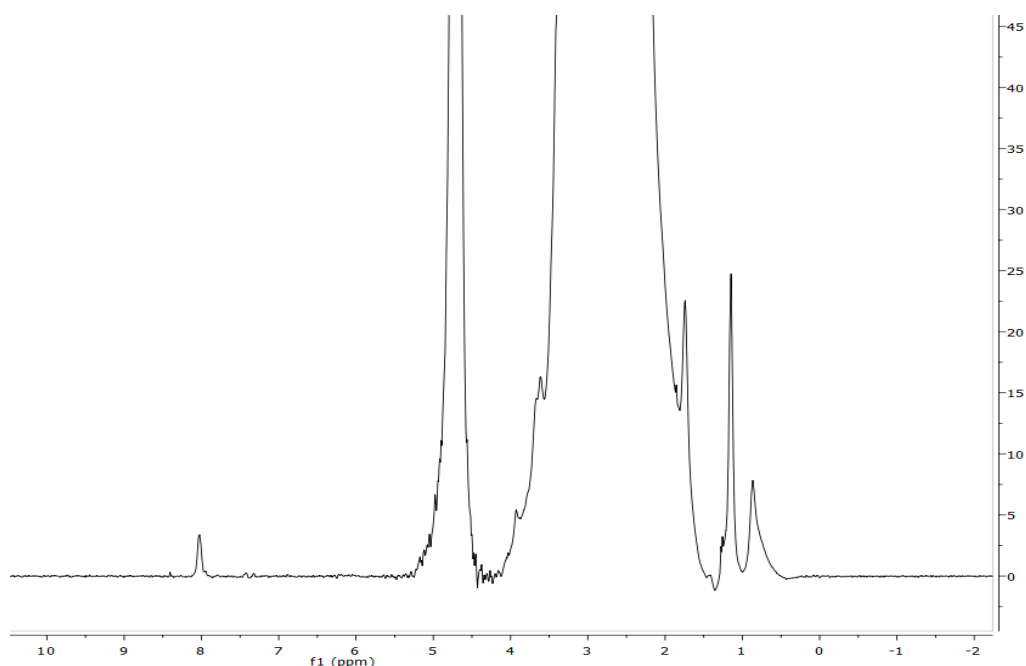
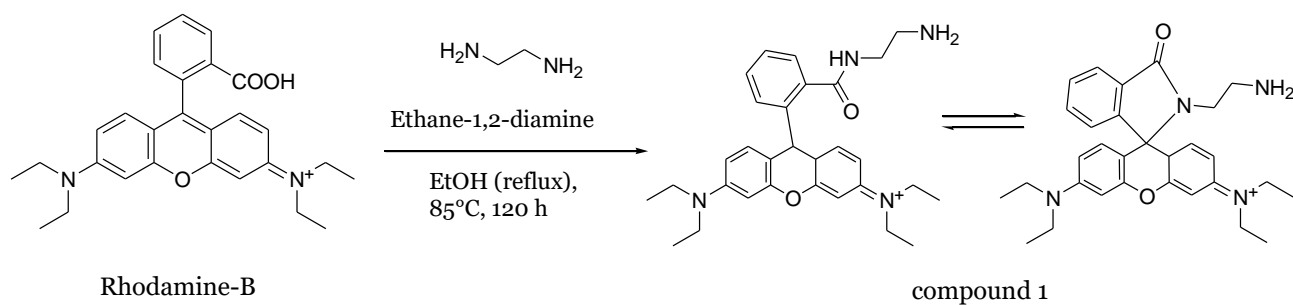


Figure 3.3.1: $^1\text{H-NMR}$ spectrum of F-bPEI1 concentrated in D_2O

3.6.3 Synthesis of compound 1

Standard procedure

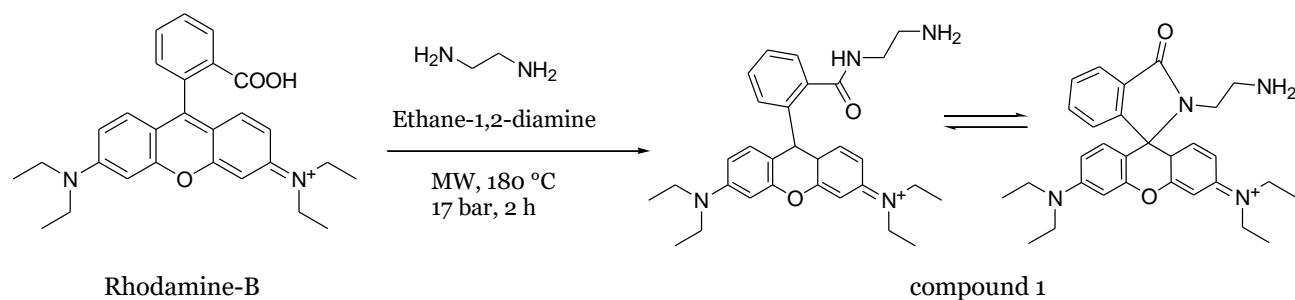


Scheme 3.3.6: standard pathway for the synthesis of compound 1

Following the procedure reported in [3], Rhodamine-B (200 mg, 0.42 mmol) was dissolved in 30 mL of ethanol. Then an excess of ethane-1,2-diamine (197.8 mg, 3.284 mmol, 0.22 mL) was added under ethanol reflux at 85°C . The reaction took place in five days, in which periodical monitoring were made. After two days, a first extraction was performed with HCl 1N and DCM to separate the organic and aqueous phases, a second extraction with NaOH 4N and water allowed to have a basic pH. Finally, the last extraction with DCM made possible the recover of the crude by

stratification, evaporation under vacuum and filtration. The crude then underwent flash chromatography with ethyl-acetate, methanol and ammonia (AcOET : MeOH = 9 : 1; MeOH : NH₄OH = 1000 : 1) as eluents, obtaining 11 mg of clean product. The yield is 40 %.

Microwave procedure



Scheme 3.3.7: microwave pathway for the synthesis of compound 1

The chromophore (500 mg, 1.044 mmol) was dissolved in a 20 mL microwave vial with 17 mL of ethanol under stirring. 0.7 mL of ethylenediamine were added dropwise to the solution. The reaction was conducted in a microwave reactor under the following conditions: 180°C, 2h, regime pressure 17 bar. The crude was then purified by flash chromatography (eluents AcOEt : MeOH 9 : 1 with addition of NH₄OH). Once isolated the product, which is in equimolar equilibrium in its two forms, the solution was evaporated under vacuum to remove the solvent, obtaining a light orange solid (yield 95.74 %). The UV-Vis analysis showed a peak of adsorption at 553,5nm. ¹H NMR (400 MHz, CDCl₃) δ 7.95-7.9 (m, 1H); 7.49-7.44 (m, 2H); 7.14-7.09 (m, 1H); 6.46 (s, 1H); 6.44 (s, 1H); 6.42-6.39 (d, 2H); 6.33-6.27 (dd, 2H); 3.39-3.31 (q, 8H); 3.24-3.19 (t, 2H); 2.48-2.42 (t, 2H); 1.21-1.16 (t, 12H).

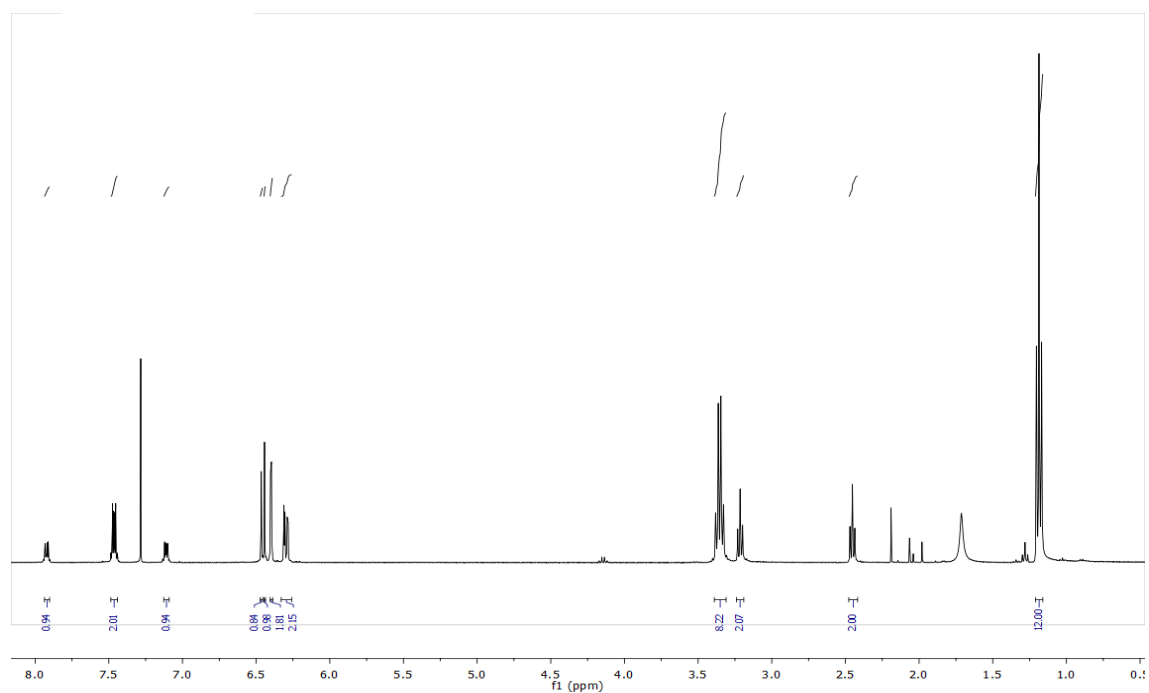


Figure 3.3.2: $^1\text{H-NMR}$ spectrum of compound **1** in CDCl_3

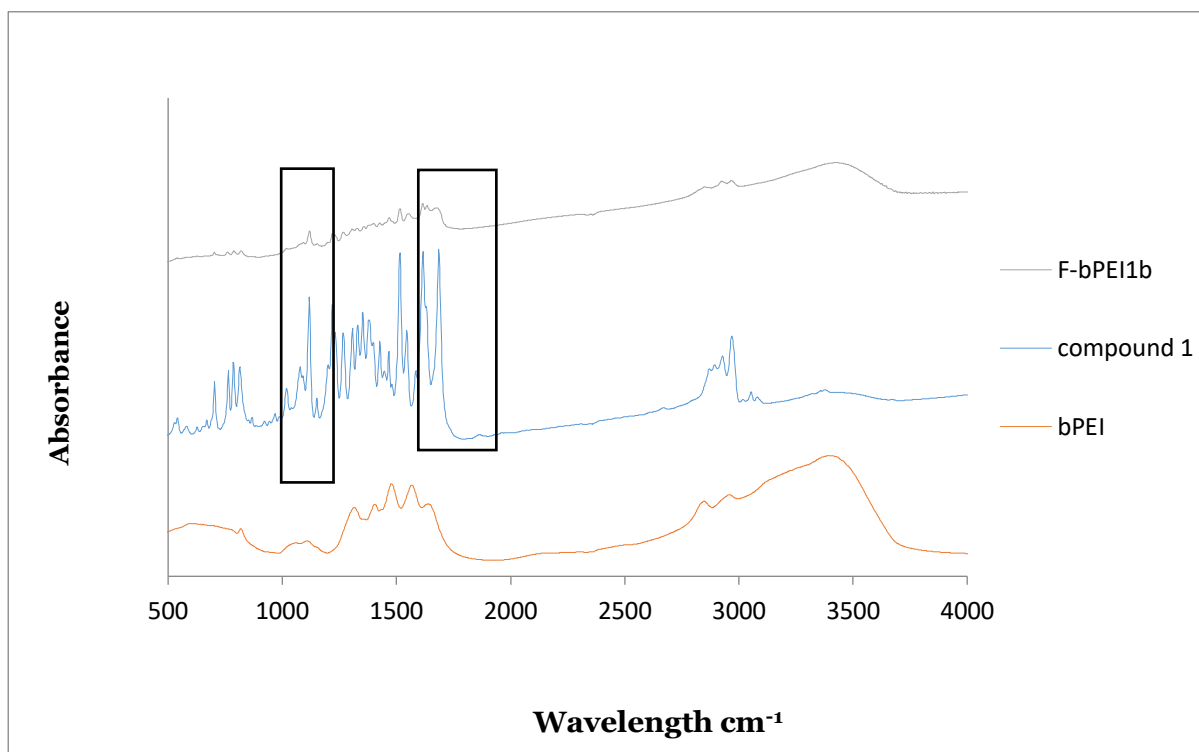
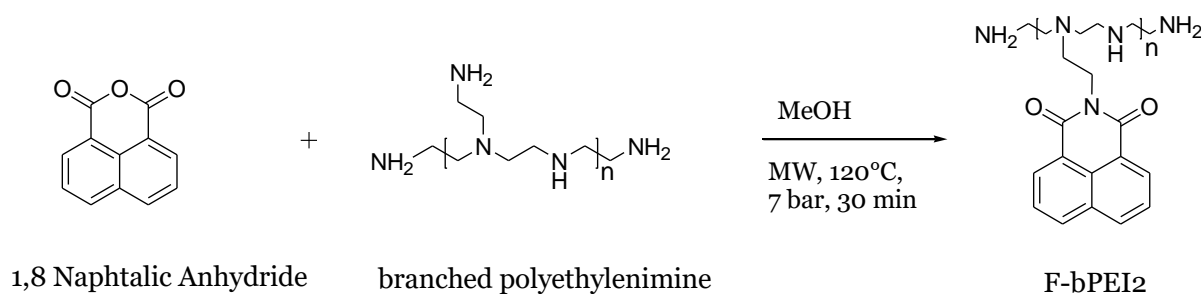


Figure 3.3.3: IR spectra of blanc bPEI, and derivative functionalized with Rhodamine B. In the spectra of compound **1** and F-bPEI**1b** it is possible to observe a peak at 1175 and between 1500-1750 cm^{-1} , relative to the imidic bond

3.6.4 Synthesis of F-bPEI2



Scheme 3.3.8: reaction pathway for the synthesis of F-bPEI2

bPEI (1 g, 7.39 mmol primary amine group) was dissolved in 15 mL of MeOH in a 20 mL microwave vial. Afterwards, 1,8-Naphthalic anhydride (293.3 mg, 1.48 mmol) was added dropwise in the solution, and stirred until total homogeneity. The synthesis took place in the microwave reactor at 120°C, 7 bar of regime pressure for 30 minutes.

The solvent was removed under reduced pressure and the crude diluted in deionized water. After filtering the solution, the liquid portion was dialyzed in a membrane with a cut-off of 12.4000 Da against ammonia and water. The dialysis took place for a week with regular replacements of the aqueous medium (10 x 1 L against ammonia, 10 x 1 L against water). Once the procedure was completed, the product was removed from the membrane and kept in solution at known concentration (44.45 mg/mL).

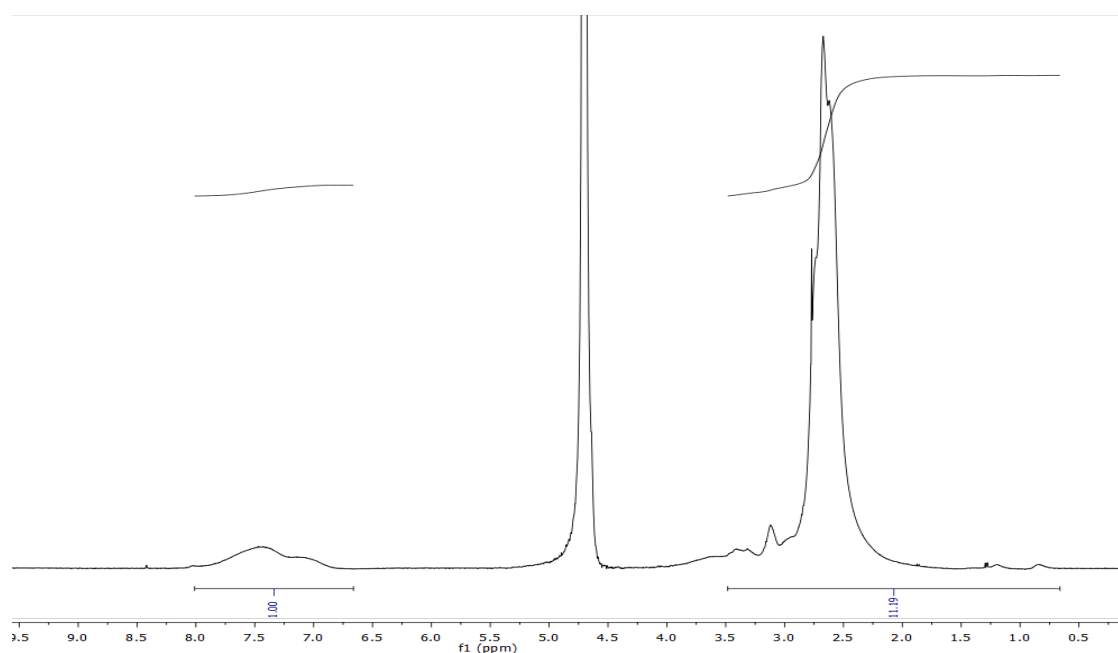
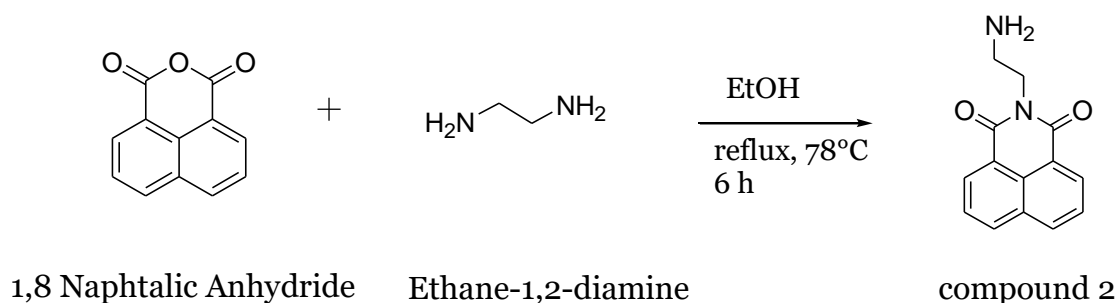


Figure 3.3.4: $^1\text{H-NMR}$ spectrum of F-bPEI2 in D_2O

3.6.5 Synthesis of compound 2



Scheme 3.3.9: synthetic pathway for the synthesis of compound 2

As reported in [4], in a flask equipped with a condenser, 1,8-Naphthalic Anhydride (200 mg, 1.01 mmol) was dissolved portionwise in ethylenediamine (0.45 mL, 6.868 mmol). The reaction was refluxed in 10 mL of EtOH for 6 hours at 78°C. After cooling, the reaction mixture was filtered, and the liquid phase evaporated under reduced pressure. The purification of the crude was achieved by flash chromatography (eluent: DCM : MeOH 9.5 : 0.5 with small addition of ammonia), resulting in a light yellow solid (yield 68.3%). The UV-Vis analysis showed a peak of adsorption at 344 nm. $^1\text{H NMR}$ (400 MHz, CDCl_3) δ 8.52-4.48 (d, 2H); 8.47-8.43 (d, 2H); 7.9-7.84 (t, 2H); 4.11-4.04 (t, 2H); 2.84-2.78 (t, 2H)

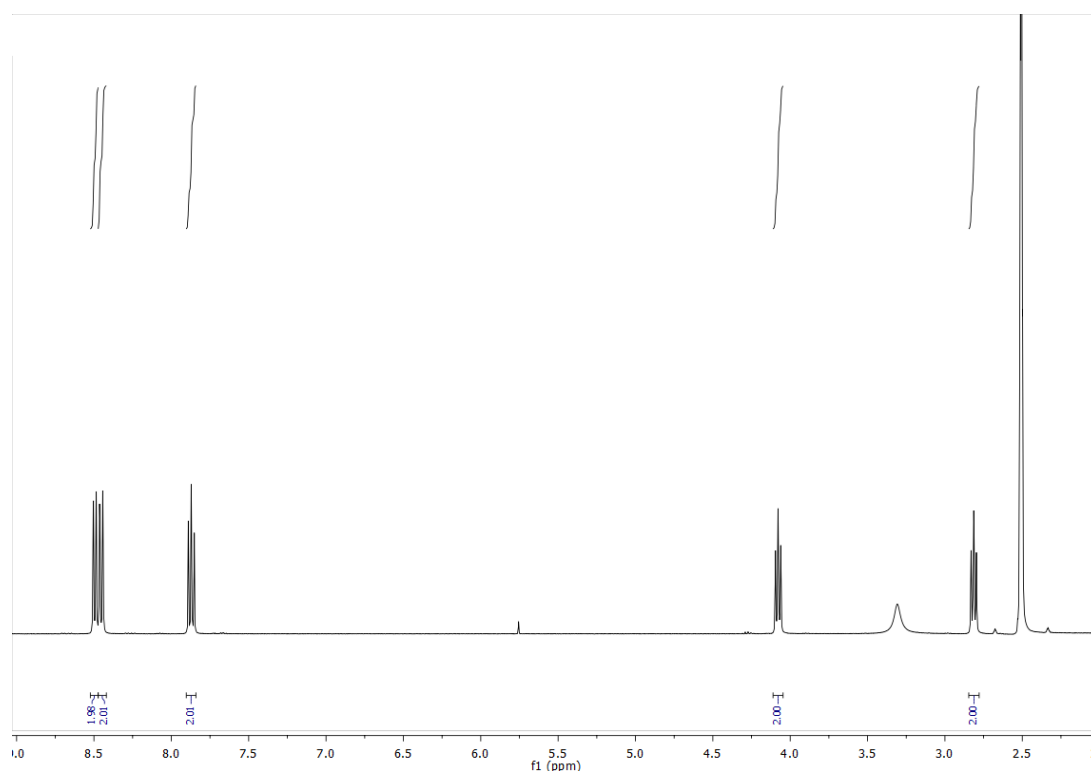


Figure 3.3.5: $^1\text{H-NMR}$ spectrum of compound 2 in CDCl_3

regular replacements of the aqueous medium (10 x 1 L against ammonia, 10 x 1 L against water). Once the procedure was completed, the product was removed from the membrane and kept in solution at known concentration (6 mg/mL).

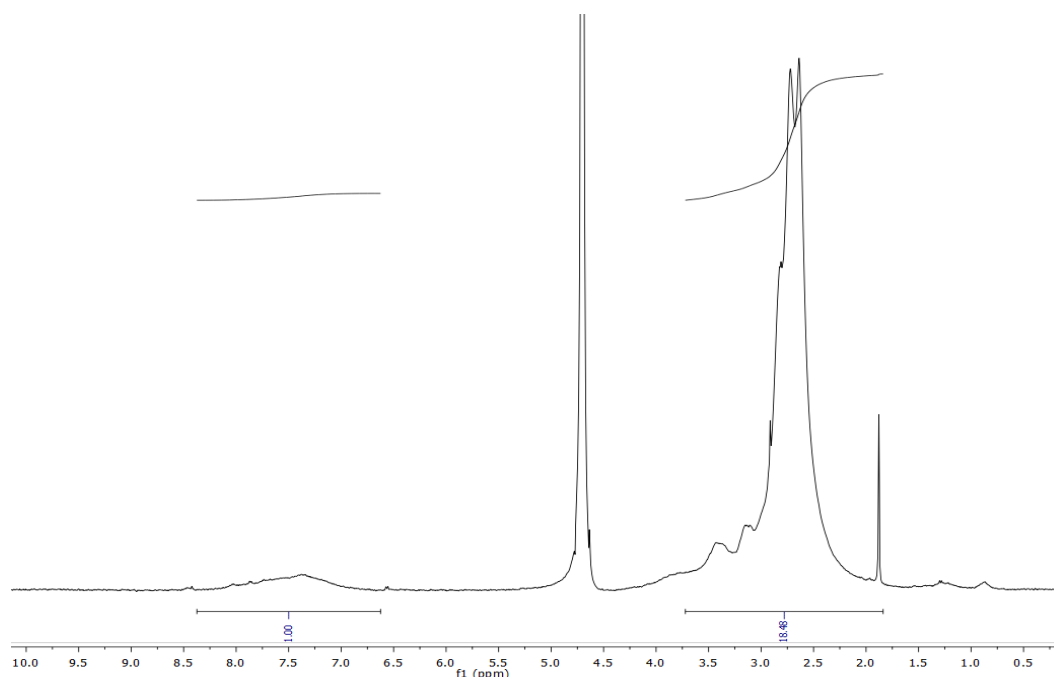
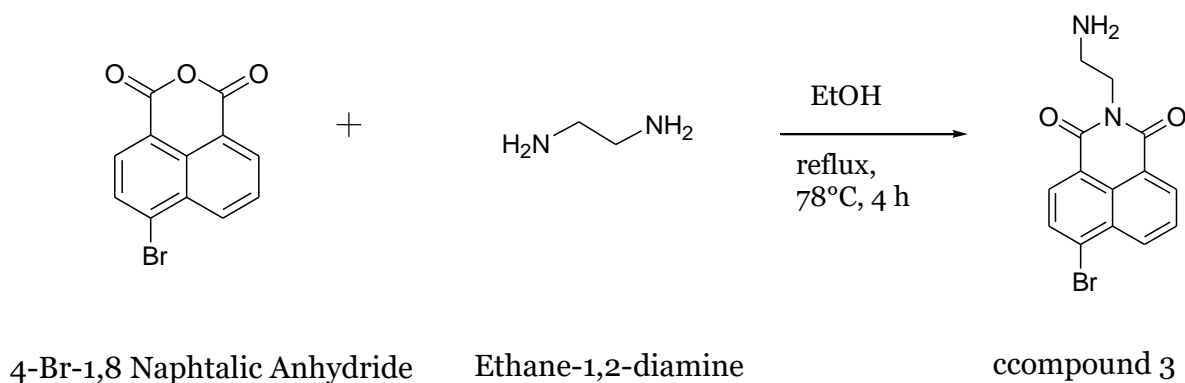


Figure 3. 3.7: $^1\text{H-NMR}$ spectrum of F-bPEI₃ in D₂O

3.6.7 Synthesis of compound 3



Scheme 3.3.11: reaction pathway for the synthesis of compound 3

As reported in [5], in a flask equipped with a condenser, 4-Br-1.8-Naphtalic Anhydride (200 mg, 1.01 mmol) was dissolved portionwise in ethylenediamine (0.1 mL, 1.202 mmol). The reaction was refluxed in 1.8 mL of EtOH for 4 hours at 78°C. After cooling, the reaction mixture was filtered, and the crude washed with ethanol. The purification of the crude was achieved by flash chromatography (eluent: DCM : MeOH 9.5 : 0.5 with small addition of ammonia), resulting in a white solid (yield 78.1%). The UV-Vis analysis showed a peak of

adsorption at 348 nm. ^1H NMR (400 MHz, CDCl_3) δ 8.63-8.53 (t, 2H); 8.38-8.33 (d, 1H); 8.27-8.2 (d, 1H); 8.04-7.97 (t, 1H); 4.11-4.03 (t, 2H); 2.86-2.77 (t, 2H).

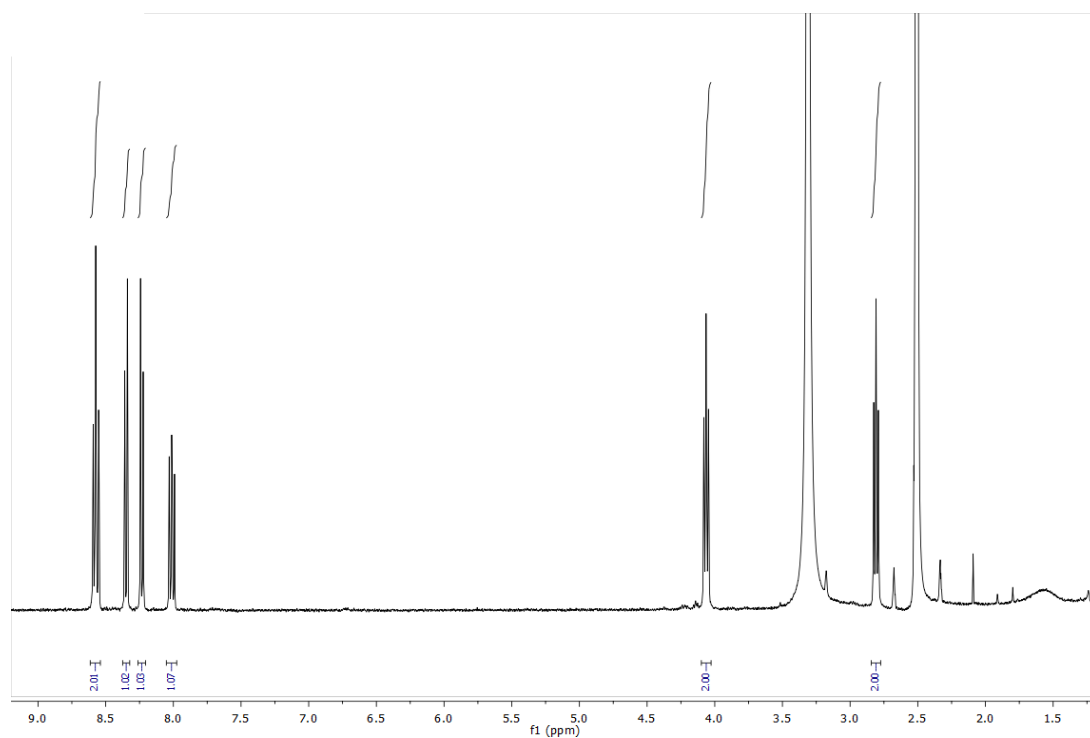


Figure 3.8: ^1H -NMR spectrum of compound **3** in CDCl_3

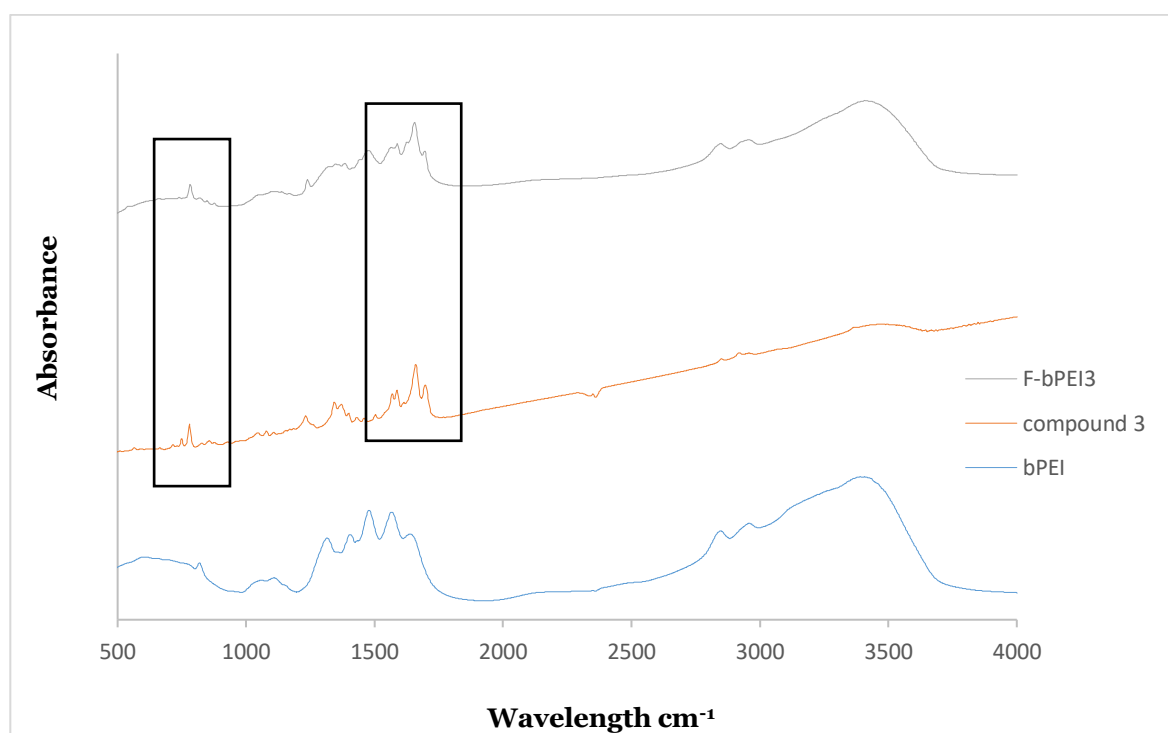
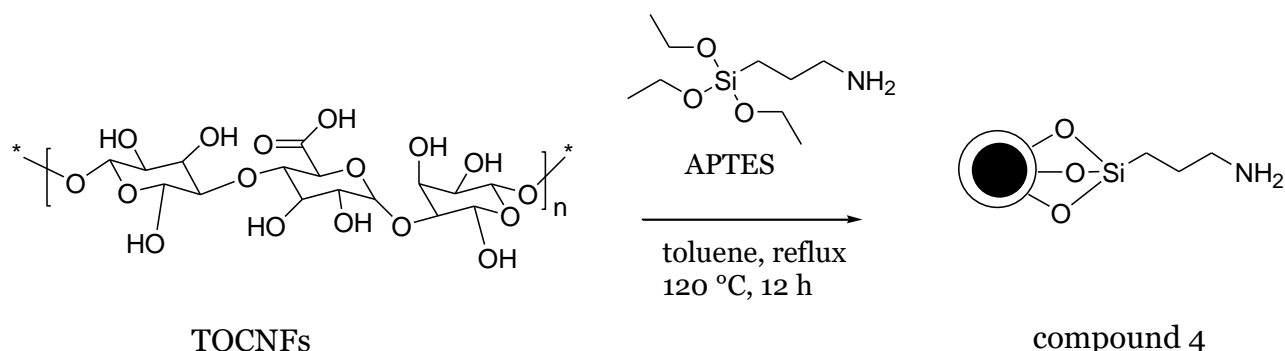


Figure 3.3.9: IR spectra of blanc bPEI, and derivative functionalized with 4-Br,1,8-Naphtalene Anhydride. In the spectra of compound **3** and F-bPEI₃ it is possible to observe a peak at 1700 and 1656 cm^{-1} ; relative to the stretching of the imidic bonds and a peak at 700 cm^{-1} , peculiar of the alkyl halide.

3.6.8 Synthesis of compound 4

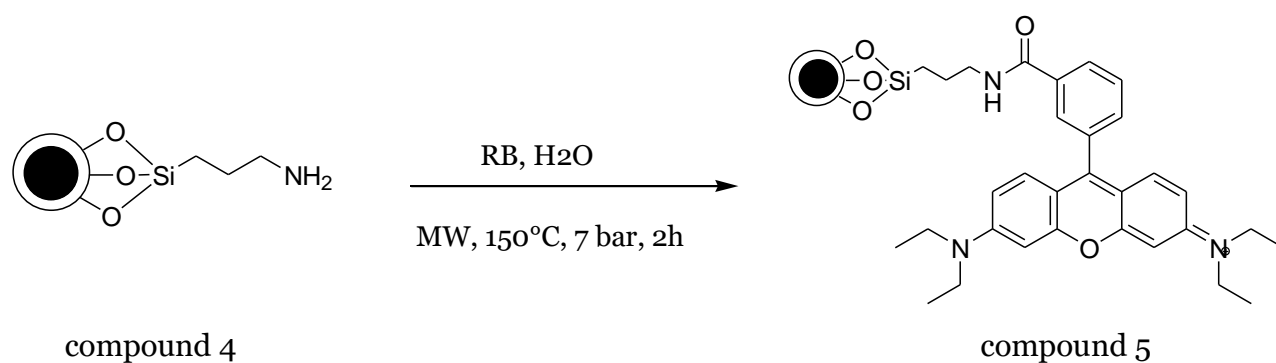


Scheme 3.3.12: reaction pathway for the synthesis of compound 4

TONCFs (500 mg) were initially dispersed in deionized water with a stoichiometric amount of NaOH, sonicated and lyophilized. Afterwards, as reported in [6], it was put in a two-necked flask with condenser under nitrogen atmosphere and dispersed in toluene (30 mL). To the suspension, 3-Amino-Propyl-Triethoxysilane (APTES, 220 mg, 1 mmol) was added dropwise. The reaction was refluxed for 12 hours at 120°C under stirring.

The product was then filtered on a Büchner funnel and washed with toluene, DCM, MeOH, AcOEt, water and acetone and dried in air on a laboratory glass. The colour of the solid changed from white to beige. Then the ICP-OES analysis was performed to estimate the amount of reacted silane (grafting of the silane of TONCFs about 10 %)

3.6.9 Synthesis of compound 5



Scheme 3.3.13: reaction pathway for the synthesis of compound 5

Compound **4** (100 mg, 0.617 mmol) was dispersed in water (10 mL) in a 15 mL microwave vial, then Rhodamine-B (59 mg, 0.123 mmol) was added to the suspension. The reaction was conducted in the microwave at 150°C, 6-7 bar for two hours. The final product was filtrated on a Büchner funnel and washed with deionized water, 0.1 M HCl_{aq}, 0.1 M NaOH_{aq}, MeOH, toluene, DCM and acetone.

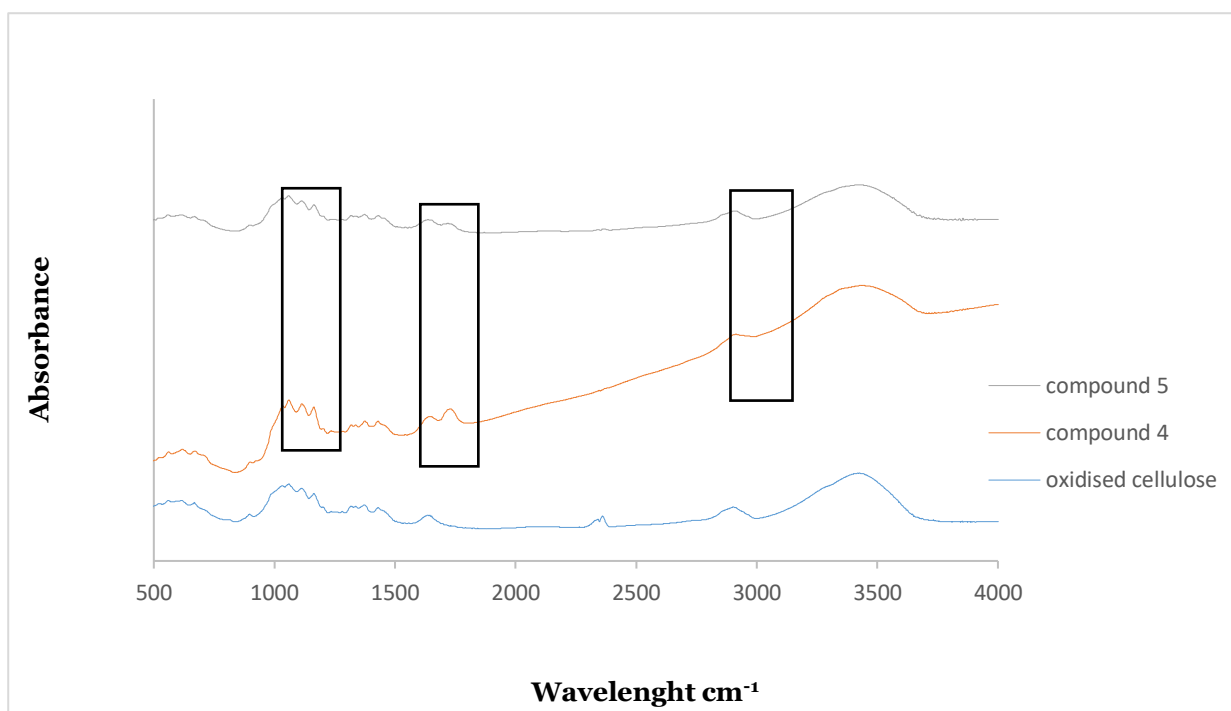
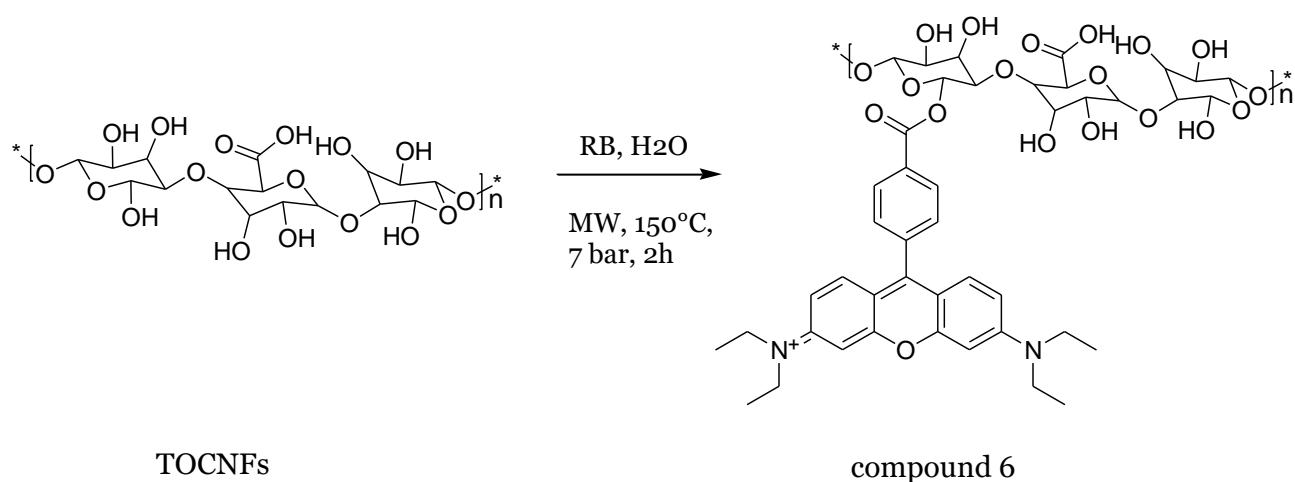


Figure 3.3.10: IR spectra of oxidised cellulose, and derivative functionalized with APTES and then with Rhodamine B. In the spectra of compound 4 and compound 5 it is possible to observe a peak at 3000 cm⁻¹; relative to the stretching of the primary and secondary amines and a peak at 1175 and between 1500-1750 cm⁻¹, relative to the imidic bond

3.6.10 Synthesis of compound 6



Scheme 3.3.14: reaction pathway for the synthesis of compound 6

Rhodamine-B (59 mg, 0.123 mmol) was dissolved in 10 mL of water under stirring in a 15 mL microwave vial. Oxidized cellulose (100 mg, 0.17 mmol) was added to the solution, obtaining a heterogeneous suspension. The reaction was carried in the microwave at 150°C, 6-7 bar for two hours. The obtained solid was then washed with deionized water, 0.1 M HCl_{aq}, 0.1 M NaOH_{aq}, MeOH, toluene, DCM and acetone. The yield achieved was almost quantitative, about the 96%.

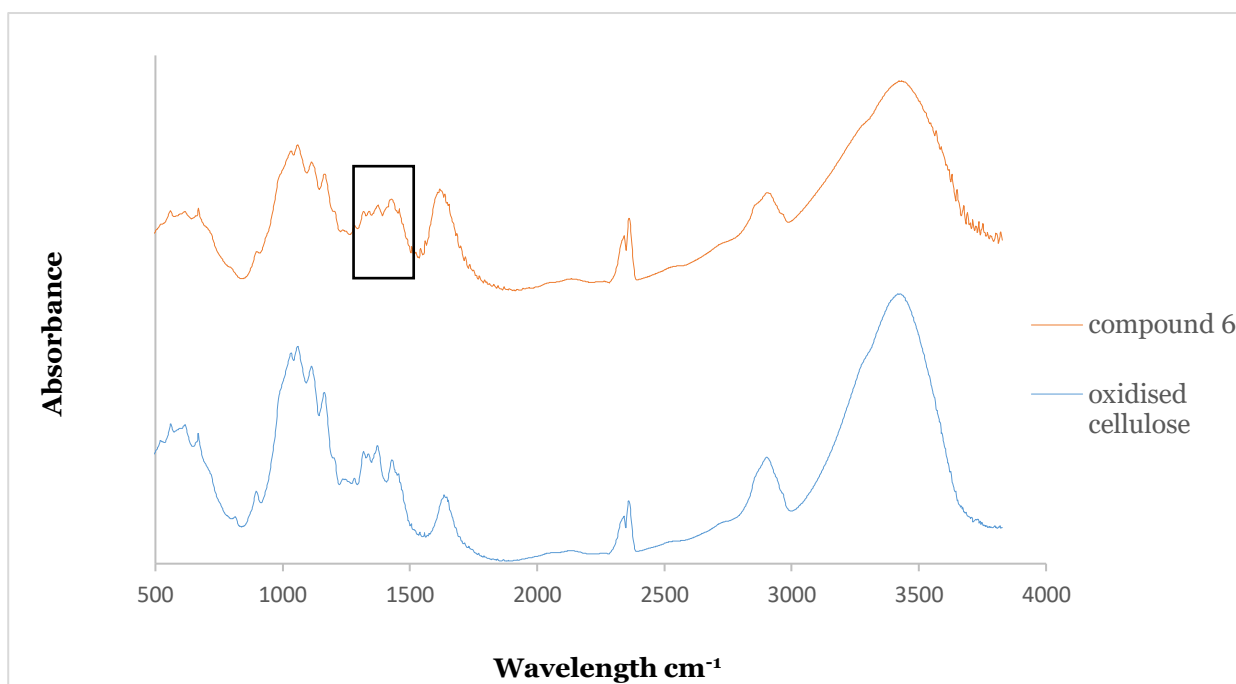


Figure 3.3.11: IR spectra of oxidised cellulose, and derivative functionalized with Rhodamine B. In the spectra of compound 6 it is possible to observe a peak at 1400 cm⁻¹; relative to the double bond C-C of the aromatics

3.6.11 Preparation of the sponges

Different amounts of oxidized cellulose were dispersed in water to obtain a homogeneous solution 3% w/v, as states the general protocol. Then a water solution of functionalized and non-functionalized bPEI in different ratios was added portionwise (see Table 2.1, 2.2, 2.3 of Results and Discussion). The mixtures were put in a well-plate and underwent the freezing and thermal protocol. Then, the sponges were washed with water (150 mL/g_{sponge}) three times and once with EtOH.

3.7 UV absorption spectroscopy

To quantify the amount of fluorophore grafted on the primary amine of bPEI, hence on the NS, the UV absorption spectroscopy was performed.

The analysis undergoes the principles here reported.

The transmittance (T) is defined by the ratio I/I_0 . On this basis, the absorbance (A) is defined as reported in Eq. 3.3:

Eq.3 5:

$$A = -\log_{10} T = \log_{10} \frac{I_0}{I}$$

Equation 3.3: relation between absorbance and transmittance

If the absorbance is known, the concentration of the absorbing species can be linearly related to it through the Lambert-Beer equation, Eq. 3.4:

Eq.3.4

$$A = \log_{10} \frac{I_0}{I} = \varepsilon CL$$

Equation 3.4: Lambert-Beer law

where ε (molar absorptivity) measures the strength of light attenuation of the chemical species at a given wavelength, C is the concentration of the absorbed species (mol/L) and d is the path length by the sample (cm).

Using this technique, a calibration line expressed in both mg/mL and $\mu\text{mol/mL}$ of compounds **1,2,3** was built by matching the Lambert-Beer law with the linear equation $y = mx + q$, where y is the absorbance measurements obtained through the UV spectroscopy, and x is the concentration. The parameters q and m (angular coefficient and intercept) are obtained by means of a linear regression of the data. The UV analysis was then performed on samples of each grafted b-PEI at different concentration. Hence, m and q are used to establish the amount of fluorophore present in each grafted polymer sample analysed, as shown in Eq. 3.5

Eq.3.6:

$$x = \frac{y - q}{m} \left[\frac{\mu\text{mol}}{\text{mL}} \right]$$

Equation 3.5: reformulation of the calibration line

The evaluation of the amount of sensor grafted on the sponges was achieved by dividing the found value of concentration by the known concentration in mg/mL of the polymeric sample.

3.7.1 UV-vis analysis of compound 1 and F-bPEI1b

Two starting reference solutions have been prepared, the first with concentration of 9.7 mg/mL while the second of 6.3 mg/mL and in both cases the solvent was acid water (0.1N HCl). The maximum value of absorption was found at a wavelength of 561.5 nm

The analysis was performed at different dilutions, as shown in Figure 3.12 and Table 3.2.

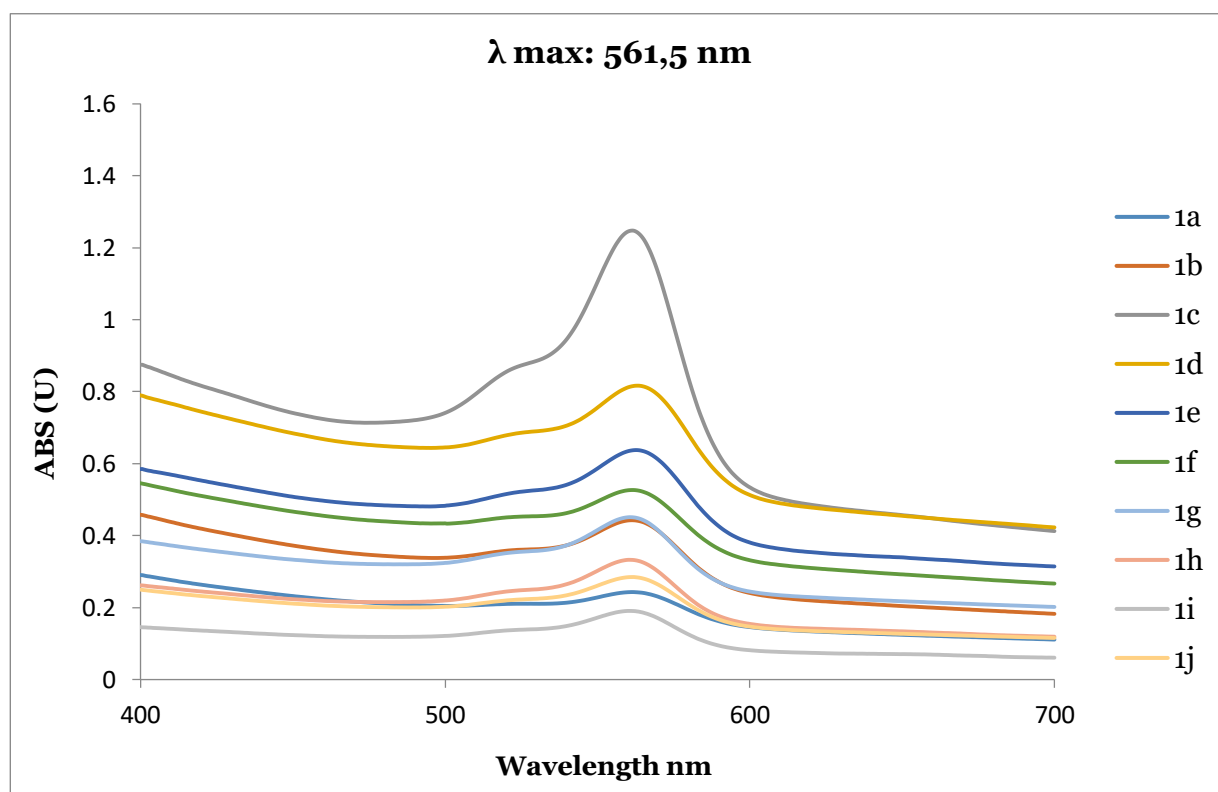
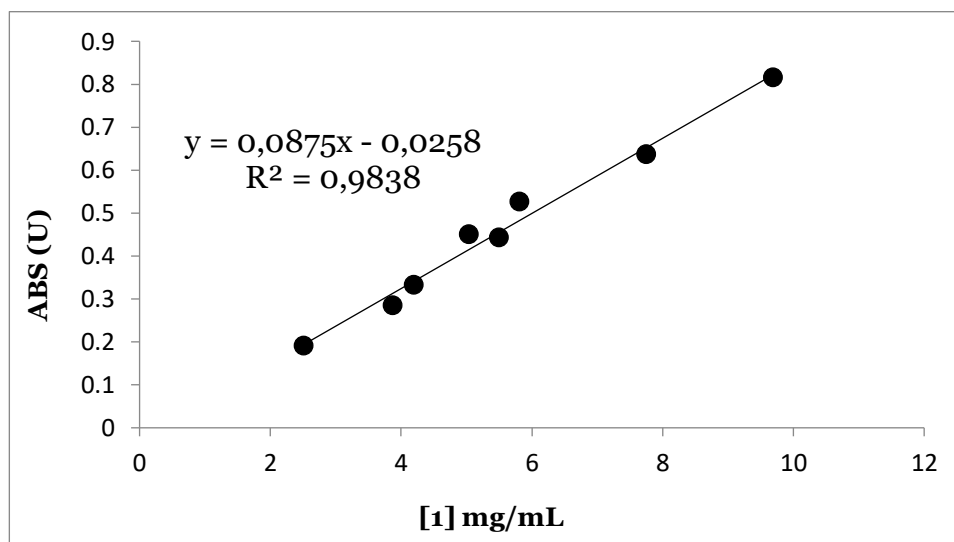


Figure 3.3.12: UV spectra at different concentrations of compound 1 in HCl 0.1N

Table 3.3.2: concentrations and measured absorptions of compound **1**

Sample	Absorption @ 561.5 nm	Concentration [mg/mL]	Concentration [μmol/mL]
1a	0.2601	5.5	11.349
1b	0.2133	4.2	8.6664
1c	0.1693	3.88	8.0061
1d	0.1297	2.52	5.1998
1e	0.2599	5.82	12.009
1f	0.3924	9.7	20.015
1g	0.3227	7.76	16.012
1h	0.2491	5.04	10.399

Then the calibration lines have been plotted with [mg/mL] and [μmol/mL] on x-axis.



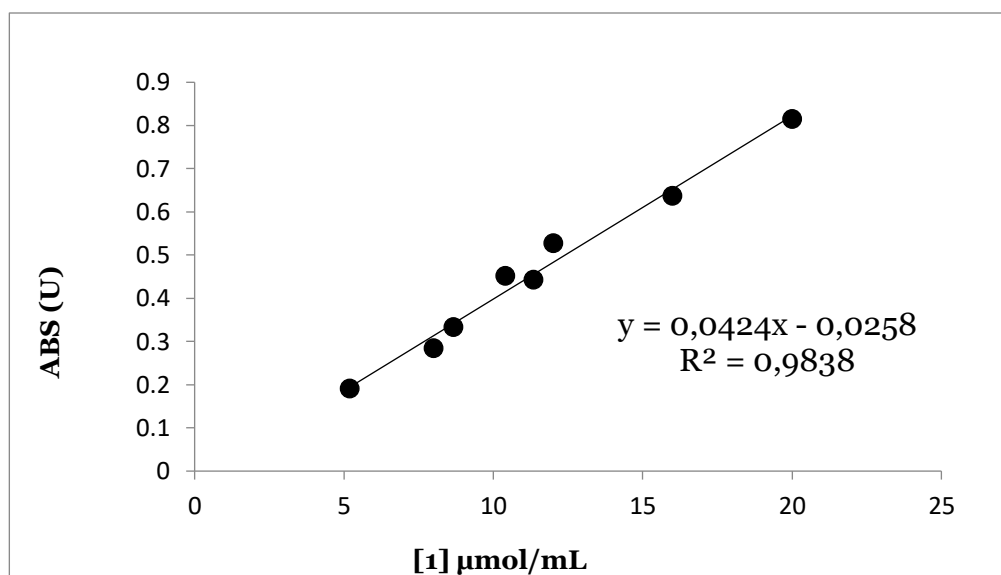


Figure 3.3.13: calibration lines of compound **1**, expressed in mg/mL and $\mu\text{mol/mL}$

Regarding the grafted polyamine, 1.8 mL of F-bPEI1b were dissolved in water and 0.2 mL of 0.1 N HCl were added, obtaining a mother solution with concentration 40 mg/mL. The solution was then diluted as reported in Figure 3.14 and Table 3.3.

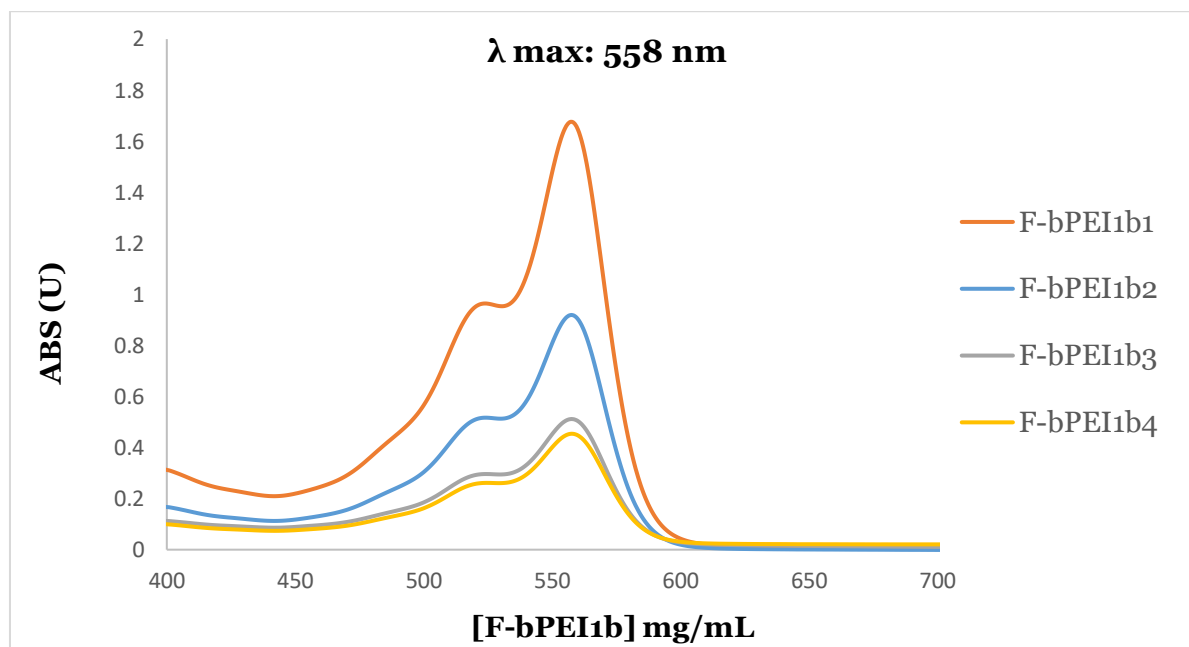


Figure 3.3.14: UV-vis spectra of F-bPEI1b in HCl 0.1N at different concentrations

Table 3.3.3: concentrations and measured absorptions of F-bPEI1b

Sample	Absorption @ 558 nm	Concentration [mg/mL]
F-bPEI1b1	1.6749	3.32
F-bPEI1b2	0.9186	1.81
F-bPEI1b3	0.5114	0.91
F-bPEI1b4	0.4539	0.79

By means of Eq.5, it was possible to calculate the amount of chromophore in each cuvette of F-bPEI1b, then the ratios fluorophore/polymer, as shown in Table 3.4.

Table 3.3.4: fluorophore present in each sample of F-bPEI1b and corresponding degree of grafting

Sample	Fluorophore in the cuvette [$\mu\text{mol/mL}$]	Fluorophore/F-bPEI1b [$\mu\text{mol/mg}$]
F-bPEI1b1	92.301	27.843
F-bPEI1b2	49.57	27.387
F-bPEI1b3	26.568	29.357
F-bPEI1b4	23.315	29.513

The obtained degree of grafting was 28.515 $\mu\text{mol/mg}$, which is impossible, since it is not coherent with the stoichiometric amount used in the reaction. A deepened explanation of this anomaly is given in the Results and Discussion section.

3.7.2 UV-vis analysis of compound 2 and F-bPEI2

10 mg of the reference compound were put into a 10 mL volumetric flask and dissolved in acid water (0.1N HCl), giving an initial concentration of the mother solution of 1 mg/mL. The peak of absorption was recorded at 344 nm.

The analysis was performed at different dilutions, as shown in Figure 3.13 and Table 3.5.

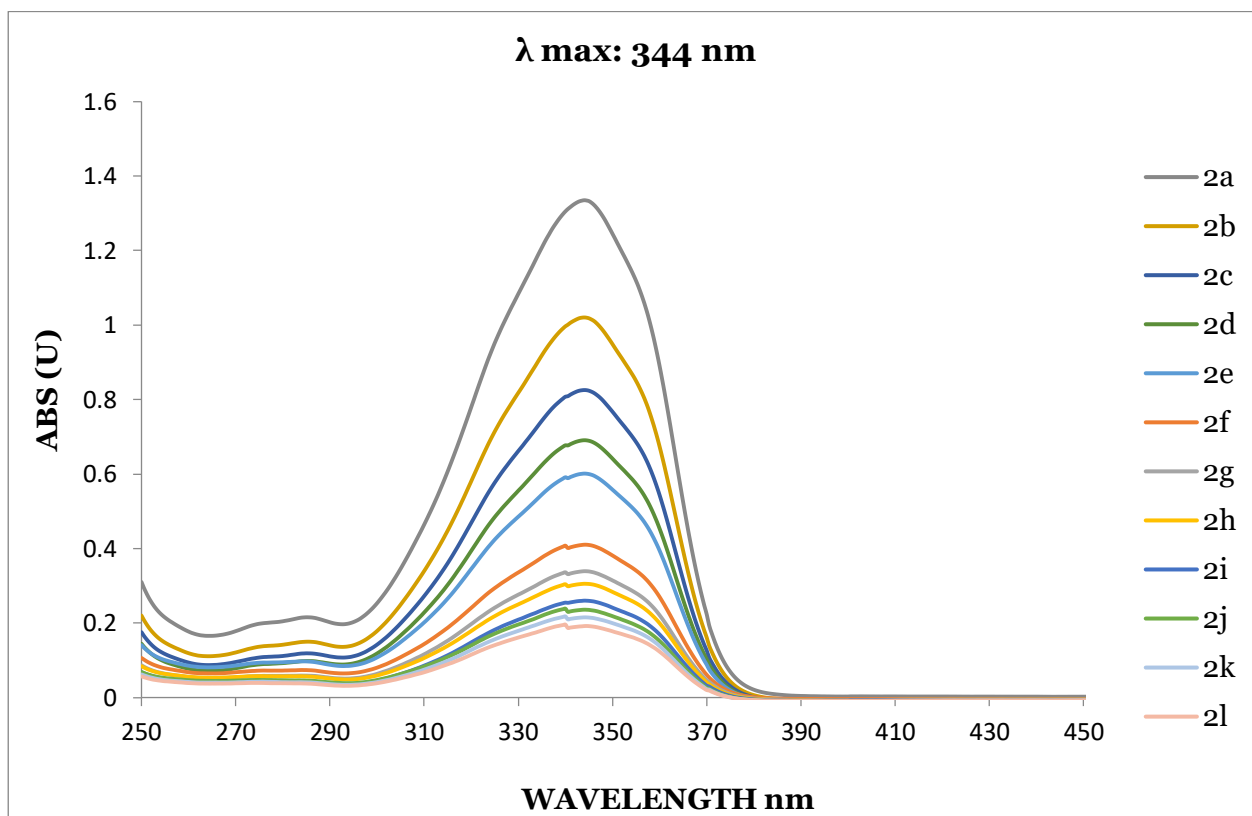
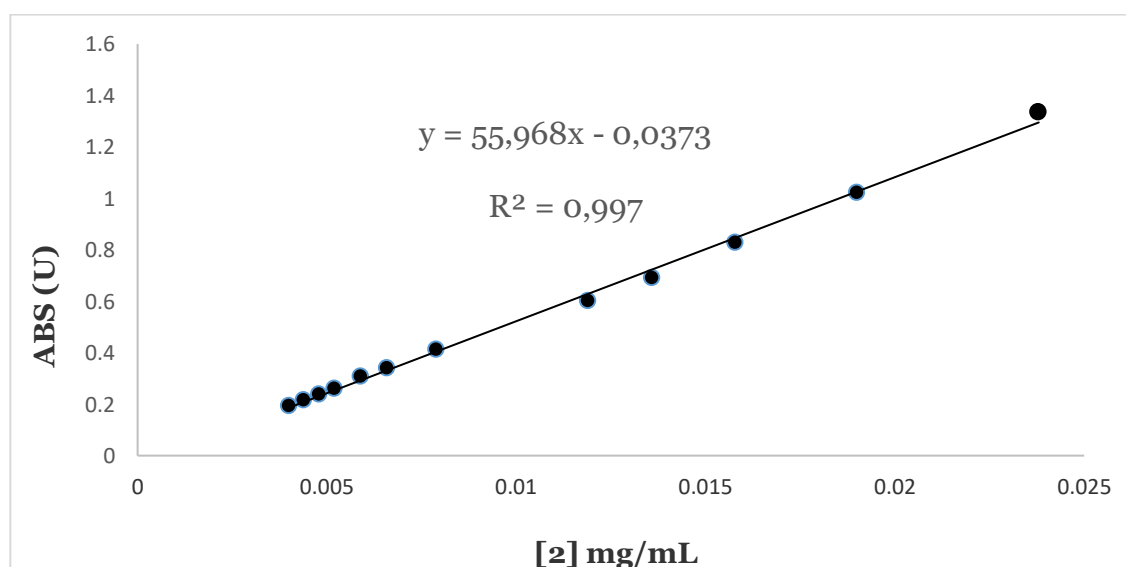


Figure 3.3.15: UV spectra at different concentrations of compound 2 in HCl 0.

Table 3.3.5: concentrations and measured absorptions of compound 2

Sample	Absorption @ 344 nm	Concentration [mg/mL]	Concentration [$\mu\text{mol/mL}$]
2a	1.3350	0.0238	0.0989
2b	1.0203	0.0190	0.0791
2c	0.8254	0.0158	0.0659
2d	0.6907	0.0136	0.0565
2e	0.6012	0.0119	0.0494
2f	0.4103	0.0079	0.0330
2g	0.3392	0.0066	0.0275
2h	0.3054	0.0059	0.0247
2i	0.2601	0.0052	0.0215
2j	0.2358	0.0048	0.0198
2k	0.2152	0.0044	0.0183
2l	0.1919	0.0040	0.0165

Calibration lines with [mg/mL] and [$\mu\text{mol/mL}$] on x-axis are reported below.



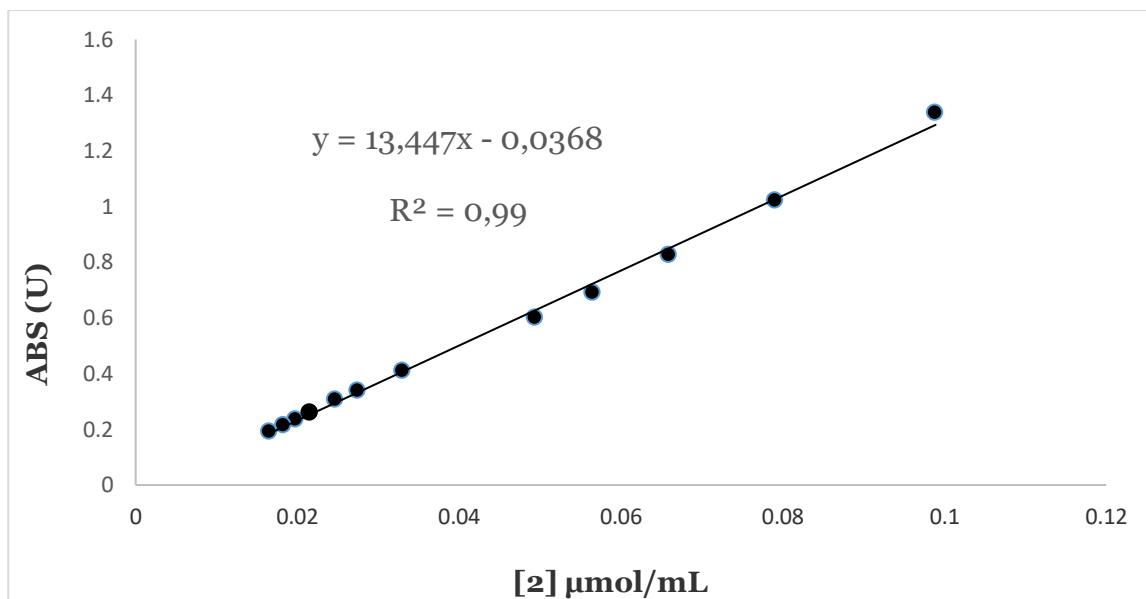


Figure 3.3.16: calibration lines of compound **2**, expressed in mg/mL and $\mu\text{mol/mL}$

1.8 mL of F-bPEI2 were dissolved in water and 0.2 mL of 0.1N HCl were added, obtaining a mother solution with concentration 40 mg/mL. The solution was then diluted as reported in Table 3.6, obtaining the spectra reported in Figure 3.15.

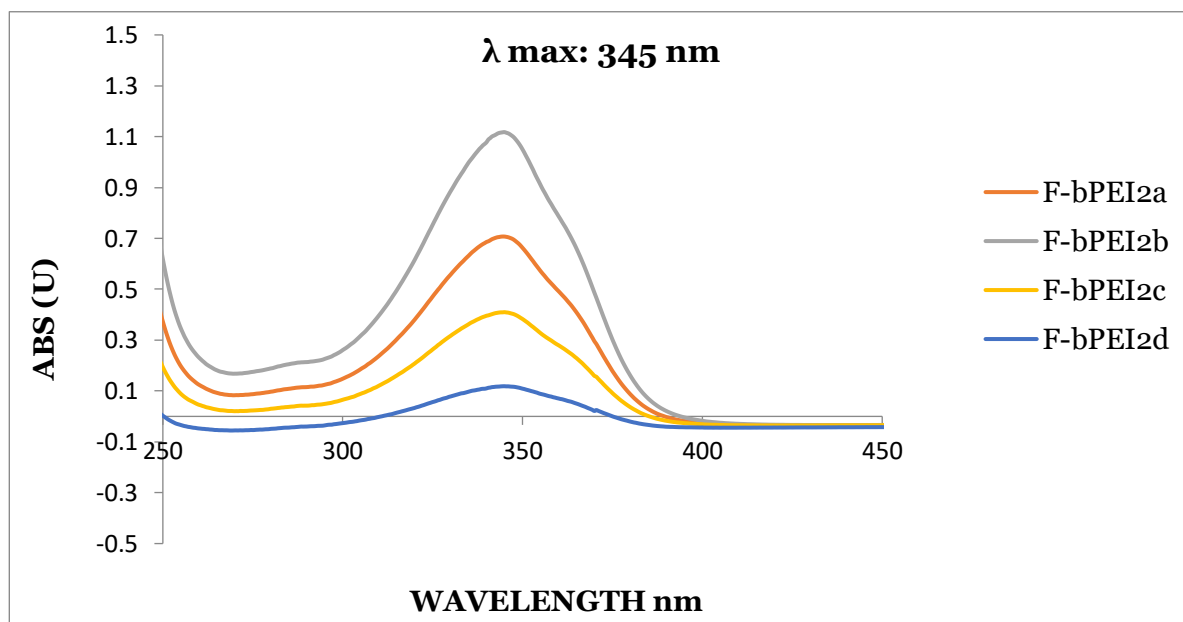


Figure 3.3.17: UV spectra of F-PEI2 in HCl 0.1N at different concentrations

Table 3.3.6: concentrations and measured absorptions of F-bPEI2

Sample	Absorption @ 345 nm	Concentration [mg/mL]
F-bPEI2a	0.7071	0.0889
F-bPEI2b	1.1177	0.1400
F-bPEI2c	0.4098	0.0560
F-bPEI2d	0.1186	0.0224

The amount of chromophore in each cuvette analysed was estimated using Eq.3.5, as reported in the next table.

Table 3.3.7: fluorophore present in each sample of F-bPEI2 and corresponding degree of grafting

Sample	Fluorophore in the cuvette[$\mu\text{mol/mL}$]	Fluorophore/F-bPEI2 [$\mu\text{mol/mg}$]
F-bPEI2a	0.0565	0.64
F-bPEI2b	0.0896	0.64
F-bPEI2c	0.0326	0.58
F-bPEI2d	0.0091	0.41

Using the values reported in **Table 3.7**, the average degree of grafting was 0.57 [$\mu\text{mol/mL}$].

3.7.3 UV-vis analysis of compound 3 and F-bPEI3

10 mg of the reference compound were put into a 10 mL volumetric flask and dissolved in acid water (0.1N HCl), giving an initial concentration of the mother solution of 1 mg/mL. The peak of absorption was found at a wavelength of 348 nm

The analysis was performed at different dilutions, as shown in Figure 3.16 and Table 3.8.

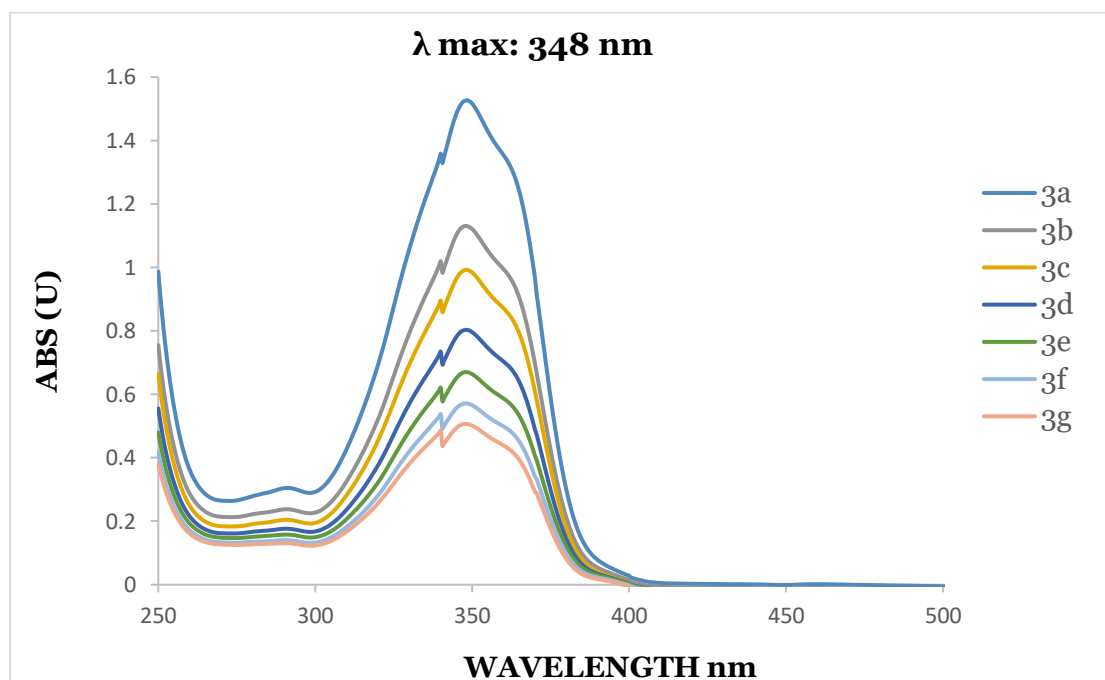


Figure 3.3.18: UV spectra at different concentrations of compound **3** in HCl 0.1N

Table 3.3.8: concentrations and measured absorptions of compound **3**

Sample	Absorption @ 348 nm	Concentration [mg/mL]	Concentration [μmol/mL]
3a	1.1309	0.0268	0.0839
3b	0.9925	0.0234	0.0734
3c	0.8032	0.0188	0.0587
3d	0.6701	0.0156	0.0490
3e	0.5715	0.0134	0.0420
3f	0.5068	0.01172	0.0367
3g	0.4769	0.0110	0.0345

Then the calibration lines have been plotted with [mg/mL] and [μ mol/mL] on x-axis.

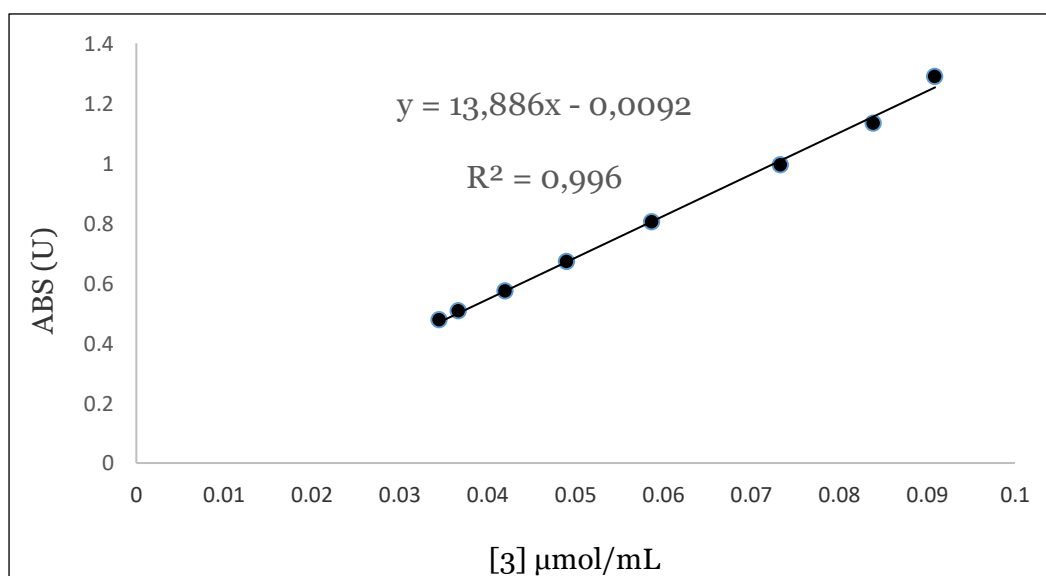
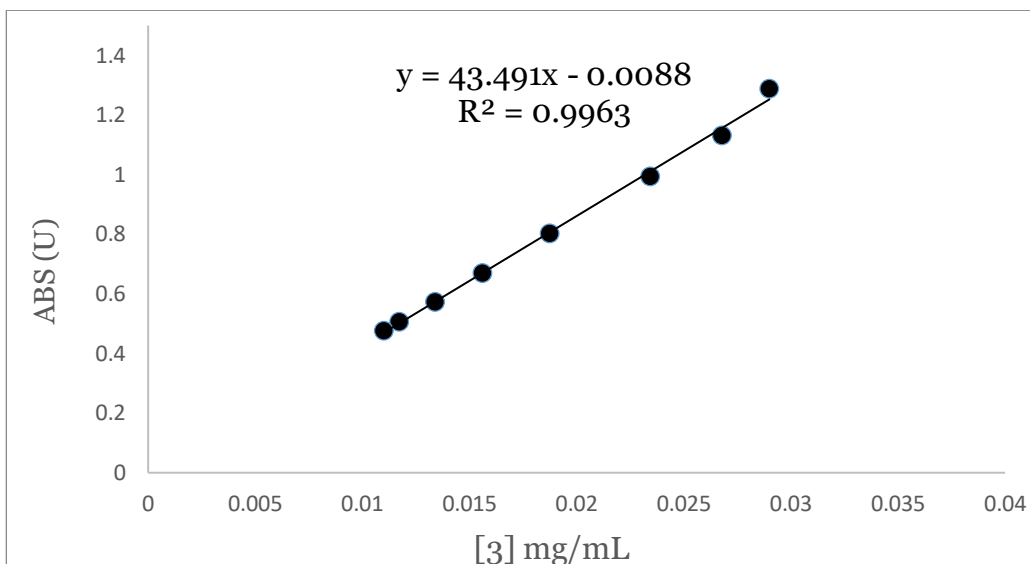


Figure 3.3.19: calibration lines of compound 3, expressed in mg/mL and $\mu\text{mol/mL}$

1.8 mL of F-bPEI₃ were dissolved in water and 0.2 mL of 0.1N HCl were added, obtaining a mother solution with concentration 5.4 mg/mL. The solution was then diluted as reported in Table 3.9, obtaining the spectra reported in Figure 3.18.

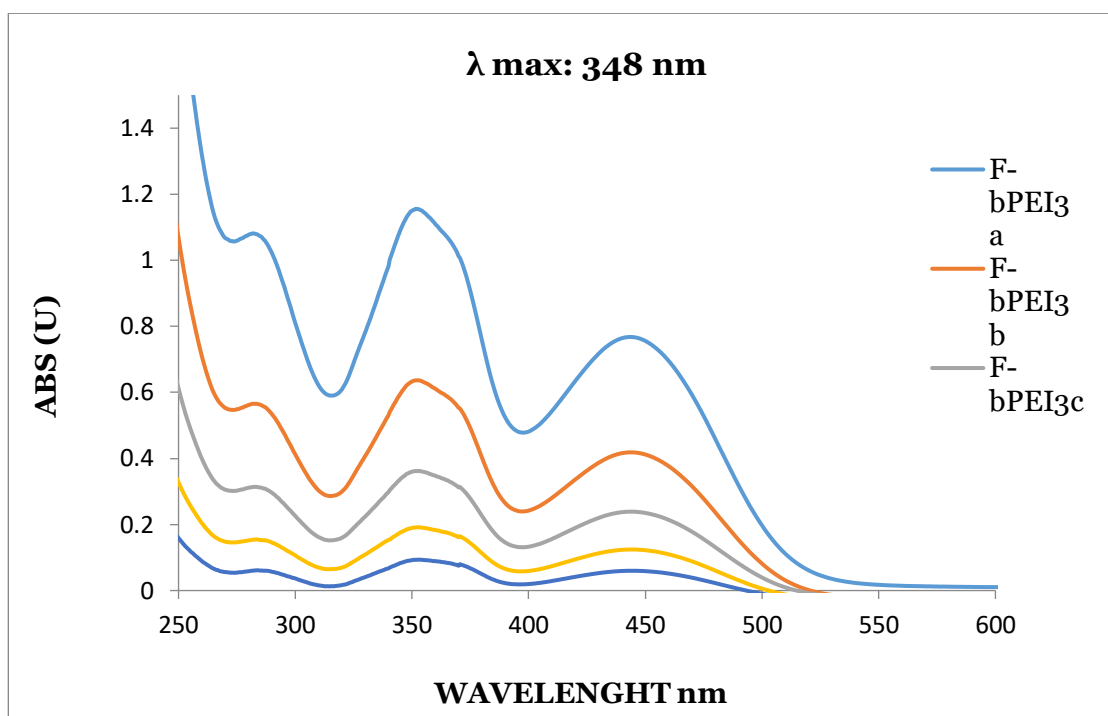


Figure 3.3.20: UV spectra of F-PEI₃ in HCl 0.1N at different concentrations

Table 3.3.9: concentrations and measured absorptions of F-bPEI₃

Sample	Absorption @ 348 nm	Concentration [mg/mL]
F-bPEI ₃ a	1.1556	0.2420
F-bPEI ₃ b	0.6361	0.1452
F-bPEI ₃ c	0.3618	0.0870
F-bPEI ₃ d	0.1909	0.0520
F-bPEI ₃ e	0.0929	0.0310

In the next table are reported the results of Eq.3.5 applied to F-bPEI₃.

Table 3.3.10: fluorophore present in each sample and corresponding degree of grafting

Sample	Fluorophore in the cuvette[$\mu\text{mol/mL}$]	Fluorophore/F-bPEI2 [$\mu\text{mol/mg}$]
F-bPEI3a	0.0839	0.35
F-bPEI3b	0.0465	0.32
F-bPEI3c	0.0267	0.31
F-bPEI3d	0.0144	0.28

From **Table 3.10**, it was possible to prove that the average degree of grafting was 0.3 [$\mu\text{mol/mL}$].

4. Conclusion and future perspective

The focus of this work was to find green and ecological strategies to functionalise a polymeric composite material with fluorophores UV-vis detectable for the monitoring of an engineered nanomaterial used for water remediation.

The properties of this material rely on the imidic bond between the carboxylic moieties of TONCFs and the primary amine of bPEI, giving the proper mechanical strength and adsorption capability of polluting heavy metal ions through their chelation done by the polyamine.

The material itself does not provoke any harm in its action environment, since several improvements in the formulation were made in order to erase the risk of toxicity of one of its components, bPEI. So, the necessity to monitor the degradation pathway of the NS become paramount. An efficient and effective strategies to check the behaviour of the problematic polymer was thought to be the selective grafting with UV fluorophores. Three different molecules were used (Rhodamine-B, 1,8-Naphthalic Anhydride and 4-Br-1,8 Naphthalic Anhydride) each of them responding at a different wavelength.

Then the synthesis of the model compound was achieved. They were synthesized performing a reaction between the pure chromophore and a diamine, in this way they had an appendage like the one present on the polymer backbone. The estimation of the degree of grafting of the fluorophore on bPEI. There are problems for the evaluation of the grafting of Rhodamine-B, since it presents incoherent results using the UV spectroscopy analysis. This issue is under investigation. Anyway, it was possible to perform the esteem of the extent of functionalization with the other two chromophores

Samples of the grafted NanoSponges underwent ecotoxicological tests, to see if the behaviour of new material and the potential modification to be applied.

These tests proved that marine biota exposed to water with low dilution (0.03 mg/L) of the material showed no fluorescence, meaning that no bioaccumulation was achieved.

Given the promising results, we now know the rightful dilution to use for the grafting of bPEI with Rhodamine-B, once it is found a solution to the problem of the degree of

grafting estimation. So, the next steps in the research will be the further decrease of concentration of the fluorophore on the polymer, then the synthesis of NS with both polymers functionalised.

5. Bibliography

1. Study, N. A. E. *et al.* Environmentally Sustainable and Ecosafe Polysaccharide-Based Materials for Water. doi:10.3390/ma11071228
2. Godwin, H. *et al.* Nanomaterial Categorization for Assessing Risk Potential To Facilitate Regulatory Decision-Making. *ACS Nano* **9**, 3409–3417 (2015).
3. Karn, B. & Otto, M. *Nanotechnology and in situ remediation: A review of the benefits and potential risks.* *Environ. Health Persp.* **117**, (2009).
4. Trujillo-Reyes, J., Peralta-Videa, J. R. & Gardea-Torresdey, J. L. Supported and unsupported nanomaterials for water and soil remediation: Are they a useful solution for worldwide pollution? *J. Hazard. Mater.* **280**, 487–503 (2014).
5. Thomas, B. *et al.* Nanocellulose, a Versatile Green Platform: From Biosources to Materials and Their Applications. *Chem. Rev.* **118**, 11575–11625 (2018).
6. Dufresne, A. *Nanocellulose: from nature to high performance tailored materials.* *De Gruyter. Nanocellulose* (2012). doi:10.1515/9783110254600
7. Wicklein, B. *et al.* Thermally insulating and fire-retardant lightweight anisotropic foams based on nanocellulose and graphene oxide. *Nature nanotechnology* **10**, (2014).
8. Habibi, Y. Chem Soc Rev Key advances in the chemical modification of nanocelluloses. 1519–1542 (2014). doi:10.1039/c3cs60204d
9. Klemm, D., Heublein, B., Fink, H.-P. & Bohn, A. *Cellulose: Fascinating Biopolymer and Sustainable Raw Material.* *Angewandte Chemie (International ed. in English)* **44**, (2005).
10. Wang, H., Gurau, G. & Rogers, R. D. Ionic liquid processing of cellulose. *Chem. Soc. Rev.* **41**, 1519–1537 (2012).
11. Metzger, J. & Hüttermann, A. *Sustainable global energy supply based on lignocellulosic biomass from afforestation of degraded areas.* *Die Naturwissenschaften* **96**, (2009).
12. Haghghi Mood, S. *et al.* Lignocellulosic biomass to bioethanol, a comprehensive review with a focus on pretreatment. *Renew. Sustain. Energy Rev.* **27**, 77–93 (2013).
13. Quiroz Castañeda, R. & Folch-Mallol, J. *Proteínas que remodelan y degradan la pared celular vegetal: perspectivas actuales.* *Biotecnología Aplicada* **28**, (2011).
14. Isogai, A., Saito, T. & Fukuzumi, H. TEMPO-oxidized cellulose nanofibers. *Nanoscale* **3**, 71–85 (2011).
15. Sogai, B. A. I. Review Development of completely dispersed cellulose nano fi bers. **94**, 161–179 (2018).
16. Shokri, J. Application of Cellulose and Cellulose Derivatives in Pharmaceutical Industries. in (ed. Godbout, K. A. E.-T. van de V. E.-L.) Ch. 3 (IntechOpen, 2013). doi:10.5772/55178
17. Boy, R., Narayanan, G. & Kotek, R. Formation of Cellulose and Protein Blend Biofibers. in *Polysaccharide-Based Fibers and Composites: Chemical and Engineering Fundamentals and Industrial Applications* 77–117 (2018). doi:10.1007/978-3-319-56596-5_5
18. Pranger, L. & Tannenbaum, R. Biobased Nanocomposites Prepared by In Situ Polymerization of

- Furfuryl Alcohol with Cellulose Whiskers or Montmorillonite Clay. *Macromolecules* **41**, 8682–8687 (2008).
19. Reid, M. S., Villalobos, M. & Cranston, E. D. Benchmarking Cellulose Nanocrystals: From the Laboratory to Industrial Production. (2017). doi:10.1021/acs.langmuir.6b03765
 20. H.P.S, A. K., Bhat, A. H. & F. Ireana Yusra, A. *Green Composites from Sustainable Cellulose Nanofibrils: A review. Carbohydrate Polymers In Press*, (2011).
 21. Siro, I. & Plackett, D. *Siro, I. & Plackett, D. Microfibrillated cellulose and new nanocomposite materials: a review. Cellulose 17, 459-494. Cellulose* **17**, (2010).
 22. Habibi, Y. Key advances in the chemical modification of nanocelluloses. *Chem. Soc. Rev.* **43**, 1519–1542 (2014).
 23. Klemm, D. *et al.* Nanocelluloses: A New Family of Nature-Based Materials. *Angew. Chemie Int. Ed.* **50**, 5438–5466 (2011).
 24. Habibi, Y., Lucia, L. A. & Rojas, O. J. Cellulose Nanocrystals: Chemistry, Self-Assembly, and Applications. *Chem. Rev.* **110**, 3479–3500 (2010).
 25. Thomas, B. *et al.* Nanocellulose , a Versatile Green Platform : From Biosources to Materials and Their Applications. (2018). doi:10.1021/acs.chemrev.7b00627
 26. El-Saied, H., H. Basta, A. & Gobran, R. *Research Progress in Friendly Environmental Technology for the Production of Cellulose Products (Bacterial Cellulose and Its Application). Polymer-plastics Technology and Engineering - POLYM-PLAST TECHNOL ENG* **43**, (2004).
 27. Bodin, A. *et al.* Influence of cultivation conditions on mechanical and morphological properties of bacterial cellulose tubes. *Biotechnol. Bioeng.* **97**, 425–434 (2007).
 28. Iguchi, M., Yamanaka, S. & J. Budhiono, A. *Bacterial cellulose—a masterpiece of nature’s arts. Journal of Materials Science* **35**, (2000).
 29. Czaja, W., Romanovicz, D. & Brown, R. M. *Structural investigation of microbial cellulose produced in stationary and agitated culture. Cellulose* **11**, (2004).
 30. Klemm, D. *et al.* Nanocelluloses as Innovative Polymers in Research and Application Polysaccharides II. in *Advances in Polymer Science* **205**, 49–96 (2006).
 31. Wang, L., Schütz, C., Salazar-Alvarez, G. & Titirici, M.-M. *Carbon aerogels from bacterial nano cellulose as anodes for lithium ion batteries. RSC Advances* **4**, (2014).
 32. K Czaja, W., J Young, D., Kaweck, M. & Malcolm Brown, R. *The Future Prospects of Microbial Cellulose in Biomedical Applications. Biomacromolecules* **8**, (2007).
 33. Li, P., Sirviö, J., Haapala, A. & Liimatainen, H. *Cellulose Nanofibrils from Nonderivatizing Urea-Based Deep Eutectic Solvent Pretreatments. ACS applied materials & interfaces* **9**, (2016).
 34. Hassan, M., P Mathew, A., Hassan, E., El-Wakil, N. & Oksman, K. *Nanofibers from bagasse and rice straw: Process optimization and properties. Wood Science and Technology* **46**, (2012).
 35. Tsuzuki, T., Rana, R., Liu, Q., Zhang, L. & Wang, X. *Production of Green Nanomaterials. ICONN 2010 - Proceedings of the 2010 International Conference on Nanoscience and Nanotechnology* (2010). doi:10.1109/ICONN.2010.6045222
 36. Moon, R. J., Martini, A., Nairn, J., Simonsen, J. & Youngblood, J. Cellulose nanomaterials review: structure, properties and nanocomposites. *Chem. Soc. Rev.* **40**, 3941–3994 (2011).
 37. Isogai, A. & Bergström, L. Preparation of cellulose nanofibers using green and sustainable chemistry. *Curr. Opin. Green Sustain. Chem.* **12**, 15–21 (2018).

38. Chen, Y., Wu, Q., Huang, B., Huang, M. & Ai, X. *Isolation and Characteristics of Cellulose and Nanocellulose from Lotus Leaf Stalk Agro-wastes*. *BioResources* **10**, (2014).
39. Chen, Y., Xu, W., Liu, W. & Zeng, G. *Responsiveness, swelling, and mechanical properties of PNIPAA nanocomposite hydrogels reinforced by nanocellulose*. *Journal of Materials Research* **30**, (2015).
40. Hamed, M. *et al.* *Highly Conducting, Strong Nanocomposites Based on Nanocellulose-Assisted Aqueous Dispersions of Single-Wall Carbon Nanotubes*. *ACS nano* **8**, (2014).
41. van de Ven, T. & Sheikhi, A. *Hairy cellulose nanocrystalloids: A novel class of nanocellulose*. *Nanoscale* **8**, (2016).
42. Abdul Rashid, E. S., Muhd Julkapli, N. & Yehye, W. A. *Nanocellulose reinforced as green agent in polymer matrix composites applications*. *Polym. Adv. Technol.* **29**, 1531–1546 (2018).
43. Dufresne, A. *Nanocellulose: A new ageless bionanomaterial*. *Materials Today* **16**, (2013).
44. Peng, Y. *et al.* *Influence of drying method on the material properties of nanocellulose I: Thermostability and crystallinity*. *Cellulose* **20**, (2013).
45. B, D. *et al.* *Utilization of various lignocellulosic biomass for the production of nanocellulose: a comparative study*. *Cellulose* **22**, (2015).
46. Mohammed, N., Grishkewich, N. & Tam, K. C. *Cellulose nanomaterials: Promising sustainable nanomaterials for application in water/wastewater treatment processes*. *Environ. Sci. Nano* **5**, 623–658 (2018).
47. Dąbrowski, A. *Adsorption — from theory to practice*. *Adv. Colloid Interface Sci.* **93**, 135–224 (2001).
48. Khajeh, M., Laurent, S. & Dastafkan, K. *Nano-adsorbents: Classification, Preparation, and Applications (with Emphasis on Aqueous Media)*. *Chem. Rev.* **113**, 7728–7768 (2013).
49. Abraham, E. *et al.* *Extraction of nanocellulose fibrils from lignocellulosic fibres: A novel approach*. *Carbohydrate Polymers* **86**, (2011).
50. Cherian, B. *et al.* *Isolation of nanocellulose from pineapple leaf fibres by steam explosion*. *Carbohydrate Polymers* **81**, (2010).
51. Hettrich, K., Pinnow, M., Volkert, B., Passauer, L. & Fischer, S. *Novel aspects of nanocellulose*. *Cellulose* **21**, (2014).
52. Geng, T. *et al.* *Journal of Environmental Chemical Engineering* *The chromogenic and fluorescent sensing properties for a water soluble polymeric chemosensor bearing rhodamine ethanediamine moieties with oxethyl (OCH₂CH₂) as a spacer*. *Biochem. Pharmacol.* **5**, 906–914 (2017).
53. Taokaew, S., Seetabhawang, S., Siripong, P. & Phisalaphong, M. *Biosynthesis and Characterization of Nanocellulose-Gelatin Films*. *Materials* **6**, (2013).
54. Ahrem, H. *et al.* *Laser-structured bacterial nanocellulose hydrogels support ingrowth and differentiation of chondrocytes and show potential as cartilage implants*. *Acta Biomater.* **10**, 1341–1353 (2014).
55. Kubiak, K. *et al.* *Complete genome sequence of *Gluconacetobacter xylinus* E25 strain—Valuable and effective producer of bacterial nanocellulose*. *Journal of Biotechnology* **176**, (2014).
56. Bhatnagar, A. & Sain, M. *Processing of Cellulose Nanofiber-reinforced Composites*. *Journal of Reinforced Plastics and Composites* **24**, (2005).

57. Rojas, J., Bedoya, M. & Ciro, Y. Current Trends in the Production of Cellulose Nanoparticles and Nanocomposites for Biomedical Applications. in 193–228 (2015). doi:10.5772/61334
58. Reid, M. S., Villalobos, M. & Cranston, E. D. Benchmarking Cellulose Nanocrystals: From the Laboratory to Industrial Production. *Langmuir* **33**, 1583–1598 (2017).
59. Mandal, A. & Chakrabarty, D. Isolation of nanocellulose from waste sugarcane bagasse (SCB) and its characterization. *Carbohydrate Polymers - CARBOHYD POLYM* **86**, (2011).
60. Lu, Z. *et al.* Preparation, characterization and optimization of nanocellulose whiskers by simultaneously ultrasonic wave and microwave assisted. *Bioresource technology* **146C**, (2013).
61. Shahabi-Ghahfarrokhi, I., Khodaiyan, F., Mousavi, M. & Yousefi, H. Preparation and Characterization of Nanocellulose from Beer Industrial Residues Using Acid Hydrolysis/Ultrasound. *Fibers and Polymers* **16**, (2015).
62. Abd Hamid, S. B., Al Amin, M. & Ali, M. Zeolite Supported Ionic Liquid Catalyst for the Synthesis of Nano-Cellulose from Palm Tree Biomass. *Advanced Materials Research* **925**, (2014).
63. Mishra, S., Thirree, J., Manent, A.-S., Chabot, B. & Daneault, C. Ultrasound-catalyzed TEMPO-mediated oxidation of native cellulose for the production of nanocellulose: Effect of process variables. *Bioresources* **6**, (2011).
64. Mishra, S., Manent, A.-S., Chabot, B. & Daneault, C. Production of nano-cellulose from native cellulose - Various options utilizing ultrasound. *Bioresources* **7**, (2012).
65. Müller, A. *et al.* The biopolymer bacterial nanocellulose as drug delivery system: Investigation of drug loading and release using the model protein albumin. *Journal of pharmaceutical sciences* **102**, (2013).
66. Loranger, E., Jradi, K. & Daneault, C. Nanocellulose Production by Ultrasound-Assisted TEMPO Oxidation of Kraft Pulp on Laboratory and Pilot Scales. *IEEE International Ultrasonics Symposium, IUS* (2012). doi:10.1109/ULTSYM.2012.0238
67. Bragd, P., van Bekkum, H. & Besemer, A. TEMPO-Mediated Oxidation of Polysaccharides: Survey of Methods and Applications: Catalytic Conversion of Renewables. Guest Editors: Herman van Bekkum and Pierre Gallezot. *Top. Catal.* **27**, (2004).
68. Tavernier, M. L., Delattre, C., Petit, E. & Michaud, P. β -(1,4)-Polyglucuronic Acids - An Overview. *Open Biotechnol. J.* **2**, 73–86 (2008).
69. Pierre, G. *et al.* TEMPO-mediated oxidation of polysaccharides: An ongoing story. *Carbohydr. Polym.* **165**, 71–85 (2017).
70. Masruchin, N., Park, B.-D., Causin, V. & Um, I. Characteristics of TEMPO-oxidized cellulose fibril-based hydrogels induced by cationic ions and their properties. *Cellulose* **22**, (2015).
71. Koga, H. *et al.* Transparent, Conductive, and Printable Composites Consisting of TEMPO-Oxidized Nanocellulose and Carbon Nanotube. *Biomacromolecules* **14**, (2013).
72. Jiang, Y., Zhao, Y., Feng, X., Fang, J. & Shi, L. TEMPO-mediated oxidized nanocellulose incorporating with its derivatives of carbon dots for luminescent hybrid films. *RSC Adv.* **6**, 6504–6510 (2016).
73. Adam, W., Saha-Möller, C. R. & Ganeshpure, P. A. Synthetic Applications of Nonmetal Catalysts for Homogeneous Oxidations. *Chem. Rev.* **101**, 3499–3548 (2001).
74. Zhang, F., Ren, H., Dou, J., Tong, G. & Deng, Y. Cellulose Nanofibril Based-Aerogel

- Microreactors : A High Efficiency and Easy Recoverable W / O / W Membrane Separation System. *Nat. Publ. Gr.* 1–7 (2017). doi:10.1038/srep40096
75. Pierre, G. *et al.* TEMPO-mediated oxidation of polysaccharides : An ongoing story. *Carbohydr. Polym.* **165**, 71–85 (2017).
76. Melone, L. *et al.* TEMPO-Oxidized Cellulose Cross-Linked with Branched Polyethyleneimine: Nanostructured Adsorbent Sponges for Water Remediation. *Chempluschem* **80**, 1408–1415 (2015).
77. Fiorati, A. *et al.* Mechanical and Drug Release Properties of Sponges from Cross-linked Cellulose Nanofibers. 848–858 (2017). doi:10.1002/cplu.201700185
78. Riva, L. *et al.* Naked-Eye Heterogeneous Sensing of Fluoride Ions by Co-Polymeric Nanosponge Systems Comprising Aromatic-Imide-Functionalized Nanocellulose and Branched Polyethyleneimine. *Chempluschem* **84**, 1512–1518 (2019).
79. Fiorati, A. *et al.* Eco-design of nanostructured cellulose sponges for sea-water decontamination from heavy metal ions. *J. Clean. Prod.* 119009 (2019). doi:10.1016/j.jclepro.2019.119009

Acknowledgements

Firstly, I would like to thank Prof. Carlo Punta for the care and attention given to me, for the availability to answer to my very and each question. His support was fundamental for the realization of this work.

I am extremelly grateful to Laura Riva: she taught me how to work in a chemistry lab and how is important to be precise and firm while facing laboratory research, with always time for a laugh. Being always available for my questions, I really appreciate her commitment to the research activity, her great knowledge of the subject and her infinite patience.

I would like to thank all the OSCM Lab research group, especially Andrea, Arianna, Martina, Fabio, Filippo and Alessandro. I would like also to thank the “intruder” Federico.